Isotope fractionation associated with direct and indirect photolysis of substituted anilines

DISS. ETH NO. 22750

ISOTOPE FRACTIONATION ASSOCIATED WITH DIRECT AND INDIRECT PHOTOLYSIS OF SUBSTITUTED ANILINES

A thesis submitted to attain the degree of

DOCTOR OF SCIENCES of ETH ZURICH

(Dr. sc. ETH Zurich)

presented by

MARCO RATTI

Dottore Magistrale in SCIENZE CHIMICHE, Università degli Studi di Milano

born on 24.09.1984

citizen of Italy

accepted on the recommendation of

Prof. Dr. Kristopher McNeill, examiner

PD Dr. Thomas B. Hofstetter, co-examiner

Dr. Silvio Canonica, co-examiner

Prof. Dr. Petr Klán, co-examiner

2015

Dank

Ich möchte meinen Betreuern, Thomas Hofstetter, Silvio Canonica und Kris McNeill, herzlich danken.

Thomas hat mir die Gelegenheit gegeben, die Doktorarbeit unter seiner Betreuung durchführen zu können. Er hat mich Schritt für Schritt mit seinem Enthusiasmus bis zum Ende der Doktorarbeit begleitet. Deswegen möchte ich ihm einen herzlichen Dank für das Vertrauen und die Geduld aussprechen. Er war immer sehr hilfsbereit in menschlichen, wissenschaftlichen, technischen und vor allem schreibtechnischen Belangen.

Ich möchte Silvio ganz herzlich danken für seine unschätzbare wissenschaftliche Beratung. Bei jedem Zweifel konnte ich bei ihm zur Besprechung vorbeikommen und bekam immer hilfreiche Lösungen. Zudem bin ich ihm für die Geduld und das Vertrauen sehr dankbar.

Ich möchte dem Leiter dieses Projekts, Kris, für das Vertrauen ganz herzlich danken. Er hat mir die Möglichkeit gegeben, an den Meetings seiner Gruppe teilnehmen zu können, wo ich immer extrem viele wertvolle Feedbacks und neue Ideen für mein Projekt bekommen habe. Leider konnte ich nicht alle Ideen weiterentwickeln. Dank der engen Zusammenarbeit mit Kris Gruppe, konnte ich jedoch sehr interessante Versuche am Laser durchführen. Für die Unterstützung bei diesen Versuchen und für die wissenschaftliche Beratungen möchte ich Paul ganz herzlich danken.

Im Übrigen möchte ich all meinen Betreuern für die Zeit, die sie mit Besprechungen in meine Schulung investiert haben, herzlich danken.

Zudem möchte ich Petr Klán für sein Interesse an dieser Arbeit und für die Übernahme des Korreferats danken.

Vielen Dank an Kov! Beim GC/IRMS traten immer wieder neue Probleme auf

und er konnte sie alle dank seiner grossen technischen Kompetenz und vor allem dank seiner Manualität beheben.

Einen herzlichen Dank an alle PhDs, die in den letzten vier Jahren in der Gruppe von Thomas gearbeitet haben: Sarah, Stephie, Marita, Reto und Rani. Ich konnte von euch allen wichtige wissenschaftliche, technische, Computer-technische oder auch organisatorische Ratschläge bekommen, die für meinen Weg hier an der Eawag extrem wichtig waren. Ihr wart immer hilfsbereit und vor allem geduldig mit mir, deswegen möchte ich euch einen grossen Dank aussprechen.

Ich möchte Jannis, Sabrina und vor allem Frank für die Beratungen und Zusammenarbeit beim Praktikum herzlich danken.

Ich möchte Philipp und allen anderen, die mir ab und zu beim Orbitrap geholfen haben, herzlich danken.

Ich möchte der Abteilung Uchem von der Eawag für die Geduld in all diesen Jahren herzlich danken. Auch dem IBP an der ETH danke ich herzlich.

Ebenfalls möchte ich der ITN CSI:ENVIRONMENT Gruppe herzlich danken. Die Meetings und die Training-Networks in ganz Europa waren immer sehr interessant. Ich möchte Henry Holmstrand und Milena für die Unterstützung während meines Secondment an der Universität von Stockholm herzlich danken.

Zum Schluss möchte ich den Personen ganz herzlich danken, die für mich am wichtigsten sind: Meine Eltern. Diese Doktorarbeit habe ich vor allem für euch zu Ende gebracht!

Table of contents

Summary

Aromatic amines are widely used chemicals in the industrial synthesis and many chemical products including pharmaceuticals, pesticides, and personal care products contain aromatic amine moieties. As a consequence of their frequent use, contamination of aquatic environment with aromatic amines occurs from point sources, such as accidental release or incomplete removal during waste treatment processes, as well as through diffuse pollution, for example when applied during pest control. In addition, aromatic amines can also be formed in the environment through the transformation of anthropogenic contaminants. Because of their considerable toxicity and carcinogenicity, quantification of the exposure of humans and the environment to this contaminant class is essential for a reliable assessment of adverse effects. Understanding the transformation processes of aromatic amines, however, is challenging due to numerous possible biological and abiotic degradation pathways. In this work, we explored the use of compound specific stable isotope analysis (CSIA) to contribute to a reliable assessment of the (bio)degradation of aromatic amines. As has been shown for some enzymatic and mineral-catalyzed oxidations of aromatic amines, changes of natural abundance $^{13}C/^{12}C$, $^{15}N/^{14}N$, and $^{2}H/^{1}H$ ratios in the residual amine enables one to identify ongoing degradation processes even if reactions take place simultaneously and regardless of contaminant dilution or phase transfer. But it is currently unknown whether CSIA is also applicable to study the important photochemical degradation of aromatic amines, because kinetic and equilibrium isotope effects of reactions of excited state species are not well understood. The specific goal of this PhD thesis was therefore to identify isotope fractionation patterns of that could enable one to track direct and indirect photolytic transformations of aromatic amines by using chlorinated anilines as model compounds.

We studied the *direct* photolysis of 2-chloro-, 3-chloro, and 4-chloroaniline in laboratory batch experiments at an irradiation wavelength of 254 nm over the pH range 2.0 to 9.0 in the presence and absence of Cs^+ used as a singlet state quencher. Photolysis leads to a dechlorination of excited state chloroaniline species and was associated with measurable C and N isotope fractionation. The extent of isotope fractionation, quantified by C and N isotope enrichment factors, ϵ_C and ϵ_N was distinctly different for each chloroaniline isomer and varied with pH and presence of Cs^+. We also observed substantial variations in the preference of light vs. heavy C and N isotopes, that is isotope fractionation was both *normal* and *inverse*.

Linear correlations of the apparent ^{13}C- and ^{15}N-kinetic isotope effects (AKIE) associated with the photolysis of 4-Cl-aniline revealed photolysis by two reaction pathways that may be due to different spin states of excited 4-Cl-aniline species. Such magnetic isotope effects were hypothesized to originate from spin-orbit coupling of unpaired electrons with spin carrying nuclei (^{13}C, ^{14}N, ^{15}N but not ^{12}C). In the presence of 1 M Cs^+ or at solution pH values below 5, we found a marked increase of ^{13}C- and ^{15}N-AKIEs that could be indicative for reactions from triplet excited states. Photolysis of 4-Cl-aniline at pH-values between 5.0 to 9.0, on the other hand, showed a correlation of increasing ^{15}N-AKIE with decreasing ^{13}C-AKIE. The latter may hint at reactions from excited singlet states because experiments at pH 7.0 and 9.0 in the presence of Cs^+, result in the former AKIE patterns. Photolytic dechlorination of 2-Cl-aniline also revealed mass independent C and N isotope fractionation. In contrast to 4-Cl-aniline, different ^{13}C- and ^{15}N-AKIEs could be assigned to protonated and neutral 2-Cl-aniline species. Only C and N isotope fractionation of the 2-Cl-anilinium cation changed in the presence of Cs^+ suggesting that AKIEs of this species reacted, at least in part, through excited singlet states. The almost negligible C isotope fractionation associated with the dechlorination of 3-Cl-aniline was also influenced by its protonation state whereas the larger N isotope fractionation did not follow this trend.

The *indirect* photolysis of a series of four *para*-substituted anilines was studied at irradiation wavelengths $\geq$ 400 nm, using aerated aqueous solutions of a model photosensitizer, namely anthraquinone disulfonate (AQDS) or methylene blue. The excited triplet states formed upon irradiation of such photosensitizers were used to mimic excited triplet states of dissolved organic matter, which are the reactive species initiating these indirect photolysis reactions in sunlit natural waters. Transformation of aniline, 4-CH_3-, 4-OCH_3- and 4-Cl-aniline photosensitized by AQDS and methylene blue is assumed to occur through an N atom oxidation mechanisms. Transformation was associated with inverse or normal N isotope fractionation, depending on the compound, whereas C isotope fractionation was negligible. The apparent ^{15}N-AKIE-values were almost identical for both photosensitizers and correlated well with the electron donating properties of the substituent at the aromatic ring. N isotope fractionation is pH-dependent in that it is dominated by H^+ exchange reactions below and N atom oxidation processes above the pK_a-value of the substituted aniline's conjugate acid. As opposed to direct photolysis, isotope fractionation could be rationalized with changes of N bonds after one electron oxidation.

The findings presented in this study show that the direct and indirect phototransformations of substituted anilines can be associated with distinctly different C and N isotope fractionation that could be detected in sunlit surface waters. Because direct and indirect photo-transformations of many aromatic amines are potentially competing reactions, the identification of specific C and N isotope fractionation patterns trends, is of great importance to assess the relative importance of those transformation pathways. A more widespread application of CSIA will benefit from further study with aromatic amines that react through other direct photolysis mechanisms than dechlorination as well as by indirect photolysis with other important transient oxidants such as reactive oxygen species (e.g. singlet oxygen, hydroxyl radical) and carbonate radical.

Riassunto

Le ammine aromatiche sono largamente utilizzate nell'industria chimica per la sintesi di prodotti farmaceutici, insetticidi, cosmetici o destinati all'uso per l'igiene personale. Le ammine aromatiche vengono rilasciate nell'ambiente, per via accidentale, antropogenica oppure attraverso gli impianti per il trattamento delle acque reflue, quando la loro rimozione risulta essere inefficiente. Trattandosi di composti altamente tossici e cancerogeni è fondamentale quantificarne l'impatto nocivo sull'ambiente e sulla salute delle persone. Tuttavia la piena comprensione dei processi di trasformazione delle ammine aromatiche risulta essere un'opera laboriosa, in seguito alle molteplici vie di degradazione (biotiche a abiotiche), alle quali questa classe di composti si sottopone nell'ambiente. In questo lavoro è stata impiegata la tecnica di analisi isotopica di composti specifici (Compound-Specific Isotope Analysis, CSIA) per effettuare una valutazione affidabile delle diverse vie di degradazione (biotiche e abiotiche) delle ammine aromatiche nell'ambiente. In passato è stato dimostrato come la variazione nel rapporto dell'abbondanza isotopica naturale ($^{13}C/^{12}C$, $^{15}N/^{14}N$, e $^{2}H/^{1}H$) abbia permesso di monitorare la degradazione delle ammine aromatiche di interesse ambientale. Ciò è stato possibile per la reazione di ossidazione delle ammine aromatiche, catalizzata per via enzimatica o da legami con la superficie di un minerale. È tuttora incerto se la tecnica di analisi CSIA sia applicabile allo studio di fotodegradazione delle ammine aromatiche. Gli effetti isotopici cinetici e di equilibrio relativi a reazioni che avvengono allo stato elettronico eccitato sono perlopiù tuttora sconosciuti. La presente tesi di dottorato ha avuto come obbiettivo lo studio del frazionamento isotopico associato alle reazioni di fotodegradazione diretta ed indiretta delle ammine aromatiche. È stato scelto di utilizzare le cloroaniline come composti di riferimento per le ammine aromatiche.

La fotolisi diretta della 2-, 3- e 4-cloroanilina è stata studiata in laboratorio mediante irradiazione di soluzioni acquose a pH variabile ad una lunghezza d'onda di 254 nm. È stato fatto uso anche di uno spegnitore (quencher, Cs^{+}) di stati elettronici eccitati di singoletto. Mediante l'uso di analisi CSIA, è stato possibile determinare il frazionamento isotopico degli atomi di carbonio e di azoto associato alla declorinazione fotolitica delle cloroaniline in soluzione acquosa.

Al variare delle condizioni sperimentali, variando dunque il pH della soluzione e facendo o meno utilizzo di Cs^{+},il frazionamento isotopico, quantificabile come fattore di arricchimento isotopico (ϵ_{C}, ϵ_{N}), è risultato essere variabile. A seconda del substrato utilizzato per la reazione, è stato possibile osservare l'arricchimento preferenziale negli atomi di C e di N dell'isotopo pesante rispetto a quello leggero e viceversa. Come risultato si ha che il fattore di arricchimento isotopico è risultato essere sia *normale* che *inverso*.

Dalle correlazioni lineari degli effetti isotopici cinetici (^{13}C- e ^{15}N-AKIE), ossevabili nel caso della fotolisi diretta della 4-cloroanilina, si evince che la reazione di fotolisi può ricondursi fondmentalmente a due differenti meccanismi di reazione, a seconda che avvenga da uno stato elettronico eccitato di singoletto o di tripletto. Si pensa dunque che le interazioni magnetiche, derivanti dall'accoppiamento del momento orbitale dell'elettrone disaccoppiato con lo spin magnetico del nucleo (^{13}C, ^{14}N, ^{15}N) diano luogo a degli effetti isotopici magnetici. Reazioni di fotolisi riconducibili allo stato elettronico eccitato di tripletto sono state individuate per le reazioni condotte a valori di pH inferiori a 5 oppure in presenza di Cs^{+} 1M, dove è stato possibile osservare un incremento sia per i valori di ^{13}C-AKIE che per quelli relativi a ^{15}N-AKIE. D'altro canto, le reazioni condotte a dei valori di pH superiori a 5, sono state associate a delle fotolisi riconducibili allo stato elettronico eccitato di singoletto. In quest'ultimo caso l'incremento si verifica solo per i valori di ^{15}N-AKIE, mentre quelli relativi a ^{13}C-AKIE tendono a diminuire. La declorinazione fotolitica della 2-cloroanilina ha prodotto anch'essa degli effetti isotopici magnetici e, a differenza del caso della 4-cloroanilina, è stato possibile assegnare valori di ^{13}C- e ^{15}N-AKIE alle specie neutra e protonata del composto. In seguito all'aggiunta di Cs^{+}, solo la forma protonata della 2-cloroanilina ha prodotto variazioni nel frazionamento isotopico del carbonio e dell'azoto, lasciando pensare che la reazione di fotodeclorinazione avvenga perlopiù da stati elettronici eccitati di singoletto. La fotolisi diretta della 3-cloroanilina ha prodotto un frazionamento isotopico, anch'esso funzione del livello di protonazione, trascurabile per l'atomo di carbonio. Mentre il frazionamento isotopico associato all'atomo di azoto, è risultato essere maggiore.

La fotolisi indiretta relativa a una serie di quattro aniline *para*-sostituite, è stata condotta in soluzioni acquose areate, contenenti fotosensibilizzatori rappresentativi della classe dei composti DOM (dissolved organic matter), mediante irraggiamento a delle lunghezze d'onda superiori ai 400 nm. L'anilina, la 4-CH_3-anilina, la 4-OCH_3-anilina e la 4-Cl-anilina reagiscono per trasferimento di carica con gli stati elettronici eccitati di tripletto dell'antrachinone-1,5-disolfonato e del blu di metilene, dando luogo ad un meccanismo di ossidazione localizzato sull'atomo di azoto. Questo tipo di trasformazione è associato con un frazionamento *normale* od *inverso* per l'atomo di azoto, a seconda dell'anilina sostituita, mentre per l'atomo di carbonio è trascurabile. I valori di ^{15}N-AKIE si sono rivelati essere piuttosto identici per entrambi i fotosensibilizzatori, dando luogo a correlazione con i sostituenti dell'anello aromatico, a seconda del loro effetto elettron-attrattore. Il frazionamento isotopico dell'atomo di azoto è risultato essere funzione del pH. Al di sotto del valore della pK_a, il frazionamento isotopico dell'azoto è risultato essere dominato dalla reazione di scambio con H^+, mentre per valori superiori alla pK_a, il frazionamento isotopico è dovuto all'ossidazione dell'atomo di azoto. Il frazionamento isotopico nella fotolisi indiretta si è dimostrato, al contrario di quella diretta, riconducibile a delle variazioni di legame coinvolgenti l'azoto, in seguito a trasferimento monoelettronico.

Le scoperte presentate in questo studio dimostrano che la fotolisi diretta ed indiretta delle aniline sostituite possono essere associate a dei frazionamenti isotopici diversi per l'atomo di C e di N nelle acque di superficie. Dato che la fotolisi diretta ed indiretta sono reazioni competitive per la trasformazione di molte ammine aromatiche, l'individuazione di specifici andamenti per il frazionamento di C ed N, è di grande impatto ambientale. L'applicazione di CSIA può essere applicata per lo studio della fotolisi diretta di altre ammine aromatiche, funzionalizzate in modo diverso da quelle clorurate, e per la fotolisi indiretta mediante l'uso di specie di ossigeno altamente reattive (ROS).

Chapter 1

Introduction

1.1 Substituted anilines as micropollutants of aquatic environments

Aromatic amines are widely used chemicals in industrial synthesis and this compound class is frequently part of the molecular structure of pharmaceuticals, pesticides and personal care products[136,159]. Pharmaceuticals derived from aromatic amines include anti-inflammatory drugs and antibiotics such as diclofenac and sulfamethoxazole. Moreover, a large variety of pesticides such as alachlor and diuron applied for crop protection represent aromatic amines, amides, and phenyl ureas[6]. In the chemical industry, substituted anilines (e.g. 2,4-dichloroaniline) is an important feed stock and precursor for the synthesis of azo dyes[51,65]. Because of their widespread use, contamination of aquatic environments with aromatic amines occurs from different sources.[114,127,128] Aromatic amines are released unintentionally into the environment through spills and due to incomplete removal in industrial and municipal waste water treatment processes. On the other hand, because of their use as active ingredients in plant protection products, aromatic amines are introduced on purpose on agricultural land, from which its chemicals are washed off during rain events[101,152]. Finally, aromatic amines are produced in the environment as a consequence of the transformation processes of pesticides,[10] dyes,[153] and explosives[58,59] under both oxic and anoxic conditions.[12,44,68,141]

Aromatic amines are usually electron-rich compounds, well soluble in polar solvents, and therefore mobile in aquatic environments.[126] Because of their considerable toxicity and carcinogenicity,[30,42] knowledge of the attenuation processes of aromatic amines in aquatic environments is key for an assessment of their impacts and adverse effects to both humans and the environment. In fact, there is a number of degradation processes in the soils and aquatic environment and their initial steps are summarized in Figure 1.1. (1) N-atom oxidation[75,78] and (2) oxidative N-atom dealkylation[52,150] can be catalyzed by both enzymes and mineral surfaces and lead to the formation of radical coupling and N-dealkylated products. The former is typically followed by polymerization reactions generating products of higher molecular weight than the reactants. (3) Aromatic amines undergo nucleophilic addition reactions to electrophilic moieties of natural organic matter (NOM) in irreversible reactions to anilino-quinones.[27,154] (4) Oxidative enzymes can carry out dioxygenations at the benzene ring resulting in substituted catechols, which are often amenable to further biodegradation.[130] (5) Under anoxic conditions, e.g. wastewater treatment plants, enzymatic reductive deamination takes place and the carboxylated products are transformed further as observed in dioxygenation processes[77,123]. Carboxylation to aminobenzoate and reductive deamination were the identified degradation steps of the reaction. In sunlit surface waters, (6) direct photolysis of chloro-substituted anilines is associated with a dechlorination reaction and the formation of stable products from radical intermediates strongly depends on the availability of dissolved O_2.[7,87,158] Finally, (7) sensitized photolysis of substituted anilines by reactive oxygen and carbonate species as well as excited triplet states of dissolved organic matter (^{3}DOM*) follows the same reaction mechanism invoked for processes (1) and (2) to radical coupling products.[9,41,99]

The large number of potentially competing attenuation processes makes the quantification of the exposure of humans and aquatic organisms to substituted anilines as well as a prediction of their possible transformation products a challenging task. Information about the predominant degradation reaction in the environment is difficult to obtain because concentration profiles cannot resolve transformation reactions occurring in parallel and may be biased by dilution and sorption of the contaminants to organic and inorganic constituents of the environmental matrices. Moreover, many of the principal reaction products are difficult to quantify because of further (metabolic) transformations. To contribute to a more reliable assessment of the transformation pathways of aromatic amines, new approaches are required that enable one to overcome the above-mentioned challenges. The overall goal of this study was therefore to explore the use of compound specific isotope analysis (CSIA) for the identification of transformation processes of aromatic amines in aquatic environments. Compound specific isotope analysis was already applied successfully for quantifying natural attenuation of various contaminant classes including chlorinated hydrocarbons[36,122], fuel constituents[116,147], and nitroaromatic explosives[58,163]. As illustrated in more detail in the following chapters, CSIA relies on the accurate quantification of changes in stable isotope composition of C, H, N and other elements in organic contaminants and the understanding of the kinetic and equilibrium isotope effects associated with the various contaminant transfor-

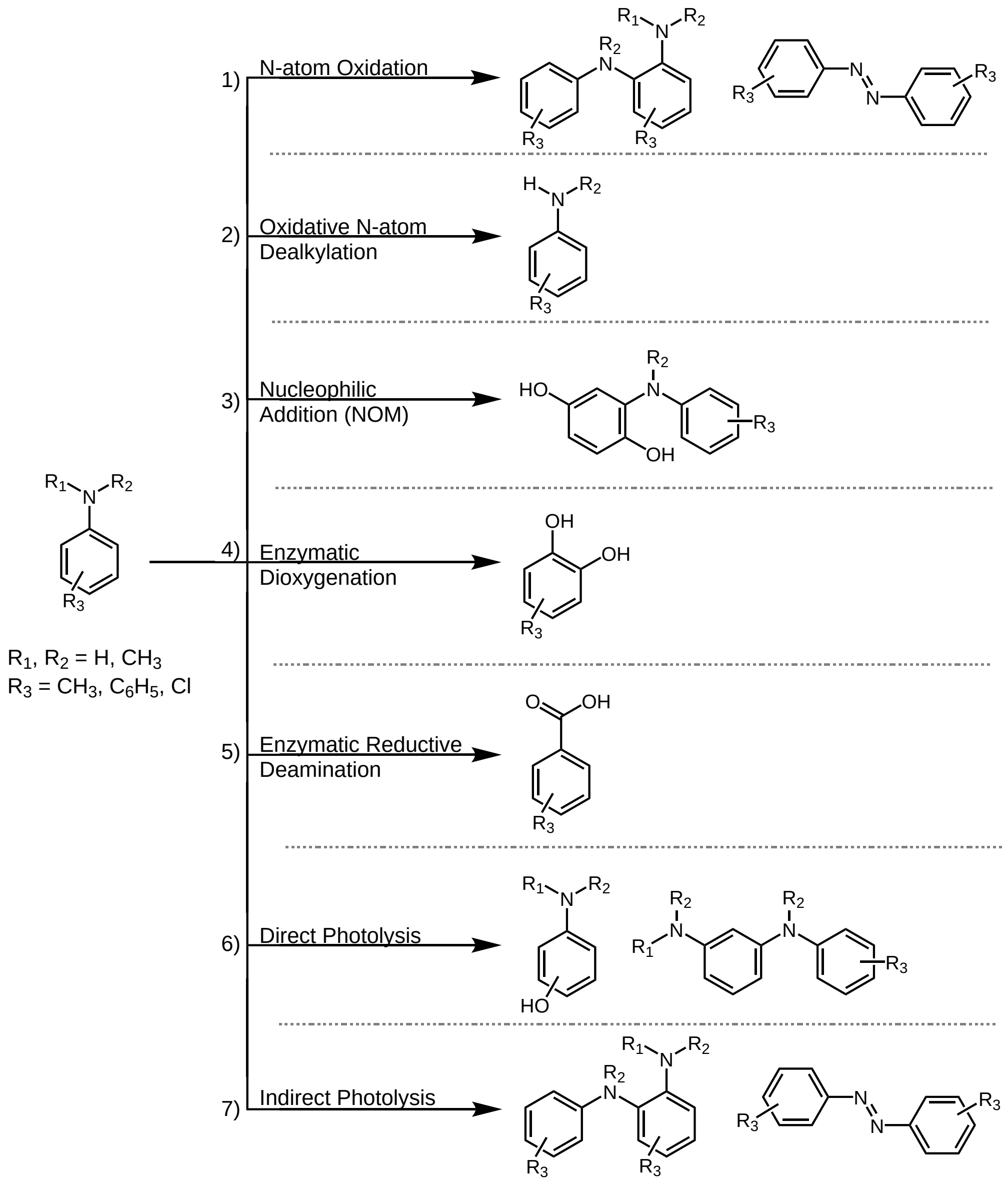

Figure 1.1 Possible elimination pathways of aromatic amines in the environment, listed with the characteristic transformation products. Halogenated, alkyl and aromatic groups are used as substituents for R_3.

mation pathways.[2,35,38,57,61,63,71,122,146] However, only very few of the degradation reactions of aromatic amines listed in Figure 1.1 are understood in terms of isotope effects and isotope fractionation.

1.2 Compound-specific isotope analysis (CSIA)

The analysis of stable isotope ratios of aromatic amines, namely $^{13}C/^{12}C$, $^{15}N/^{14}N$, and $^{2}H/^{1}H$, is accomplished by coupling gas chromatography to isotope ratio mass spectrometry (GC/IRMS).[35,57] Elemental isotope ratios, denoted here with E for either C, N, and H (where h and l stands for heavy and light isotopes), are usually expressed as stable isotope signatures (δ^{h}E) in ‰, e.g. δ^{13}C, δ^{15}N and δ^{2}H. Their value referred to an internationally defined standard material (eq. 1.1).

$$\delta^{\mathrm{h}}\mathrm{E} = \frac{(^{\mathrm{h}}\mathrm{E}/^{\mathrm{l}}\mathrm{E})_{\mathrm{sample}}}{(^{\mathrm{h}}\mathrm{E}/^{\mathrm{l}}\mathrm{E})_{\mathrm{standard}}} - 1 \tag{1.1}$$

Transformations of aromatic amines are associated with changes of isotope ratios of the considered molecule and this phenomenon is called isotope fractionation. The observed isotope fractionation refers to the variation of the isotopic signature of a compound, $\delta^{\mathrm{h}}\mathrm{E}$, in comparison to its initial value, $\delta^{\mathrm{h}}\mathrm{E}_0$. Isotope fractionation is proportional to the fractional conversion of a compound and the extent of isotope fractionation is quantified with isotope enrichment factors, ϵ_{E}, which always refer to the isotopic change in the entire molecule.[35] This relationship is shown in the Rayleigh equation (eq. 1.2), where C/C_0 is the fraction of remaining reactant.

$$\frac{\delta^{\mathrm{h}}\mathrm{E} + 1}{\delta^{\mathrm{h}}\mathrm{E}_0 + 1} = \left(\frac{C}{C_0}\right)^{\epsilon_{\mathrm{E}}} \tag{1.2}$$

Isotope enrichment factors (ϵ_{E}) are obtained from linear regression with a log-linearized form of the Rayleigh equation. ϵ_{E}-values are pertinent to an aromatic amine and a transformation process. The isotope fractionation quantified for the bulk compound with an ϵ_{E}-value, reflects the kinetic isotope effect (KIE) of the reacting bonds. One central hypothesis of CSIA is that every transformation pathway is associated with a characteristic KIE, which reflect the (small) differences in activation energy of molecules carrying light and heavy isotopes, respectively.[166] KIEs of electronic ground state reactions are therefore defined as ratios of reaction rate constant ratio of the light ($^{\mathrm{l}}k$) to heavy ($^{\mathrm{h}}k$) isotopologue (eq. 1.3). Note that labels for the considered isotopic elements (E) are not shown for convenience here.

$$\mathrm{KIE} = \frac{{}^{\mathrm{l}}k}{{}^{\mathrm{h}}k} \tag{1.3}$$

Primary KIEs are observed when bonds are broken or formed during the rate-limiting step of a reaction whereas KIEs are secondary, if isotopic substitution is not at the reactive position. Kinetic isotope effects are *normal*, i.e. > 1, when the light isotopologues react faster than the heavy ones, while the effect is *inverse* in the opposite case. To obtain *apparent* kinetic isotope effects (AKIEs) from isotope enrichment factors, one typically neglects secondary isotope effects. The derivation is straightforward when taking into account the dilution of a KIE by nonreactive atoms as well as intramolecular isotopic composition as in eq. 1.4.

$$\mathrm{AKIE_E} = \frac{1}{1 + (n/x) \cdot z \cdot \epsilon_\mathrm{E}} \tag{1.4}$$

where n is the number of isotopic atoms of an element, x denotes atoms at the reactive site, and z quantifies the number of chemically equivalent reactive sites in the aromatic amine.[37]

Compound-specific isotope analysis is particularly useful when several elements are considered simultaneously, especially because artifacts from the masking of KIEs by isotope-independent rate-limiting steps can be circumvented.[35,170] Such multi-dimensional isotope fractionation analysis typically involves the correlation of isotope fractionation of two elements as proxy for a transformation process. In this study, this approach was implemented for C and N isotopes as in eq. 1.5. The ratio of changes of N and C isotope signatures, $\Delta\delta^{15}\mathrm{N}/\Delta\delta^{13}\mathrm{C}$, is approximately equivalent to the ratio of isotope enrichment factors, $\epsilon_\mathrm{N}/\epsilon_\mathrm{C}$ and proportional to the ratio of $(\mathrm{AKIE} - 1)$-values for the reactions considered.[163]

$$\frac{\Delta\delta^{15}\mathrm{N}}{\Delta\delta^{13}\mathrm{C}} \approx \frac{\epsilon_\mathrm{N}}{\epsilon_\mathrm{C}} \propto \frac{\mathrm{AKIE_N^{-1}} - 1}{\mathrm{AKIE_C^{-1}} - 1} \tag{1.5}$$

1.3 Isotopic analysis of thermal vs. photochemical transformation processes of aromatic amines

Degradation processes (1), (2), and (4) shown in Figure 1.1 have already been studied by compound-specific isotope analysis in laboratory model systems. Previous work by Skarpeli-Liati et al. and Pati et al.[102,133–135] showed that bonding changes at the N atom after one electron oxidation and dioxygenation of the aromatic ring indeed lead to characteristic primary N isotope fractionation. Fractionation of C isotopes, in contrast, was mostly minor. The tighter bonding to N in the transition state of the two reactions was hypothesized to lead to the considerably inverse isotope effects. The correlation of C and N isotope fractionation resulted in patterns, which suggest that such processes could be distinguished even if they occurred simultaneously. However, this comparison is currently limited to oxidative processes of ground state reactants and the isotope effects of other reactions, especially those occurring from excited state species of aromatic amines are completely unknown.

In fact, the few studies on the isotope fractionation associated with photochemical contaminant transformation suggest that isotope effects are more difficult to understand than for ground-state reactions. Examples for the direct photolysis of atrazine and bromophenols show that the observed fractionation of C, N, H, and Br isotopes could no longer be rationalized in terms of bond cleavage reactions.[56,168] Instead, it was suggested that magnetic interactions of excited state species with at least partial radical character led to magnetic isotope effects. It is well known that electronic excited states, which may be considered as biradicals because they have two unpaired electrons, can undergo spin-orbit coupling with magnetic moments of different isotopic nuclei leading to preferential conversion of spin states during intersystem crossing.[17–19,149,160] To date, however, there is no evidence for a contribution of magnetic isotope effects from photophysical processes to isotope fractionations in photochemical transformation of aromatic amines. Furthermore, it is unknown whether such effects differ from that of indirect photolytic processes, which can be assumed to follow the trends observed for enzymatic and mineral-catalyzed oxidation reactions.

1.4 Goals and approach

The goal of this work was to investigate the magnitude and variability of isotope fractionation of direct and indirect photolytic degradation of aromatic amines and to contribute to the assessment of environmentally relevant degradation processes by CSIA. We selected 2-chloro-, 3-chloro-, and 4-chloroaniline as model compounds to study C and N isotope fractionation in laboratory model system and address the following, specific objectives.

1. The *direct photolysis* of the three chloroaniline isomers involves a heterolytic dechlorination reaction. Previous work showed that despite this apparent similarity, the mechanisms of 2-Cl-, 3-Cl-, and 4-Cl-aniline photolysis are quite different.[5,45,48,53,94,95,97,98] 4-Cl-aniline reacts to a variety of products via a biradical intermediate whereas the radical character of the photolysis of 2-Cl- and 3-Cl-aniline is less certain. Through a comparison of the C and N isotope effects associated with the photolysis of the three chloroaniline isomers, we aimed at identifying

    (a) typical C and N isotope fractionation patterns that would enable one to track photolytic dechlorinations.

    (b) In addition, these experiments were made to obtain insights into the origin of C and N isotope fractionation and delineate the contribution of photophysical reactions (i.e., from magnetic isotope effects) vs. bond cleavage reactions.

2. The *indirect photolysis* of aromatic amines occurs through oxidations by transient photooxidants, which are often generated through light absorption of dissolved organic matter (^{3}DOM*).[155,156] Through the study of the oxidation of a series of four, *para*-substituted anilines, namely aniline, 4-CH_3-, 4-OCH_3-, and 4-Cl-aniline, by excited triplet states of an anthraquinone disulfonate and methylene blue, we aimed at

(a) identifying differences in C and N isotope fractionation between direct and indirect photolysis with multi-dimensional isotope analysis ($\Delta\delta^{15}N/\Delta\delta^{13}C$) and

(b) quantifying the effects of different photooxidants and aromatic substituents on the apparent ^{15}N- and ^{13}C-kinetic isotope effects.

The results of the PhD thesis are presented in the following way. In Chapter 2, we present the results from the study of 4-Cl-aniline photolysis at an irradiation wavelength of 254 nm. The detailed analysis of 4-Cl-aniline disappearance kinetics and elucidation of products show that the observable isotope fractionation is due to the initial step in the photolysis reaction. Experiments carried out over the pH-range 2 to 9 as well as in the presence of a singlet quencher[74,118] illustrate a substantial variability of isotope effects depending on reactions from excited triplet and singlet states. In Chapter 3, the systematic investigation of isotope fractionation under different experimental conditions is extended to 2-Cl- and 3-Cl-aniline. The comparison not only reveals substantial differences in isotope fractionation behaviour of the three chloroaniline isomers but also suggests that anilinium cations and neutral species photolyse by different mechanims. In Chapter 4, we show evidence for substituent-dependent N isotope effects associated with the N atom oxidation of four substituted anilines. In contrast to direct photolytic reactions, isotope fractionation can be explained by bonding changes at the N atom without contributions from magnetic interactions. Conclusions of the PhD thesis with regard to the overall goals are discussed in Chapter 5.

Chapter 2

Isotope Fractionation Associated with the Direct Photolysis of 4-Chloroaniline

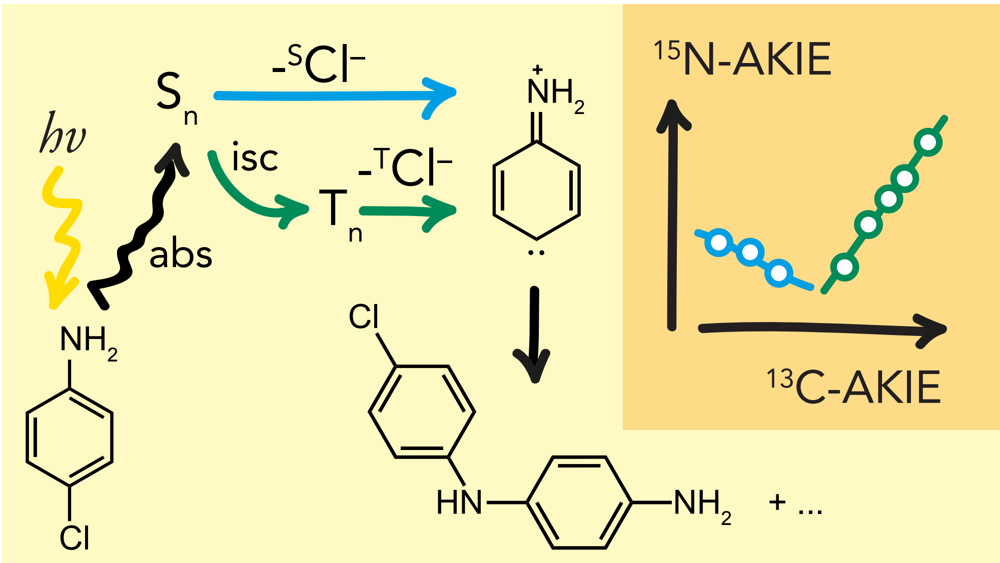

M. Ratti, S. Canonica, K. McNeill, P. R. Erickson, J. Bolotin and T. B. Hofstetter. Isotope fractionation associated with the direct photolysis of 4-chloroaniline. *Environ. Sci. Technol.*, 49:4263-4273, **2015**

Abstract

Compound-specific isotope analysis is a useful approach to track transformations of many organic soil and water pollutants. Applications of CSIA to characterize photochemical processes, however, have hardly been explored. In this work, we systematically studied C and N isotope fractionation associated with the direct photolysis of 4-Cl-aniline used as a model compound for organic micropollutants that are known to degrade via photochemical processes. Laboratory experiments were carried out at an irradiation wavelength of 254 nm over the pH range 2.0 to 9.0 as well as in the presence of Cs^+ as a quencher of excited singlet 4-Cl-aniline at pH 7.0 and 9.0. We observed considerable variation of C and N isotope enrichment factors, ϵ_C and ϵ_N, between -1.2 ± 0.2‰ to -2.7 ± 0.2‰ for C and -0.6 ± 0.2‰ to -9.1 ± 1.6‰ for N, respectively, which could not be explained by the speciation of 4-Cl-aniline alone. In the presence of 1 M Cs^+, we found a marked increase of apparent ^{13}C-kinetic isotope effects (^{13}C-AKIE) and decrease of 4-Cl-aniline fluorescence lifetimes. Our data suggest that variations of C and N isotope fractionation originate from heterolytic dechlorination of excited triplet and singlet states of 4-Cl-aniline. Linear correlations of ^{13}C-AKIE vs. ^{15}N-AKIE were distinctly different for these two reaction pathways and may be explored further for the identification of photolytic aromatic dechlorination reactions.

2.1 Introduction

Compound-specific stable isotope analysis enables tracking the transformation of many different micropollutants in the environment. Isotope fractionation measured in individual compounds can often be rationalized in terms of bonding changes along the reaction pathway and is therefore a valuable proxy for determining the type of reaction that initiates contaminant degradation[2,35,38,57,61,146]. The combined evaluation of isotope fractionation from several elements such as C, H, N, and Cl is especially valuable in identifying degradation pathways even if reactions take place simultaneously[38,71]. While apparent kinetic isotope effects (AKIEs) and isotope fractionation patterns of many substitution and redox reactions have been characterized in recent years,[1,26,55,60,80,84,88,102,104,116,135,147,162–164] little is known about isotope fractionation during photolytic transformations of organic contaminants. It is currently unclear whether such processes are accompanied by isotope fractionation trends that could be assigned specifically to photochemical transformations in the environment.

Bonding changes, especially bond cleavage reactions in the rate-limiting step, are typically considered the primary source of isotope fractionation[86,166]. In photochemical processes, however, additional factors make it more difficult to rationalize isotope fractionation. The direct photolysis of atrazine and the associated fractionation of C and N is an interesting, illustrative example[56]. The observed, inverse apparent C and N isotope fractionation of atrazine could not be reconciled with the fact that transformation is a dechlorination reaction leading to hydroxyatrazine. A C–Cl bond cleavage is expected to give rise to normal instead of inverse isotope fractionation and cannot explain why fractionation of N isotope is large even though none of the five N atoms are directly involved in the reaction. The results were hypothesized to originate from magnetic interactions of excited state species with at least partial radical character as magnetic isotope effects. Several other examples of such mass *in*dependent isotope effects in the transformation of both organic and inorganic contaminants are known and include other elements like Br and Hg[11,137,161,168]. Apparently, excited state radicals can undergo spin-orbit coupling with magnetic moments of different isotopic nuclei leading, for example, to preferential conversion of spin states during intersystem crossing[17–19,142,149,160]. Isotope fractionation associated with photochemical pollutant transformation is thus likely accompanied by magnetic isotope effects (or combinations thereof) originating from photophysical processes.

These phenomena are, unfortunately, poorly understood in photochemical pollutant transformation processes and it was the goal of the present study to explore the consequences for pollutant isotope fractionation in more detail. In this work, 4-chloroaniline (4-Cl-aniline) was used as a model compound for pharmaceuticals, pesticides, and industrial chemicals that are known to degrade via photochemical processes in surface waters[14,15,20]. Moreover, the reaction routes of direct photolysis of 4-Cl-aniline via carbene intermediates are well characterized[45,48,53,95,98]. Specifically, we investigated (i) whether direct photolysis of 4-Cl-aniline gives rise to characteristic C and N isotope fractionation trends that could be used as proxies for photochemical degradation, (ii) if our observations apply for variable environmental conditions, and (iii) to what extent photochemical isotope fractionation differs from that reported for biological and abiotic transformation of substituted anilines and aromatic *N*-alkyl amines[134,135].

Oxidation of substituted anilines can occur at the N atom by various abiotic oxidants, including MnO_2,[78] photochemically produced reactive intermediates such as excited triplet states of chromophoric natural organic materials and carbonate radicals[23,112] as well as enzymatically via dioxygenation of the aromatic ring[130]. Both abiotic and enzymatic mechanisms exhibit only minor normal ^{13}C-AKIEs ($\leqslant 1.003$), whereas N isotope fractionation is inverse and much larger for enzymatic processes (^{15}N-AKIEs between 0.987 and 1.006)[102,134]. The ^{15}N-AKIEs for the N atom oxidation mechanism, however, are quite sensitive to the type and position of aromatic substituents thus making extrapolations of isotope effects from one compound to another challenging. In addition, at pH-values close to and below the pK_a of the substituted aniline's conjugate acid, oxidation isotope effects become negligible when compared to the large ^{15}N-equilibrium isotope effects associated with deprotonation[115,133,134]. Here, we studied the C and N isotope fractionation of direct photolysis of 4-Cl-aniline in aqueous solution over a wide pH range (2.0 to 9.0) to account for possible influence of H^+-exchange reactions in ground and excited states. We performed isotopic analyses of 4-Cl-aniline from experiments in batch reactors, as well as quantitative and qualitative product analysis by GC/MS and LC-MS/MS, respectively. In addition, the effect of singlet quenchers was investigated with time-resolved laser spectroscopy.

2.2 Experimental Section

A list of chemicals including their purities and suppliers can be found in the Supporting Information (SI).

2.2.1 Chemical and isotopic analysis

Concentrations of 4-Cl-aniline were measured by reversed phase HPLC as reported previously using a Dionex UltiMate 3000 equipped with a UV-Vis detector and a Supelcosil LC-18 column (25 cm $\times$4.6 mm, 5μm)[133]. Eluents consisted of 40/60 vol % mixtures of methanol and 1 mM KH_2PO_4 at a flow rate of 1 mL min^{-1} and a sample injection volume of 20 μL. All concentrations were measured in duplicates and are reported as arithmetic mean. Transformation products were identified by liquid chromatography coupled to an LTQ (Linear Trap Quadrupole) Orbitrap mass spectrometer (Thermo) with electrospray ionization as documented previously[134,135]. For liquid chromatographic separation an Atlantis C-18 column (3.0$\times$ 150 mm, 3 μm particle size, Waters) and an XBridge C-18 column (2.1$\times$ 50 mm, 3.5 μm particle size, Waters) were used and a gradient was run from a ratio of 90/10 to 5/95 vol % of H_2O/MeOH. Both eluents contained 0.1 vol % formic acid. 4-Aminophenol and aniline were available as commercial standards for product identification while the dimers, trimers, and tetramer photoproducts were defined qualitatively based on exact molecular mass and fragmentation pattern of each detected product. Possible molecular structures were postulated as shown in the Supporting Information (SI).

Stable C and N isotope signatures ($\delta^{13}C$, $\delta^{15}N$) of 4-Cl-aniline were measured using a gas chromatograph (Trace GC / Trace GC Ultra, Thermo) coupled to an isotope ratio mass spectrometer (Delta Plus XL / V Plus, Thermo) as described previously[133]. The combustion interface was equipped with a Ni/Pt reactor[138]. The aqueous 4-Cl-aniline solutions were adjusted to pH 7.0 prior to extraction by solid-phase microextraction using a PDMS/DVB-fiber (Supelco). Stable C and

N isotope signatures (δ^{13}C-, δ^{15}N-) of 4-Cl-aniline are given as arithmetic mean ($\pm\sigma$) of triplicate measurements in per mil (‰). Isotopic standard materials purchased from Indiana University were used to report δ^{13}C- and δ^{15}N-values relative to Vienna PeeDee Belemnite and air, respectively. C and N isotope analysis was performed within the method quantification limits of the SPME-GC/IRMS procedure of 1.0 to 2.5 μM for δ^{13}C and δ^{15}N [72]. Samples were diluted to concentrations yielding peak amplitudes between 0.5 and 3 V. A standard bracketing procedure, referenced to a calibrated in-house standard of 4-Cl-aniline of known δ^{13}C and δ^{15}N-values, was used to ensure accuracy of the isotope ratio measurements.

2.2.2 Photochemical Experiments

Four different series of photochemical experiments were performed in this study; (*a*) for investigation of C and N isotope fractionation, (*b*) for examination of rate constants and reaction kinetics at pH 7.0 at various initial substrate concentrations, (*c*) for quantification of the pH-dependence of direct 4-Cl-aniline photolysis rate constants, and (*d*) for determining fluorescence lifetimes.

Experiments (*a*) to (*c*) were carried out in glass-stoppered quartz tubes (OD 18 mm, ID 15 mm) filled with 20 mL of aerated and buffered solution, typically 10 mM phosphate buffer in the pH range 2.0 to 9.0. For isotope fractionation experiments of type (*a*), initial 4-Cl-aniline concentrations generally amounted to 80 μM to ensure substrate concentrations above the method quantification limits at 95% turnover. Control experiments for quantification of non-reactive losses and isotope fractionation of 4-Cl-aniline were set up identically but not irradiated. Concentration-dependent C and N isotope fractionation was studied with 50 to 300 μM of 4-Cl-aniline. The same setup was also used to check for the effects of buffer type (phosphate vs. formate), buffer concentration (10 vs. 25 mM), and Cl^- concentrations (up to 100 mM). Experiments with Cs^+ as a singlet quencher were carried out in 10 mM phosphate buffer containing 1 M CsCl at pH 7.0 and 9.0.

Quartz tubes were introduced in a DEMA 125 merry-go-round photoreactor (Hans Mangels GmbH, Bornheim-Roidorf, Germany) equipped with a low-pressure mercury (LP Hg) lamp (Heraeus Noblelight model TNN 15/32, nominal power 15

W) and a quartz cooling jacket[24]. A recirculating pure water bath kept reaction the temperature at 25.0 ± 0.2 ℃. Direct photolysis experiments were started by irradiation of monochromatic light at a wavelength of 254 nm and stopped by removing the quartz tubes from the light sources. This wavelength was selected for the following reasons. Both neutral and protonated 4-Cl-aniline absorb light efficiently at 254 nm so that the pH dependence of the reaction can be studied within experimental timeframes of a few hours. Under the selected experimental conditions, light absorption and reactions of other solution constituents such as polymeric reaction products can be avoided, which would otherwise preclude a rigorous interpretation of product formation. Finally, the mechanism of direct 4-Cl-aniline photolysis does not change at higher irradiation wavelengths. Between 9 and 12 samples consisting of the entire volume of a 20 mL quartz tube were collected at different time points depending on the decay kinetics of 4-Cl-aniline until fractional conversion exceeded 95%. Samples were split for measurement of substrate concentrations, C and N isotope ratios, identification of reaction products, and UV-vis absorbance.

Experiments of type (*b*) with C_0 from 5 to 300 μM at pH 7.0 and (*c*), with C_0 of 5 μM and pH from 2.0 to 9.0, were carried out identically except for the sampling strategy. In this case, 500 μL of aqueous sample was withdrawn from two, simultaneously irradiated quartz tubes at predefined time points for concentration measurements only. Experiments of type (*b*) were all performed within a single day in presence and absence of a wire cloth to access the kinetics of fast reactions. The photon fluence rate employed to determine photolysis quantum yields and to compare photolysis rate constants, was measured by chemical actinometry using an aqueous atrazine solution[24].

Time-resolved fluorescence lifetimes (τ_{F}) measurements of experiments (*d*) in presence of NaCl and CsCl were carried out with a time-correlated single-photon counting (TCSPC) system (HALCYONE; Ultrafast Systems). A Solstice amplified Ti:Sapphire ultrafast laser (795 nm, 3.2 W, FWHM $\sim$ 80 fs; Newport Spectra-Physics) was used. The excitation wavelength of 280 nm was generated by a Topas optical parametric amplifier (Light Conversion, Vilnius, Lithuania) and directed to a 100 μM 4-Cl-aniline aqueous solution. The fluorescence emission was collected by an achromatic doublet lens and directed through a double monochromator onto an avalanche photodiode detector. The fluorescence wavelength monitored was 356 nm. For each decay profile, TCSPC data was collected until 1500-2000 photon counts at the peak emission time were obtained. The rate of data collection was kept near 5% of the maximum possible counts per second to avoid pile-up artifacts.

2.2.3 Data evaluation

Isotope fractionation

For interpretation of experiments of type (*a*), we calculated C and N isotope enrichment factors, ϵ_{C} and ϵ_{N}, from linear regression analysis of δ^{13}C- and δ^{15}N-values, respectively, vs. the fractional amount of reactant conversion, which is quantified from the remaining reactant concentration (C/C_0, eq. 2.1). The corresponding apparent ^{13}C- and ^{15}N-kinetic isotope effects (AKIEs) were obtained from eq. 2.2 based on the assumption that secondary isotope effects are negligible and that isotope ratios change only at reactive atoms and are invariant at nonreactive ones. Therefore, n, in eq. 2.2 equals 6 for derivation of ^{13}C-AKIEs and 1 for ^{15}N-AKIEs. Isotope fractionation measured in replicate experiments was reconciled as using the Pitman estimator[129].

$$ln\left(\frac{\delta^{\mathrm{h}}\mathrm{E}+1}{\delta^{\mathrm{h}}\mathrm{E}_0+1}\right) = \epsilon_{\mathrm{E}} \cdot ln\left(\frac{C}{C_0}\right) \tag{2.1}$$

$$\mathrm{AKIE}_{\mathrm{E}} = \frac{1}{1+n\cdot\epsilon_{\mathrm{E}}} \tag{2.2}$$

where $^{\mathrm{h}}\mathrm{E}_0$ and $^{\mathrm{h}}\mathrm{E}$ stand for the initial isotope signatures of an element (E) as well as for those at different stages of the reaction, respectively. All uncertainties associated with ϵ- and AKIE-values are given as 95 % confidence intervals.

Contributions of 4-Cl-aniline deprotonation to C and N isotope fractionation in photochemical experiments where calculated with eqs. 2.3 to 2.4. Equilibrium isotope effects associated with the deprotonation of 4-Cl-aniline's conjugate acid (BH^+), $\mathrm{EIE}_{\mathrm{E}}^{\mathrm{BH}^+}$, were taken from Skarpeli-Liati et al.[134] and $\mathrm{AKIE}_{\mathrm{E}}^{\mathrm{B}}$ denote AKIEs for photolysis of the neutral 4-Cl-aniline species. Using the apparent pK-value, $\mathrm{p}K^{\star}_{\mathrm{BH}^+}$, which specifies the pH-value, at which neutral and protonated 4-Cl-aniline species contribute equally to the the *rate* of photolysis (see below), we calculated the corresponding apparent fraction of protonated 4-Cl-aniline base, $\alpha^{\star}_{\mathrm{BH^+}}$ (eq. 2.4).

$$\epsilon_{\mathrm{E}} = \frac{1}{\alpha^{\star}_{\mathrm{BH^+}} \cdot \mathrm{EIE}_{\mathrm{E}}^{\mathrm{BH^+}} \cdot \mathrm{AKIE}_{\mathrm{E}}^{\mathrm{B}} + \left(1 - \alpha^{\star}_{\mathrm{BH^+}}\right) \mathrm{AKIE}_{\mathrm{E}}^{\mathrm{B}}} - 1 \tag{2.3}$$

$$\alpha^{\star}_{\mathrm{BH^+}} = \frac{1}{1 + 10^{\mathrm{pH} - \mathrm{p}K^{\star}_{\mathrm{BH^+}}}} \tag{2.4}$$

Rates of 4-Cl-aniline disappearance

All rate constants shown in this work were corrected for a constant photon fluence rate of $(7.3 \pm 0.7) \cdot 10^{-5}$ einstein m^{-2} s^{-1} using atrazine as chemical actinometer (see SI section S2.2 for details). We evaluated the reaction kinetics of 4-Cl-aniline disappearance from experiments of type (*b*, variable initial concentration) based on a simplified kinetic model shown below. 4-Cl-aniline could thus be transformed photochemically (compound **1** in eq. 2.5) as well as through the oxidation by a photolysis intermediate to different products (P_1, P_2). According to Othmen et al.[98], the reactive intermediate is assumed to be a 4-iminoquinone O-oxide (compound **7** in eq. 2.6). Numbers in bold face in eqs. 2.5-2.7 refer to the reaction scheme presented in detail in the discussion section.

$$\mathbf{1} \xrightarrow{k_1} \mathbf{7} \tag{2.5}$$

$$\mathbf{1} + \mathbf{7} \xrightarrow{k_2} \mathrm{P}_1 \tag{2.6}$$

$$\mathbf{7} \xrightarrow{k_3} \mathrm{P}_2 \tag{2.7}$$

where k_1 is reaction rate constant for 4-Cl-aniline photolysis, k_2 is the bimolecular rate constant for the oxidation of 4-Cl-aniline by **7**. k_3 in eq. 2.7 stands for the lumped reaction rate constants for all reactions of the **7** that do not involve 4-Cl-aniline[98]. We obtained a rate expression for the disappearance of 4-Cl-aniline (eq.

2.9) making a steady-state approximation for **7** (eq. 2.8).

$$[\mathbf{7}]_{ss} = \frac{k_1[\mathbf{1}]}{k_2[\mathbf{1}] + k_3} \tag{2.8}$$

$$-\frac{d[\mathbf{1}]}{dt} = k_1[\mathbf{1}] + k_2[\mathbf{1}][\mathbf{7}]_{ss} \tag{2.9}$$

$$= k_1[\mathbf{1}]\frac{2k_2[\mathbf{1}] + k_3}{k_2[\mathbf{1}] + k_3} \tag{2.10}$$

The analytical solution to eq. 2.10 was obtained from a rearranged form of eq. 2.10 shown in eq. 2.11. Integration of eq. 2.11 between time intervals 0 and t with initial concentration $[\mathbf{1}]_0$ leads to eq. 2.12. The latter was solved for k_1 and the ratio k_2/k_3 by nonlinear regression of time t vs. measured 4-Cl-aniline concentrations. Data were corrected with a light attenuation factor at 254 nm, S_{254}, that accounted for the light absorption by dissolved species and the geometry of the reactors.[156] A fixed standard deviation of $\Delta\ t = \pm 5$ sec was assumed as uncertainty for solving eq. 2.12 using Igor Pro software (Wavemetrics Inc.).

$$\frac{k_2}{k_1 k_3} \cdot \frac{d[\mathbf{1}]}{2\frac{k_2}{k_3}[\mathbf{1}] + 1} - \frac{1}{k_1}\frac{d[\mathbf{1}]}{[\mathbf{1}]} = dt \tag{2.11}$$

$$\frac{1}{2k_1} ln \left(\frac{2\frac{k_2}{k_3}[\mathbf{1}] + 1}{2\frac{k_2}{k_3}[\mathbf{1}]_0 + 1} \right) + \frac{1}{k_1} ln \left(\frac{[\mathbf{1}]_0}{[\mathbf{1}]} \right) = t \tag{2.12}$$

In addition to the above kinetic model (eqs. 2.5-2.7), we quantified the pseudo-first order disappearance rate constant of 4-Cl-aniline at initial states of the reaction taking into account data points up to 50% substrate transformation ($k_{obs}^{initial}$) as well as for later stages of the reaction ($k_{obs}^{C/C_0 \leq 50\%}$).

Experiments of type (c) were evaluated according to procedures described by Canonica et al.[24] to derive the pH-value, at which neutral and protonated 4-Cl-aniline species contribute equally to the photolysis rate given the irradiation wavelength of 254 nm. This pH value was later used as apparent pK-value, p$K^{\star}_{BH^+}$, to assess and evaluate pH-dependent isotope fractionation. Briefly, photon fluence-based rate constants, $k^{\mathrm{app}}_{\mathrm{E}^0_P}$, were calculated from pseudo-first order disappearance rate constants at a given solution pH and the photon fluence rates, E^0_P (einstein m^{-2} s^{-1}) at 254 nm derived by chemical actinometry. The rate constants of neutral and protonated 4-Cl-aniline species, $k^{\mathrm{B}}_{\mathrm{E}^0_P}$ and $k^{\mathrm{BH}^+}_{\mathrm{E}^0_P}$, were obtained from linear regression of eq. 2.13 where α_{BH^+} follows from eq. 2.4 and is the fraction of protonated 4-Cl-aniline with $\mathrm{p}K_{\mathrm{BH}^+}$ of 4.0[126]. $\mathrm{p}K^{\star}_{\mathrm{BH}^+}$ (eq.2.15) follows from the assumption that neutral and protonated species contribute equally to the disappearance of the substrate (eq. 2.14).

$$k^{\mathrm{app}}_{\mathrm{E}^0_P} = k^{\mathrm{B}}_{\mathrm{E}^0_P} + \left(k^{\mathrm{BH}^+}_{\mathrm{E}^0_P} - k^{\mathrm{B}}_{\mathrm{E}^0_P}\right) \cdot \alpha_{\mathrm{BH}^+} \tag{2.13}$$

$$\alpha_{\mathrm{BH}^+} \cdot k^{\mathrm{BH}^+}_{\mathrm{E}^0_P} = \left(1 - \alpha_{\mathrm{BH}^+}\right) \cdot k^{\mathrm{B}}_{\mathrm{E}^0_P} \tag{2.14}$$

$$\mathrm{p}K^{\star}_{\mathrm{BH}^+} = \mathrm{p}K_{\mathrm{BH}^+} + log\left(\frac{k^{\mathrm{BH}^+}_{\mathrm{E}^0_P}}{k^{\mathrm{B}}_{\mathrm{E}^0_P}}\right) \tag{2.15}$$

2.3 Results and Discussion

2.3.1 Direct Photolysis of 4-Chloroaniline

The direct photolysis of 4-Cl-aniline in solutions (80 μM) buffered at pH 7.0 led to complete transformation within less than 20 minutes and was accompanied by moderate normal C and N isotope fractionation of equal magnitude (Figures 2.1a-b). Bulk C and N isotope enrichment factors, ϵ_C and ϵ_N, were identical and amounted to -1.2 ± 0.2‰ (Table 2.1, entry 9). Product analyses revealed the formation of coupling products including dimers, trimers, and tetramers of partially dechlorinated 4-Cl-aniline as documented in the Supporting Information in Figures S2.2-S2.5.

As illustrated in Figure 2.2, direct photolysis of 4-Cl-aniline has previously been shown to lead to the heterolytic dechlorination of excited state species of 4-Cl-aniline (compound **2** in Figure 2.2) generating a reactive carbene intermediate (**3**, 4-iminocyclohexa-2,5-dienylidene)[45,48,53,98]. The carbene (**3**) can subsequently react to stable products along four different pathways, namely through (i) coupling with another equivalent of the substrate, (ii) addition of molecular O_2 followed by substrate addition, (iii) H atom abstraction, and (iv) addition of H_2O[98]. According to the published rate constants for the reaction of **3**,[98] pathway (ii) should be largely dominant (86% at 80 μM 4-Cl-aniline, see SI section S2.2) in aerated solution (270 μM of O_2), making the 4-iminoquinone O-oxide (**7**) a central intermediate. The latter was shown to react fast with 4-Cl-aniline (5×10^8 M^{-1} s^{-1}), but other reactions of **7** were not characterized. In our experiments, we exclusively observed coupling products suggesting a predominant reaction of 4-Cl-aniline via pathways (i) and (ii). In fact, many of the coupling products detected at high peak intensities such as 4-hydroxy-4'-chlorodiphenylamine (Figure S2.3) contained Cl and O atoms[47]. The relative abundance of oxygenated coupling products increased with increasing solution pH value of the buffer solution (see discussion of pH-dependence below), and could thus imply reaction of hydroxide at imine functional groups[28,121,131]. Neither aniline (**9**) nor 4-aminophenol (**10**) were found, which, according to Figure 2.2, would be indicative of pathways (iii) and (iv). Our observations imply that 4-Cl-aniline did not only react through dechlorination by direct photolysis but also through oxidation of 4-Cl-aniline by intermediate **7** and, to a minor extent, by intermediate **3**.

2.3.2 Photochemical vs. oxidative reaction of 4-Cl-aniline and origin of isotope fractionation

The pathways of 4-Cl-aniline transformation at pH 7.0 were evaluated based on a kinetic analysis of experiments performed with different initial substrate concentrations ranging from 5 to 300 μM (see detailed discussion in Section S2.2 of the Supporting Information). All data were fit successfully to eq. 2.12 as shown in Figures S2.1a-e. Disappearance kinetics of 4-Cl-aniline were slightly biphasic, that is a faster initial transformation to approximately 50% turnover was followed by a slower removal of the substrate from solution. A compilation of the rate constants of photochemical removal of 4-Cl-aniline, k_1, pseudo-first order reaction rate constants for initial disappearance, $k_{\text{obs}}^{\text{initial}}$, and at more than 50% turnover, $k_{\text{obs}}^{C/C_0 \leq 50\%}$, are shown in Table S2.1 and compared in Figure 2.3a. k_1-values were identical within uncertainty to $k_{\text{obs}}^{C/C_0 \leq 50\%}$. Rate constants of initial 4-Cl-aniline transformation, $k_{\text{obs}}^{\text{initial}}$, in contrast, were twice as large as k_1 and $k_{\text{obs}}^{C/C_0 \leq 50\%}$. The ratios $k_{\text{obs}}^{\text{initial}}/k_{\text{obs}}^{C/C_0 \leq 50\%}$ indeed ranged from 1.9 ± 0.3 to 2.2 ± 0.3, except for C_0 of 300 μM, where the uncertainty was large (Figure 2.3a, Table S2.1). This observation implies that at initial stages of the reaction, two substrate molecules are removed per photochemically transformed 4-Cl-aniline, which corresponds to the stoichiometric upper limit for contribution of 4-Cl-aniline oxidation by **7** as suggested in Figure 2.2, pathway (ii). This interpretation is also supported by data for the k_2/k_3-ratios (Table S2.1), which hint at an efficient removal of **7** through reaction with the substrate. As soon as approximately 50% of the substrate are removed, however, k_1 corresponds to $k_{\text{obs}}^{C/C_0 \leq 50\%}$, suggesting that 4-Cl-aniline is transformed primarily through direct photolysis.

We also assessed the contribution of 4-Cl-aniline photolysis vs. its oxidation by iminoquinone intermediates from C and N isotope fractionation. Due to the analytical constraints of stable isotope analysis (see above), the lowest initial substrate concentrations accessible for C and N isotope fractionation measurements were 50 and 80 μM, respectively. The C and N isotope enrichment factors, ϵ_{C} and

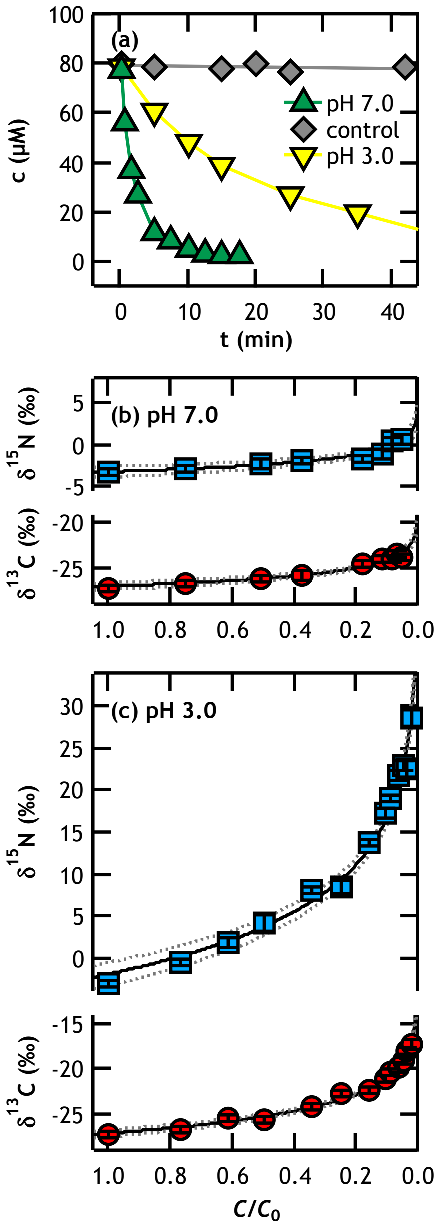

Figure 2.1 (a) 4-Cl-aniline concentration in photochemical experiments at pH 3.0 and 7.0 as well as non-irradiated controls at pH 7.0; C and N isotope signatures (δ^{13}C (circles) and δ^{15}N (squares) of 4-Cl-aniline vs. remaining substrate fraction, C/C_0 at solution pH of 7.0 (panel b) and pH 3.0 (panel c). Uncertainties represent standard deviations of triplicate measurements. Solid lines correspond to calculated isotope fractionation using eq. 2.1; gray dashed-lines indicate 95% confidence interval of the fit. Control experiments did not show C and N isotope fractionation (data not shown).

Table 2.1 C and N isotope enrichment factors (ϵ_C, ϵ_N), apparent ^{13}C-, ^{15}N-kinetic isotope effects (^{13}C-, and ^{15}N-AKIE) and the slope of the nitrogen vs. carbon isotope fractionation ($\Delta\delta^{15}N/\Delta\delta^{13}C$). [a,b]

Entry	pH	ϵ_C (‰)	ϵ_N (‰)	^{13}C-AKIE [c] (-)	^{15}N-AKIE (-)	$\Delta\delta^{15}N/\Delta\delta^{13}C$ (-)
1	2.0	-2.0 ± 0.2	-3.8 ± 0.5	1.0123 ± 0.0012	1.0038 ± 0.0005	1.9 ± 0.3
2	2.0 [d]	n.d. [e]	-4.0 ± 0.3	n.d.	1.0040 ± 0.0003	n.d.
3	2.0 [f]	-2.1 ± 0.2	-2.8 ± 0.2	1.0126 ± 0.0010	1.0028 ± 0.0002	1.4 ± 0.3
4	2.0 [g]	-1.9 ± 0.3	-2.4 ± 0.5	1.0114 ± 0.0016	1.0025 ± 0.0005	1.3 ± 0.3
5	3.0	-2.7 ± 0.2	-8.1 ± 0.6	1.0167 ± 0.0011	1.0081 ± 0.0006	3.0 ± 0.3
6	3.0 [d]	n.d.	-9.1 ± 1.6	n.d.	1.0092 ± 0.0016	n.d.
7	4.0	-2.3 ± 0.1	-5.2 ± 0.6	1.0141 ± 0.0006	1.0052 ± 0.0006	2.3 ± 0.2
8	5.0	-1.5 ± 0.2	-0.6 ± 0.2	1.0090 ± 0.0015	1.0006 ± 0.0002	0.4 ± 0.1
9	7.0	-1.2 ± 0.2	-1.2 ± 0.2	1.0073 ± 0.0012	1.0012 ± 0.0002	0.9 ± 0.3
10	7.0 [h]	-1.8 ± 0.3	-2.3 ± 0.3	1.0109 ± 0.0020	1.0023 ± 0.0003	1.2 ± 0.3
11	9.0	-0.8 ± 0.2	-2.2 ± 0.3	1.0046 ± 0.0012	1.0022 ± 0.0003	2.6 ± 0.7
12	9.0 [h]	-2.3 ± 0.4	-2.6 ± 0.5	1.0142 ± 0.0025	1.0026 ± 0.0005	1.1 ± 0.4

[a] All experiments were carried out at 80 μM initial concentration in 10 mM phosphate buffer adjusted to the given pH unless stated otherwise; [b] all uncertainties correspond to 95% confidence intervals; [c] calculated from eq. 2.2; [d] formate buffer 10 mM; [e] n.d. = not determined; [f] phosphate buffer 25 mM; [g] phosphate buffer 25 mM, 100 mM NaCl; [h] 1 M CsCl

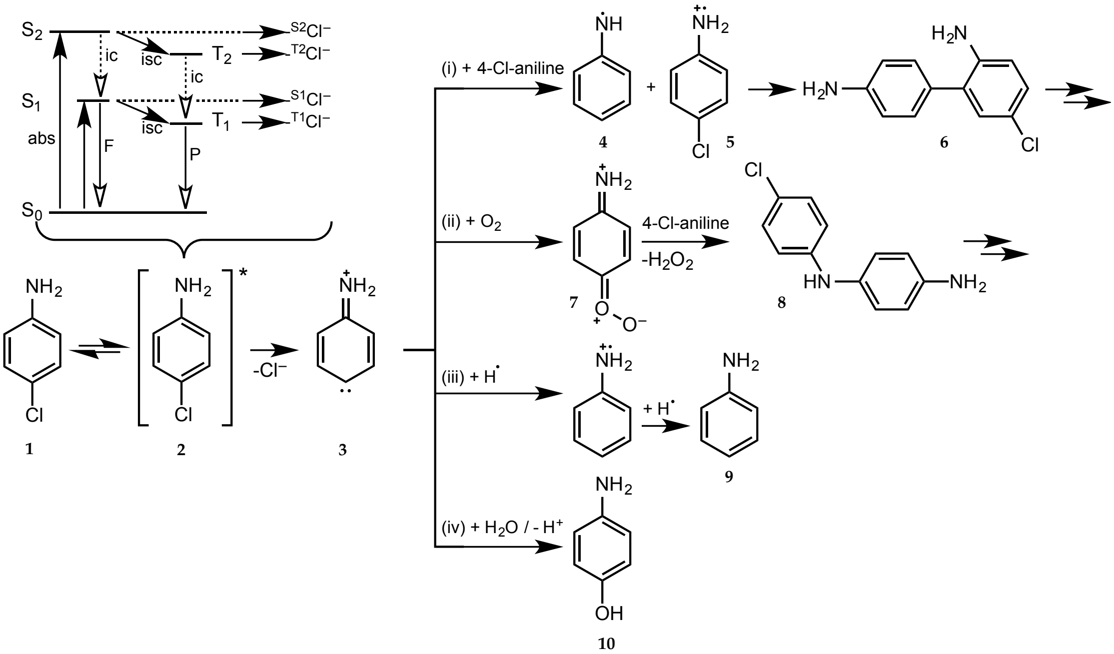

Figure 2.2 Pathways of direct photolysis of 4-Cl-aniline (**1**): excited species **2** populate singlet states (S_1, S_2) after light absorption (abs) from which they are converted to the ground state (S_0) through internal conversion (ic), fluoresence (F), and intersystem-crossing (isc) to triplet states (T_1, T_2, etc., two excited states are shown for illustration). P stands for phosphorescence. Both S_i and T_i states can dechlorinate ($-^{S_i}\mathrm{Cl}^-$, $-^{T_i}\mathrm{Cl}^-$) to a protonated carbene, **3**, 4-iminocyclohexa-2,5-dienylidene. Compound **3** can react along four reaction pathways, leading to reactive 4-iminoquinone O-oxides (**7**) and coupling products. Compounds **6** and **8** are examples for a variety of structures found by LC/HRMS as documented in the SI, aniline (**9**), and 4-aminophenol (**10**) as described in the text.

ϵ_N are shown in Figure 2.3b. Regardless of C_0, we found ϵ_C-values to be confined to a narrow range between −1.2‰ to −1.6‰. C isotope enrichment therefore does not reveal any change of reaction mechanisms associated with different shares of photochemical vs. oxidative 4-Cl-aniline transformation.

The ϵ_N-values, on the other hand, increased from -1.2 ± 0.2‰ to $+1.0 \pm 0.3$‰, that is N isotope fractionation changed from normal at lower C_0 to inverse at the highest C_0 of 270 μM. The inverse ϵ_N-value of $+1.0 \pm 0.3$‰ is identical within uncertainty of our previous data for the N atom oxidation of 4-Cl-aniline by MnO_2 at pH 7.0 ($+1.3 \pm 0.2$‰)[134]. Based on the currently available evidence,[89,134,135] it

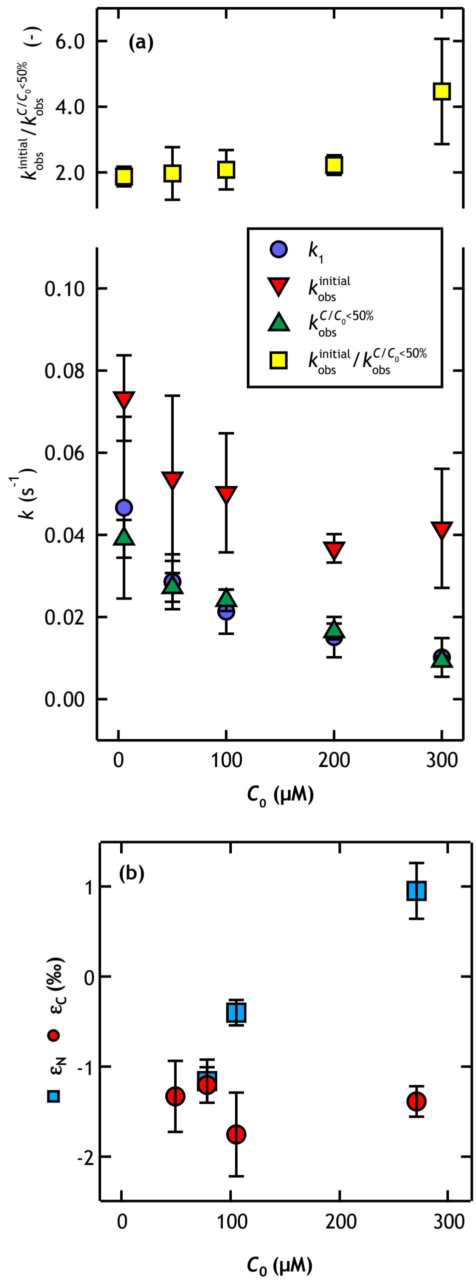

Figure 2.3 (a) Comparison of reaction rate constants from experiments with different initial 4-Cl-aniline concentrations. k_1 was obtained from fitting eq. 2.12, $k_{\rm obs}^{\rm initial}$ and $k_{\rm obs}^{C/C_0 \leq 50\%}$ follow from linear regressions of a subset of the kinetic data as described in the SI section S2.2; (b) C and N isotope enrichment factors, $\epsilon_{\rm C}$ and $\epsilon_{\rm N}$, for 4-Cl-aniline photolysis at pH 7.0 for various initial substrate concentrations. Uncertainties represent 95% confidence intervals.

is unknown if and to what extent, ϵ_N-values for N atom oxidation of 4-Cl-aniline depend on the oxidant used and whether our numbers can be compared directly. Our ϵ_N-data for photochemical experiments at high initial substrate concentrations nevertheless suggest that chemical oxidation of 4-Cl-aniline by **7** can contribute to the observable N isotope fractionation given that not more than 50% of 4-Cl-aniline react via this pathway. A more detailed elucidation of the reaction mechanisms at high initial substrate concentrations is beyond the scope of our work. The significance of the chemical oxidation pathway for N isotope fractionation in photochemical experiments, however, appears much smaller at lower initial substrate concentrations.

At C_0 of 100 μM, ϵ_N is normal and the trend to normal N isotope fractionation is even stronger at C_0 of 80 μM. The kinetic analysis discussed above implied that the disappearance of 4-Cl-aniline after 50% conversion is only due to photolysis. In fact, δ^{15}N-trends in Figure 2.1b for C_0 of 80 μM do not show any inverse N isotope fractionation at initial states of the reaction (i.e., $C/C_0 \geq 0.5$) that would point to an impact of N atom oxidation reactions. Isotope fractionation associated with the disappearance of 4-Cl-anilne was constant over time and with increasing fractional conversion as implied by eq. 2.1. This behavior is typical for transformations according to one mechanism or a constant combination of different mechanisms throughout the entire reaction. Moreover, quantifications of isotope fractionation as ϵ-values are determined by data points obtained at increasing fractional conversion, that is $C/C_0 \ll 0.5$[86]. Based on this reasoning, we conclude that isotope fractionation arising at $C/C_0 \leq 0.5$ can be apportioned to photochemical transformation without notable contributions from the oxidation of 4-Cl-aniline by **7**.

2.3.3 pH-Dependence

To explore the origins of C and N isotope fractionation, photolysis experiments were conducted over a pH range from 2.0 to 9.0. Fluence-based reaction rate constants increased with pH as shown in Tables S2.2 and S2.3. Note that the molar absorption coefficient of the protonated 4-Cl-aniline species at the irradiation wavelength λ of 254 nm, $\varepsilon_{254}^{\mathrm{BH}^+}$, is only 16 ± 9 m^2 mol^{-1} and thus much smaller than that of the neutral compound ($\varepsilon^{\mathrm{B}}_{254} = 311 \pm 15$ m^2 mol^{-1}) while the quantum yield is roughly pH-independent. Therefore, the pH-value, at which both species contribute equally to the disappearance of 4-Cl-aniline given our experimental conditions (2.65 ± 0.10, eq. 2.15) is below the p$K_{\mathrm{BH^+}}$ of 4-Cl-aniline's conjugate acid (4.0). C and N isotope fractionation was also strongly pH-dependent as illustrated from the comparison of data from experiments performed at pH 7.0 vs. pH 3.0 in Figures 2.1b/c, as well as from the compilation of C and N isotope enrichment factors in Figure 2.4. ϵ_{C}- and ϵ_{N}-values vary between -0.8 ± 0.2‰ and -2.7 ± 0.2‰ as well as -0.6 ± 0.2‰ and -8.1 ± 0.6‰, respectively (Table 2.1).

C and N isotope fractionation was larger under acidic conditions (2.0 to 4.0) and peaked at pH 3.0. ϵ_{C}-values decreased monotonicly towards pH 9.0 (Figure 2.4b), whereas no such trend was observed for ϵ_{N} (Figure 2.4a). The pH-dependence of ϵ_{C} and ϵ_{N}, however, is inconsistent with what would be expected if C and N isotope fractionation arose from the combination of (i) a deprotonation of the 4-Cl-anilinium cation at pH < 2.65 in the ground state and (ii) subsequent transformation (i.e., dechlorination) of excited species. As shown by Skarpeli-Liati et al.[133,134], C and N isotope fractionation associated with H$^+$-exchange at the amino group can indeed lead to more negative ϵ_{N}- and slightly more positive ϵ_{C}-values as indicated by the solid lines in Figure 2.4. If H$^+$-exchange at the N-atom was solely responsible for the pH dependence, however, bulk enrichment factors would approach a constant level of C and N isotope fractionation at pH-values that differed from the p$K^{\star}_{\mathrm{BH^+}}$ by ± 2 units. This expectation cannot be reconciled with the the fact that ϵ_{C}- and ϵ_{N}-values are less negative at pH 2.0 compared to pH 3.0 as well with the variation of isotope enrichment factors above pH 5.0. Even though C and N isotope fractionation due to ground state deprotonation EIEs does occur, experimental data clearly disagree with the modeled scenario. It is thus questionable whether H$^+$-exchange processes are responsible for the bell-shaped pH-dependence even if one takes into account that the acidity of excited state species can deviate from its ground state analogs by several pK_a units[74,105,144,149].

The coupling products of 4-Cl aniline photolysis detected at pH 5.0 and 9.0 were identical to those found at pH 7.0. A noticeable increase of relative peak intensity with increasing pH was found only for the hydroxylated chlorodiphenylamine (Figure S2.3). Below pH 5.0, no evidence for reaction products was found

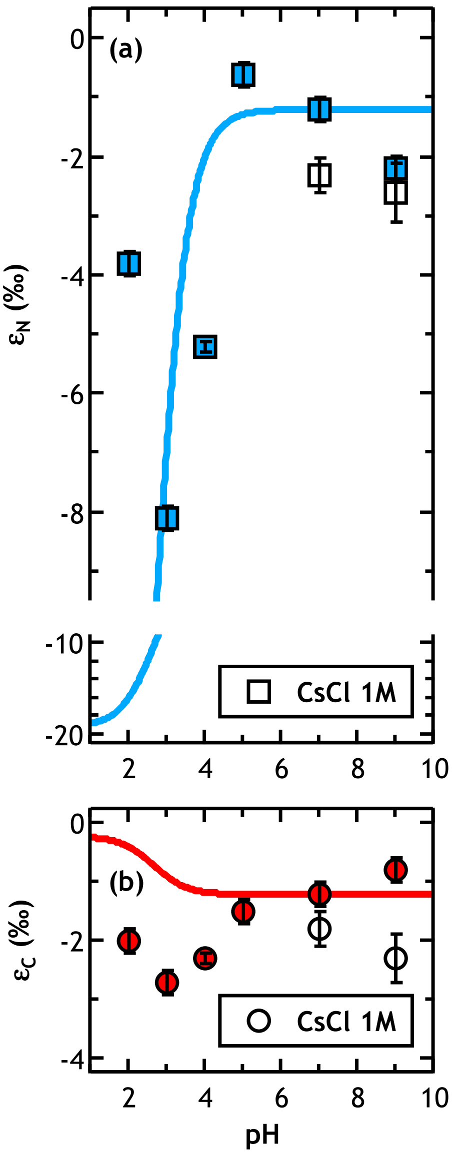

Figure 2.4 ϵ_{N} and ϵ_{C}-values associated with the direct photolysis of 4-Cl-aniline at solution pH-values between 2.0 and 9.0. The blue and red line represent ϵ-values that were calculated with eq. 2.3 under the assumption that ground-state deprotonation contributed to C and N isotope fractionation. Bright blue and yellow markers stand for experiments performed in presence of 1 M CsCl used as singlet quencher. Uncertainties represent 95% confidence intervals.

with the applied LC/HRMS procedure in agreement with less likely coupling reaction among protonated 4-Cl-aniline and the reactive intermediate **7**[98] and/or a different reaction mechanism at low pH-values. UV/Vis spectra recorded for λ of 200-400 nm during the experiments (Figure S2.6) revealed increasing light absorption of the solutions with reaction progress. We attribute this result to the formation of coloured coupling products during the reaction. A comparison of light absorption at exhaustive irradiation of 4-Cl-aniline over the entire pH range (up to 2.3 hours) suggest that the extent of coupling product formation is smaller at lower pH. This observation corroborates the findings made with high-resolution mass spectrometry.

2.3.4 Photophysical processes

We probed for potential contributions of photophysical processes to the observed isotope fractionation with photolysis experiments that were carried out in presence of CsCl. Cs^+ was used as singlet quencher to decrease the lifetime of excited singlet states via increased intersystem-crossing and thus increased excited triplet state formation[118]. Addition of 1 M of Cs^+ decreased the fluorescence lifetimes, τ_F, from 0.464 ± 0.004 to 0.292 ± 0.003 nanoseconds while addition of the same amount of Na^+ exerted a much smaller effect (Table S2.4). As shown in Figure 2.5a, normalized τ_F decreased by a factor of 1.6 due to the presence of 1 M Cs^+ whereas this ratio is only 1.1 in solutions containing 1 M Na^+.

The consequences of the presence of 1 M of Cs^+ for ϵ_C- and ϵ_N-values measured at pH 7.0 and 9.0 are shown in Figures 2.4, parts a and b and the corresponding data is shown in Table 2.1 (entries 9 to 12). ϵ_C-values were up to 1.5‰ more negative than in the absence of Cs^+ whereas a change of ϵ_N was found primarily at pH 7.0. We compared this shift of isotope fractionation behavior to effects of buffer concentration (10 mM vs. 25 mM), buffer type (phosphate vs. formate), and NaCl content at pH 2.0 and 3.0 (entries 1-6 in Table 2.1). These experimental parameters caused only minor changes of N isotope fractionation compared to experiments carried out in the standard setup. Because C isotope fractionation and the correlated C and N isotope fractionation, $\Delta\delta^{15}N/\Delta\delta^{13}C$, were identical within experimental uncertainty, we consider the impact of these experimental

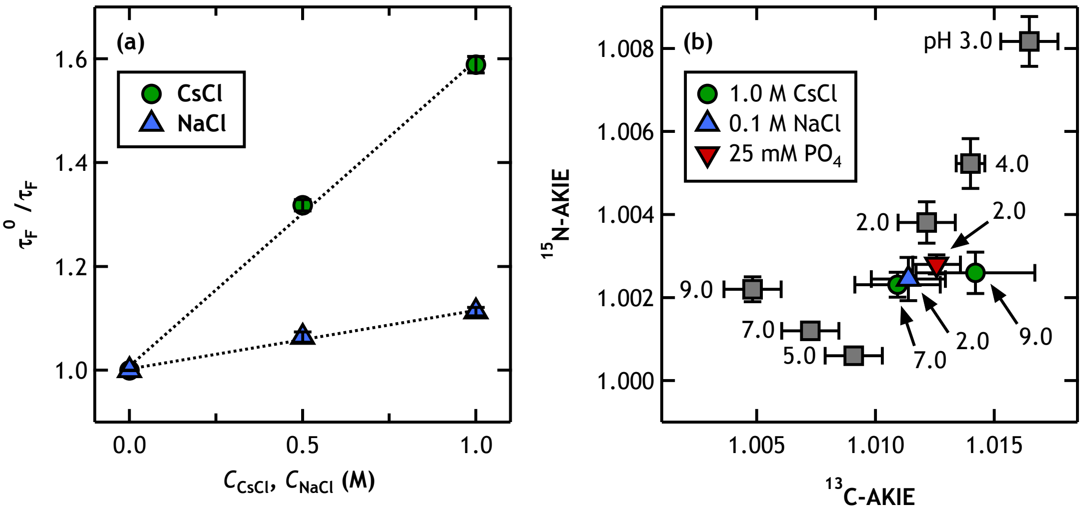

Figure 2.5 Panel (a): Fluorescence lifetimes of excited 4-Cl-aniline singlet species, τ_F, in presence of different CsCl and NaCl concentrations at pH 7.0. τ_F^0 denotes the lifetimes in absence of Cs^+ and Na^+, respectively, and was 0.464 ± 0.004 nanoseconds; panel (b): Correlation of ^{13}C- and ^{15}N-AKIEs measured at different pH values (labels). Data from Table 2.1. Uncertainties correspond to 95% confidence intervals.

factors as insignificant compared to addition of Cs^+ as singlet quencher. The above observations illustrate that C and N isotope fractionation is susceptible to the population of excited states from which 4-Cl-aniline is dechlorinated and that heterolytic dechlorination (**2** $\rightarrow$ **3** in Figure 2.2) is indeed a source of isotope fractionation. While we cannot quantify the relative shares of dechlorination from excited singlet vs. triplet states, our data implies that reactions via excited triplet states (e.g., in the presence of 1 M Cs^+) are more likely responsible for C and N isotope fractionation or lead to larger isotope fractionation. Excited triplet states of 4-Cl-aniline have indeed been postulated to determine reactivity[45,53]. Dechlorination from singlet states, in contrast, are either less isotope sensitive and mask isotope fractionation from triplet state reactions or exhibit distinctly different isotope fractionation behavior.

2.3.5 Origin of isotope fractionation and kinetic isotope effects

The considerable variability of C and N isotope enrichment factors with solution pH and presence or absence of singlet quenchers points to a combination of isotope-sensitive reactions. We hypothesize that the heterolytic C–Cl bond cleavage in excited states is the primary source of photochemically induced isotope fractionation but it is challenging to assign "typical" ^{13}C- and ^{15}N-AKIEs to this process. The ^{13}C-AKIE-values found here are 2- to 5-fold smaller than for C–Cl bond cleavages associated with elimination and reduction reactions (approx. 1.03)[3,4,36,60,92,171]. The ^{15}N-AKIE, in contrast, coincides with secondary effects for aromatic N atoms such as in oxidation reactions of N-containing organic pollutants[62,103,162–164].

Figure 2.5b shows that the ^{13}C- and ^{15}N-AKIEs correlate nicely. Data for experiments performed at pH-values pH 5.0 to 9.0 as well as those for pH 2.0 to 5.0 including the ones at pH 7.0 and 9.0 with singlet quencher follow two distinctly different, linear trends. Linear correlations of AKIEs from different isotopic elements within a molecule, like correlations of isotope signatures (e.g., $\Delta\delta^{15}\mathrm{N}/\Delta\delta^{13}\mathrm{C}$) and ϵ-values for two elements, are robust evidence that transformation proceed via a common mechanism or a combination of mechanisms[35,86]. Therefore, we hypothesize that the two data regimes are indicative for 4-Cl-aniline transformation by different reaction mechanisms. The identity of these mechanisms is yet unknown but our data offers room for interesting speculations.

In the first regime (pH 5.0 to 9.0), a slight increase of ^{15}N-AKIE-values correlates with a similarly small decrease of ^{13}C-AKIEs (and vice versa). Such a trend rules out that an intrinsic KIE, e.g., for dechlorination, is masked because masking would result in decreasing KIEs of both elements. The second regime (pH 2.0 to 5.0 and experiments with singlet quencher) features a relationship, in which increasing ^{13}C- and ^{15}N-AKIE align linearly. It is interesting to note that AKIEs obtained at pH 7.0 and 9.0 are present in both regimes. This observation excludes 4-Cl-aniline speciation in the ground state and in excited states as source of different isotope fractionation. Rather, these two data points suggest that photophysical processes contribute to or even determine the isotope effect. ^{13}C- and

^{15}N-AKIE larger than 1.010 and 1.002, respectively, would point to reactions from excited triplet states because this regime includes the experiment carried out in the presence of Cs^+ as singlet quencher ($-^{T_i}Cl^-$ in Figure 2.2). Consequently, ^{13}C-AKIEs below 1.010 would stand for dechlorinations from singlet states ($-^{S_i}Cl^-$, Figure 2.2). Note that the postulated contribution of singlet state reactions contradicts previous studies made for photolysis of 4-Cl-aniline in water and organic solvents, which suggested that dechlorination occurred exclusively from excited triplet states[45,53]. Here, changes in solution pH not only affect N isotope fractionation through H^+ exchange equilibria but also determine the population of singlet and triplet excited states of 4-Cl-aniline and thus KIEs associated with the dechlorination reaction from different spin states. Triplet state dechlorinations exhibit much larger KIEs than dechlorinations from excited singlet states. The smaller ^{13}C- and ^{15}N-AKIEs for dechlorinations from the singlet states can, in part be due to their significantly shorter lifetimes[45]. The latter may have led to a partial masking of C and N isotope fractionation from C–Cl bond cleavage. In addition, the two different AKIE regimes in Figure 2.5b suggest that magnetic interactions determined the population of singlet vs. triplet states from which dechlorination occurred with different, excited-state-specific isotope effects.

2.4 Implications

Our study illustrates that isotope fractionation associated with the photolysis of organic compounds is difficult to rationalize based on bond cleavages only. Instead, the sensitivity of excited state populations and intersystem crossing to isotopic substitution shows that photochemical contaminant transformations give rise to potentially unique isotope fractionation trends that differ from thermal reactions. In fact, ^{15}N-AKIEs for enzyme- and mineral-catalyzed oxidation of substituted anilines are mostly inverse (i.e. < 1) due to the formation of transient imine bonds. ^{13}C-AKIE-values are close to unity[102,134,135] and thus substantially smaller than what is reported here for photolytic dechlorination. These differences in both C and N isotope fractionation can be exploited for the distinction of reaction pathways in situations were multiple degradation processes can take place[35,163]. In contrast to biological and abiotic reactions, however, we lack a quantitative understanding for the factors determining the magnitude of isotope effects. The substantial variability of C and N isotope enrichment currently precludes quantification of the extent of contaminant transformation based on the ϵ_{C}- and ϵ_{N}-values listed in Table 2.1. Given that the observed isotope effects were very sensitive to excited spin state populations, we also anticipate that our findings are difficult to extrapolate to other chlorinated anilines. Further insights of the isotope sensitivity of photophysical processes is required to assess photolytic processes of aquatic micropollutants with chloro-aniline substructures such as diclofenac[84] and diflubenzuron with CSIA.

Acknowledgement

This work was supported by the EU Initial Training Network CSI:Environment (Grant agreement no. 264’329).

Supporting Information to Chapter 2

S2.1 Chemicals

Chemicals and gases were purchased from various manufacturers and used without further treatment. A list of compound names, purities, and suppliers follows. 4-Chloroaniline (>98%), potassium phosphate monobasic (>99%), were purchased from Sigma-Aldrich (Buchs SG, Switzerland); hydrochloric acid (32%) and sodium hydroxide (98%), sodium chloride (>99%) were from Merck (Dietikon, Switzerland); methanol (for HPLC gradient) from Acros Organics (Geel, Belgium); All aqueous solutions were prepared in nanopure water (18.2 MΩ-cm, Barnstead NANOpure Diamond Water Purification System).

The carrier and reference gas for GC and GC/IRMS included helium (He, 99.999%), N_2 (99.9999%), CO_2 (99.999%), H_2 (99.999%), synthetic air (20 ± 1% O_2 in N_2, 99.9995%), O_2 (99.9995%) and, N_2 (99.9995%) from Carbagas (Rümlang, Switzerland). All aqueous solutions were prepared in nanopure water (18.2 MΩ-cm, Barnstead NANOpure Diamond Water Purification System).

S2.2 Rates of 4-Cl-aniline disappearance

S2.2.1 Kinetic model for 4-Cl-aniline transformation

A simplified reaction model derived from Figure 2.2 in the main paper was employed to fit the kinetic data for the phototransformation of 4-chloroaniline. In aerated solution (as for all experiments performed in this study), the reaction of the carbene 4-iminocyclohexa-2,5-dienylidene (**3**) with oxygen (reaction (ii) in Fig. 2.2) is the dominant pathway for the consumption of the carbene. The fraction of **3** reacting with O_2 depends on the concentration of 4-Cl-aniline (e.g., 94.4%, 85.6% and 67.2% for [4-Cl-aniline] = 5 μM, 80 μM and 300 μM, respectively). The reaction of **3** with 4-Cl-aniline represents a minor reaction pathway (e.g., 0.7%, 9.9% and 29.3% for [4-Cl-aniline] = 5 μM, 80 μM and 300 μM, respectively) and was neglected in the simplified model. Also neglected were the other reactions of **3**. No reductants (but transformation products) are present in solution, and the reaction of **3** with H_2O or OH^- has a maximum contribution of 5% to the total consumption of **3**. We thus focus our attention on the product of reaction (ii), assumed to be 4-iminoquinone O-oxide (**7**) by Othmen et al.[98], who determined its second-order rate constant for reaction with 4-Cl-Aniline to be 5×10^8 M^{-1} s^{-1}. This carbene-oxygen adduct should be the key intermediate of 4-Cl-aniline photolysis able to oxidize 4-Cl-aniline. Unfortunately, no other rate constants are available for **7**, but we assume that **7** undergoes other reactions, in addition to the one with 4-Cl-aniline, following pseudo-first-order kinetics to give further products. Thus the phototransformation kinetics of 4-Cl-aniline upon direct photolysis can be derived using the following simplified reaction scheme (eqs. S2.1-S2.3).

$$\mathbf{1} \xrightarrow{k_1} \mathbf{7} \tag{S2.1}$$

$$\mathbf{1} + \mathbf{7} \xrightarrow{k_2} \mathrm{P}_1 \tag{S2.2}$$

$$\mathbf{7} \xrightarrow{k_3} \mathrm{P}_2 \tag{S2.3}$$

where k_1 is a pseudo-first-order rate constant describing the formation of **7** upon photolysis of the substrate **1**, k_2 is the second-order rate constant for the reaction of **7** with the substrate (see the aforementioned literature value), and k_3 is a lumped pseudo-first-order rate constant describing all further transformation pathways of **7**. The rate expression for the disappearance of 4-Cl-aniline (**1**) follows from the steady-state approximation of **7** (eqs. 2.8-2.9 in the main paper) leading to the analytical solution in eq. 2.12.

$$\frac{1}{2k_1} ln \left(\frac{\frac{2k_2}{k_3}[\mathbf{1}] + 1}{\frac{2k_2}{k_3}[\mathbf{1}]_0 + 1} \right) + \frac{1}{k_1} ln \left(\frac{[\mathbf{1}]_0}{[\mathbf{1}]} \right) = t \tag{S2.4}$$

Eq. S2.4 was solved for k_1 and the ratio k_2/k_3 by nonlinear regression of measured 4-Cl-aniline concentrations vs. time t, weighted by a fixed standard deviation of $\Delta\ t = \pm 5$ sec, using Igor Pro software (Wavemetrics, Lake Oswego, OR). In addition to the above kinetic model (eqs. S2.1-S2.3), we quantified the pseudo-first order disappearance rate constant of 4-Cl-aniline at initial states of the reaction taking into account data point up to 50% substrate transformation ($k_{\text{obs}}^{\text{initial}}$) as well as for later stages of the reaction ($k_{\text{obs}}^{C/C_0 \leq 50\%}$).

The results of the modeling exercise for five experiments with initial 4-Cl-aniline concentrations, C_0, from 5 μM to 300 μM are shown in Figures 2.3 panel a (in the main paper) and S2.1 and as well as in Table S2.1. The following observations and conclusions can be made:

1. Equation S2.4 adequately describes the disappearance kinetics of 4-Cl-aniline for each of the initial concentrations chosen (Figure S2.1, panels a-e). All fitted parameters are shown in Table S2.1. Values for k_1 decrease with increasing initial concentration of 4-Cl-aniline from 0.047±0.022 to 0.010±0.005 s^{-1} despite correction for the distinctly different light attenuation factors of the five experiments. Some k_1-values overlap within their 95% confidence interval in agreement with the assumption that the rate constant of 4-Cl-aniline photolysis should be independent of C_0. However, the four-fold difference between k_1 at 5 μM and 300 μM implies that other factors can affect the photolysis of 4-Cl-aniline in a way that reaction rate constants depend on initial substrate concentrations. Such a reduction of k_1 with increasing C_0 of 4-Cl-aniline is expected to arise from a reduced formation of one of the excited state precursors of the carbene, or an enhanced deactivation of such excited states, leading to a reduced yield of carbene formation. Note that this explanation is speculative and requires experimental confirmation, which is beyond the scope of the present work.

2. The comparison of k_1 with $k_{\text{obs}}^{\text{initial}}$, $k_{\text{obs}}^{C/C_0 \leq 50\%}$, as well as the ratio of the latter two variables consistently show that photochemical transformation of 4-Cl-aniline and its oxidation by **7** are of equal importance at initial stages of the reaction.

   (i) The overall rate constant of initial 4-Cl-aniline removal, $k_{\text{obs}}^{\text{initial}}$, is twice as large as the rate constant for reaction at more than 50% of substrate removal ($k_{\text{obs}}^{C/C_0 \leq 50\%}$). It is interesting to note that the distinction between fast initial vs. slow subsequent 4-Cl-aniline transformation can be made at approximately 50% substrate turnover even though experiments were conducted at different C_0. We assume that the shift of reaction rates indicates a transition from 4-Cl-aniline transformation by direct photolysis and oxidation by **7** vs. transformation by direct photolysis only. Apparently, the contribution of **7** seems to become negligible at comparable substrate turnover despite different C_0. This finding is consistent with the hypothesis that **7** may efficiently react with phototransformation products of 4-Cl-aniline, which would reduce the importance of the first term on the left-hand side of eq. S2.4 during the course of the reaction.

(ii) $k_{\mathrm{obs}}^{C/C_0 \leq 50\%}$ equals k_1 suggesting that the these two rate constants reflect exclusively the photochemical reactivity.

(iii) The ratio of $k_{\mathrm{obs}}^{\mathrm{initial}}/k_{\mathrm{obs}}^{C/C_0 \leq 50\%}$ and $k_{\mathrm{obs}}^{\mathrm{initial}}/k_1$ equals 2 except in experiments with C_0 of 300 μM. The ratio of 2 implies that at initial stages of the reaction, two substrate molecules are removed per photochemically transformed 4-Cl-aniline, which is the stoichiometric upper limit for contribution of 4-Cl-aniline oxidation by **7**. This conclusion is supported by large k_2/k_3-ratios obtained from fitting our date to eq. S2.4. Note however, that this parameter can only be determined with large uncertainties. Large k_2/k_3-ratios mean that at initial stages of the transformation of 4-Cl-aniline, reaction of **7** with 4-Cl-aniline is more important than further transformation of **7** to (coupling) products.

3. For the interpretation of 4-Cl-aniline isotope fractionation, we assume that (i) the contribution of substrate oxidation by **7** gradually decreases as the reaction progresses and (ii) that after 50% of substrate conversion, 4-Cl-aniline is transformed exclusively through direct photolysis.

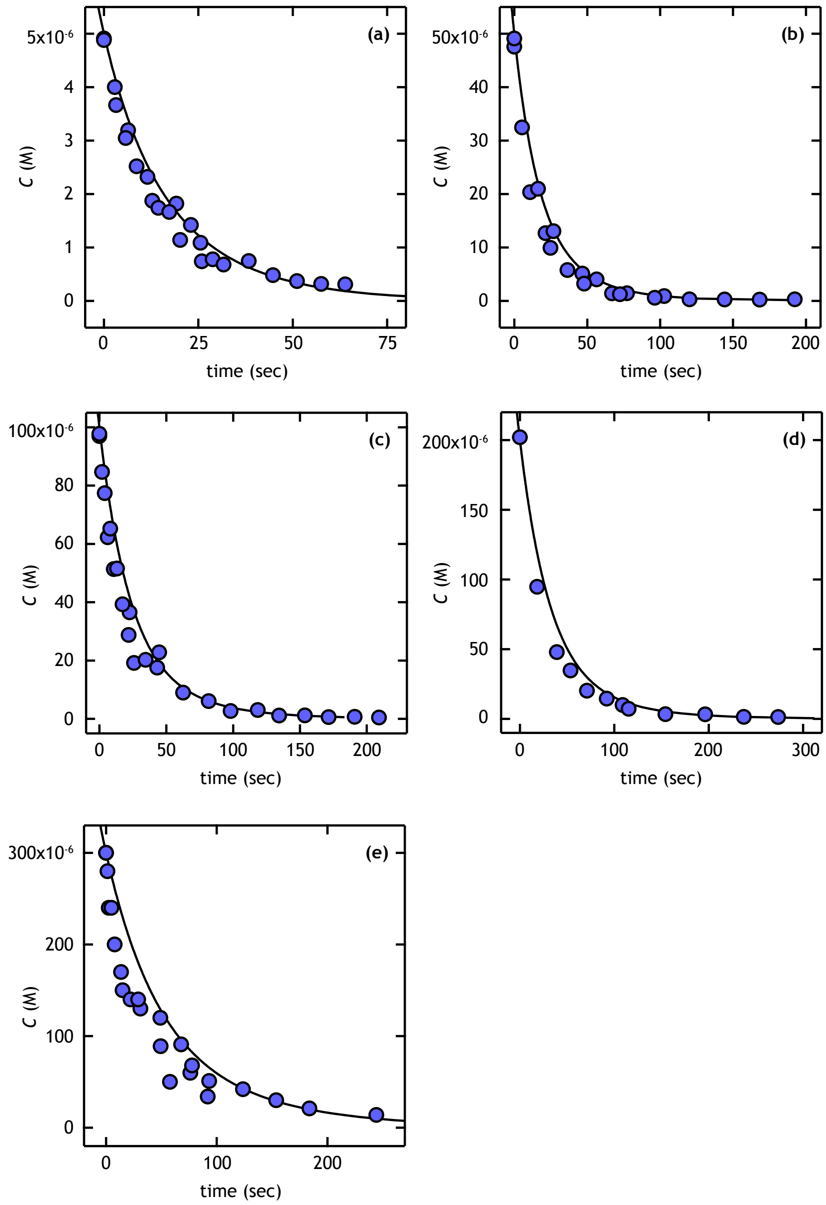

Figure S2.1 Modeling 4-Cl-aniline concentrations vs. time points corrected for light screening at $\lambda = 254$ nm using eq. S2.4 for different initial substrate concentrations: (a) 5 μM, (b) 50 μM, (c) 100 μM, (d) 200 μM, (e) 300 μM. Note that corrected time points were fitted vs. measured concentrations. Values for k_1 indicate the rate constant of photochemical transformation as in Table S2.1.

Table S2.1 Reaction rate constants for 4-Cl-aniline photolysis and related parameters obtained through kinetic modeling according to eqs. S2.1-S2.3. See text for definition of parameters. Uncertainties correspond to 95% confidence intervals.

C_0 (10^{-6} M)	k_1 (s^{-1})	k_2/k_3 (M^{-1})	$k_{obs}^{initial}$ (s^{-1})	$k_{obs}^{C/C_0 \leq 50\%}$ (s^{-1})	$k_{obs}^{initial}/k_{obs}^{C/C_0 \leq 50\%}$ ($-$)
5	$(4.7 \pm 2.2) \cdot 10^{-2}$	$(1.0 \pm 2.8) \cdot 10^{5}$	$(7.3 \pm 1.0) \cdot 10^{-2}$	$(3.9 \pm 0.5) \cdot 10^{-2}$	1.9 ± 0.3
50	$(2.4 \pm 0.7) \cdot 10^{-2}$	$(2.5 \pm 6.5) \cdot 10^{5}$	$(5.4 \pm 2.0) \cdot 10^{-2}$	$(2.7 \pm 0.3) \cdot 10^{-2}$	2.0 ± 0.8
100	$(2.1 \pm 0.5) \cdot 10^{-2}$	$(8.3 \pm 8.5) \cdot 10^{4}$	$(5.0 \pm 1.5) \cdot 10^{-2}$	$(2.4 \pm 0.3) \cdot 10^{-2}$	2.1 ± 0.6
200	$(1.5 \pm 0.5) \cdot 10^{-2}$	$(4.8 \pm 5.5) \cdot 10^{4}$	$(3.7 \pm 0.3) \cdot 10^{-2}$	$(1.7 \pm 0.2) \cdot 10^{-2}$	2.2 ± 0.3
300	$(1.0 \pm 0.5) \cdot 10^{-2}$	$(1.1 \pm 3.6) \cdot 10^{4}$	$(4.1 \pm 1.5) \cdot 10^{-2}$	$(9.3 \pm 1.1) \cdot 10^{-3}$	4.5 ± 1.6

S2.2.2 Data analysis

At aqueous 4-Cl-aniline concentrations $\geq 5\mu$M low optical density conditions for photochemical experiments are not fulfilled. Light attenuation and screening by substrate and product molecules and the ensuing decrease of the photon fluence rate in the reactor tubes were accounted for according to procedures described by Wenk et al.[156]. To this end, we corrected the sampling time points, t_{sampling}, at which samples were withdrawn from the reactors for concentration analysis with a light screening factor at wavelength λ of 254 nm, S_{254}, as well as with for photon fluence rate variations with atrazine by chemical actinometry (atr in equations below).[22] Corrected time points, t^* followed from t_{sampling} as in eq. S2.5.

$$t^* = t_{\text{sampling}} \cdot \mathrm{S}_{254}^{t_{\text{sampling}}} \cdot k_{\text{corr}}^{\text{atr}} \tag{S2.5}$$

where $\mathrm{S}_{254}^{t_{\text{sampling}}}$ and $k_{\text{corr}}^{\text{atr}}$ are derived as in eqs. (S2.6-S2.8) with n of 10^3, b_i is the length of a chord and R is the radius of the quartz tube, $k_{\text{reference}}^{\text{atr}}$ is the reference decay constant for atrazine, and k_j^{atr} is its value at the day j of measurement. $a_{254}^{t_{\text{sampling}}}$ is the absorption coefficient at 254 nm.

$$\mathrm{S}_{254}^{t_{\text{sampling}}} = \frac{\sum_{i=0}^{n} b_i \cdot \dfrac{1 - e^{-2.303 \cdot b_i \cdot a_{254}^{t_{\text{sampling}}}}}{2.303 \cdot b_i \cdot a_{254}^{t_{\text{sampling}}}}}{\sum_{i=0}^{n} b_i} \tag{S2.6}$$

$$b_i = 2R\sqrt{\frac{i}{n}\left(1 - \frac{i}{n}\right)} \tag{S2.7}$$

$$k_{\text{corr}}^{\text{atr}} = \frac{k_j^{\text{atr}}}{k_{\text{reference}}^{\text{atr}}} \tag{S2.8}$$

Table S2.2 Photon-fluence based, pseudo-first order reaction rate for the neutral ($k^{\mathrm{B}}_{\mathrm{E}^0_P}$) and conjugated acidic ($k^{\mathrm{BH}^+}_{\mathrm{E}^0_P}$) form of 4-Cl-aniline, measured at constant photon fluence rate at $\lambda = 254$nm. $\varepsilon^{\mathrm{B}}_{254}$ and $\varepsilon^{\mathrm{BH}^+}_{254}$ are the molar absorption coefficients while ϕ^{B} and ϕ^{BH^+} are the quantum yields obtained for 4-Cl-aniline in its neutral and conjugated acidic form. Uncertainties are 95% confidence intervals.

$k^{\mathrm{B}}_{\mathrm{E}^0_P}$ (m^2 einstein^{-1})	$\varepsilon^{\mathrm{B}}_{254}$ (m^2 mol^{-1})	ϕ^{B} (mol einstein^{-1})	$k^{\mathrm{BH}^+}_{\mathrm{E}^0_P}$ (m^2 einstein^{-1})	$\varepsilon^{\mathrm{BH}^+}_{254}$ (m^2 mol^{-1})	ϕ^{BH^+} (mol einstein^{-1})
622 ± 88	311 ± 15	0.869 ± 0.129	28 ± 3	16 ± 9	0.759 ± 0.416

Table S2.3 Photon-fluence based, pseudo-first order reaction rate constants for the photolysis of 4-Cl-aniline at $\lambda = 254$nm at different solution pH-values. Uncertainties are 95% confidence intervals.

pH (-)	$k^{\mathrm{app}}_{\mathrm{E}^0_P}$ (m^2 einstein^{-1})
2	34 ± 1
3	86 ± 3
4	283 ± 48
5	401 ± 114
7	605 ± 67
9	438 ± 259

S2.3 Fluorescence quenching by CsCl

Table S2.4 Fluorescence lifetimes τ_{F} of 4-Cl-aniline during photolysis in the presence CsCl or NaCl. τ^0_{F} refers to 4-Cl-aniline solution without any salt addition. Uncertainties are 95% confidence intervals.

NaCl (M)	CsCl (M)	τ_{F} (ns)	$\tau^0_{\mathrm{F}}/\tau_{\mathrm{F}}$ (-)
0	0	0.464 ± 0.004	1
0	0.5	0.352 ± 0.003	1.318 ± 0.011
0	1.0	0.292 ± 0.003	1.589 ± 0.016
0.5	0	0.436 ± 0.004	1.064 ± 0.010
1.0	0	0.417 ± 0.003	1.113 ± 0.008

S2.4 Product Analysis

The following compilation of reaction products was made for experiments carried out with 80 μM initial 4-Cl-aniline concentration. Note that neither 4-aminophenol nor aniline was detected in any experiment.

S2.4.1 Identification of possible coupling products (CP)

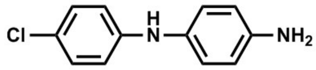

(i)

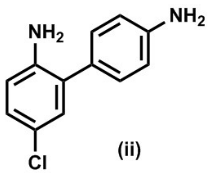

(ii)

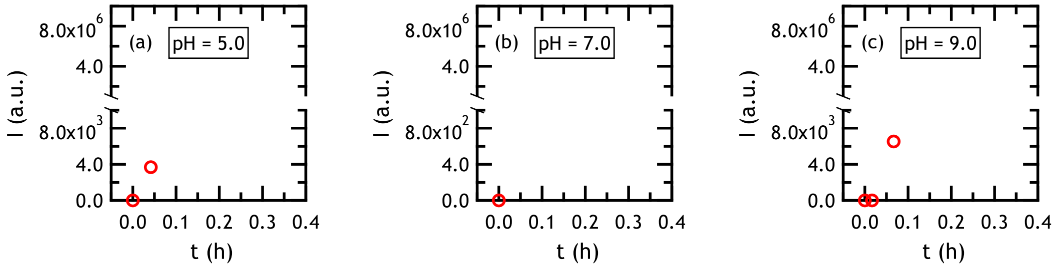

Figure S2.2 MS signal intensity represented in arbitrary units (a.u.) over irradiation time in hours (h) relative to the formation of one of the possible isomers with chemical formula $C_{12}H_{11}ClN_2$ over a pH range from 5.0 to 9.0 (a-c). Two possible identified compounds are 4-chloro-4′-aminodiphenylamine (i) and 5-chloro-1,1′-biphenyl-2,4′-diamine (ii).

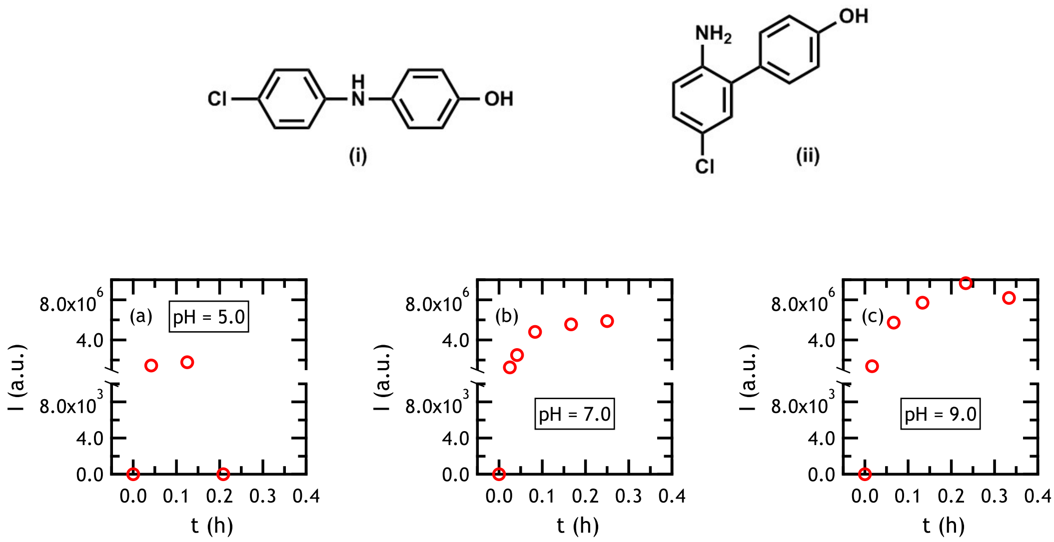

Figure S2.3 MS signal intensity represented in arbitrary units (a.u.) over irradiation time in hours (h) relative to the formation of one of the possible isomers with chemical formula $C_{12}H_{10}ClNO$ over a pH range from 5.0 to 9.0 (a-c). Two possible identified compounds are 4-hydroxy-4′-chlorodiphenylamine (i) and 5-chloro-4′-hydroxy-1,1′-biphenyl-2-amine (ii).

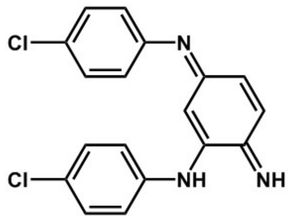

(i)

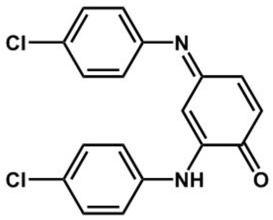

(ii)

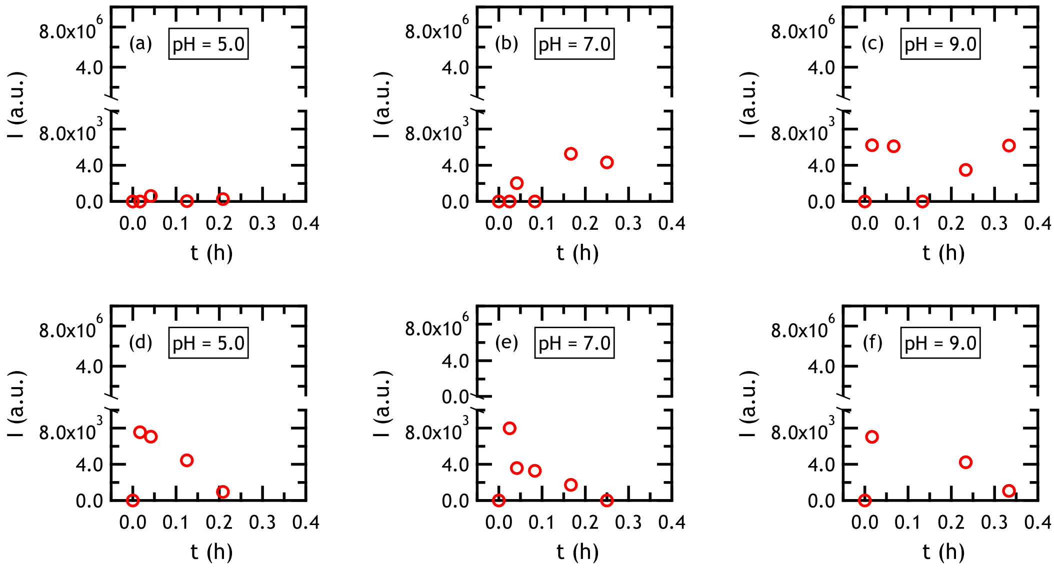

Figure S2.4 MS signal intensity represented in arbitrary units (a.u.) over irradiation time in hours (h) relative to the formation of one of the possible isomers with chemical formula $C_{18}H_{13}Cl_2N_3$ (i) over a pH range from 5.0 to 9.0 (a-c) and to the formation of one of the possible isomers with chemical formula $C_{18}H_{12}Cl_2N_2O$ (ii) over a pH range from 5.0 to 9.0 (d-f)

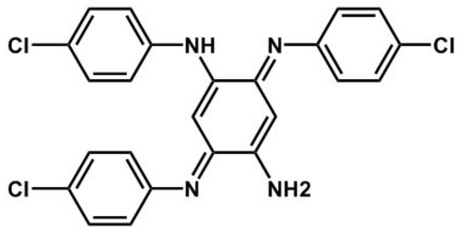

(i)

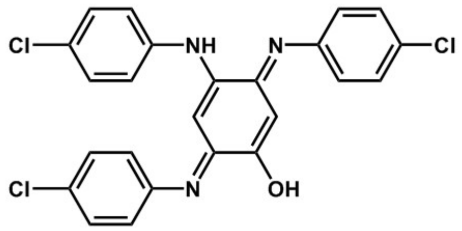

(ii)

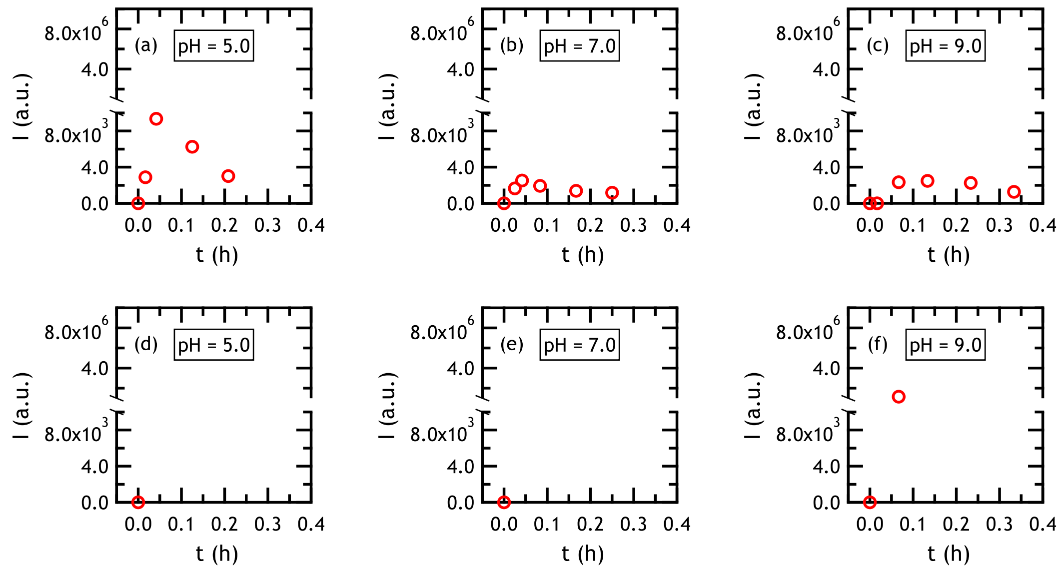

Figure S2.5 MS signal intensity represented in arbitrary units (a.u.) over irradiation time in hours (h) relative to the formation of one of the possible isomers with chemical formula $C_{24}H_{17}Cl_3N_4$ (i) over a pH range from 5.0 to 9.0 (a-c) and to the formation of one of the possible isomers with chemical formula $C_{24}H_{16}Cl_3N_3O$ (ii) over a pH range from 5.0 to 9.0 (d-f).

S2.5 UV-Vis Spectra

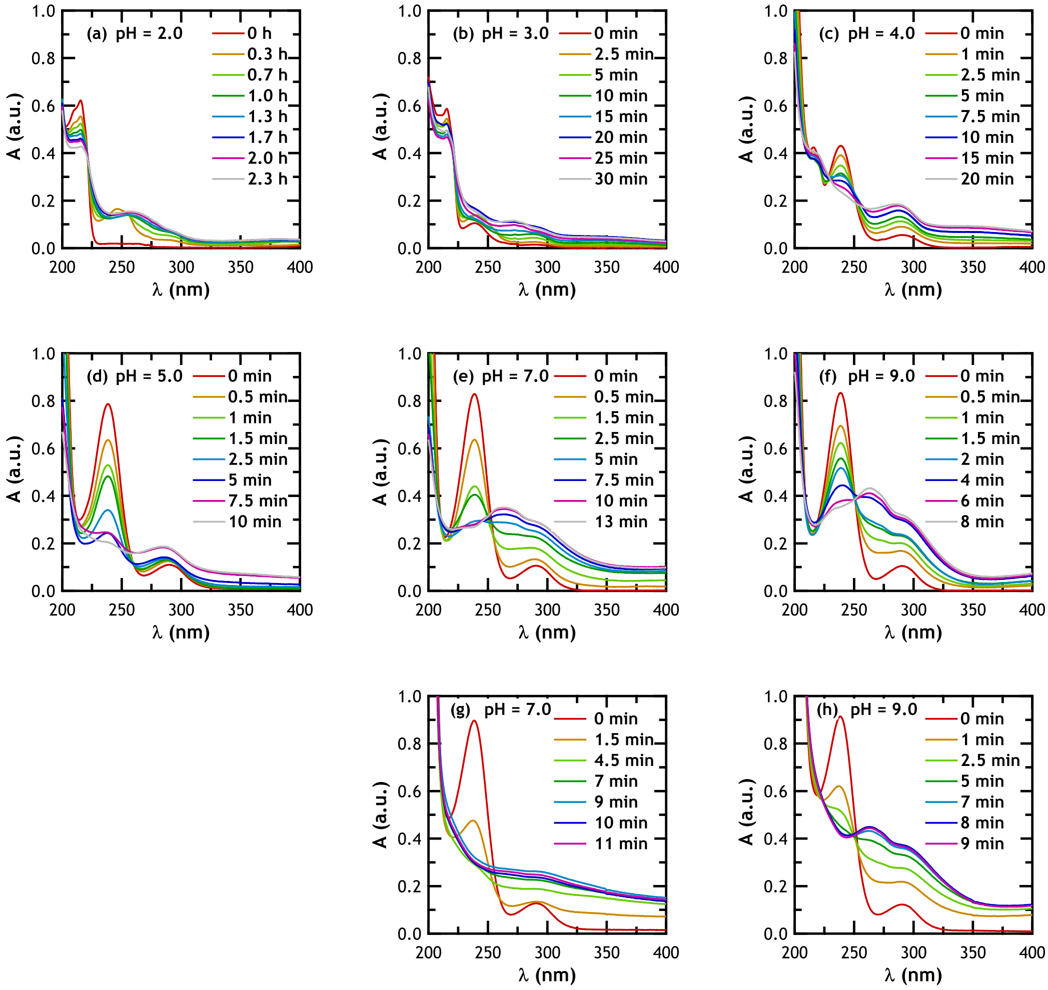

Figure S2.6 UV-Vis absorbance spectra reative to the direct photolysis of 4-Cl-aniline recorded in the UV range from 200 to 400 nm over a pH-range from 2.0 to 9.0 (a - f) and in presence of CsCl 1M (g - h)

Chapter 3

Isotope Fractionation Associated with the Photochemical Dechlorination of Chloroanilines

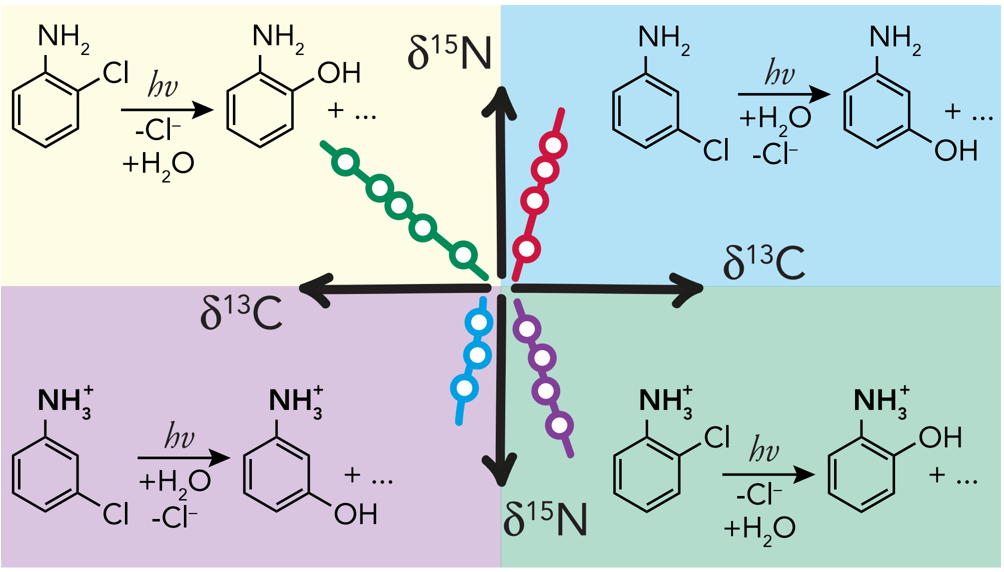

M. Ratti, S. Canonica, K. McNeill, J. Bolotin and T. B. Hofstetter. Isotope fractionation associated with the photochemical dechlorination of chloroanilines. *Environ. Sci. Technol.*, 49:9797-9806, **2015**

Abstract

Isotope fractionation associated with the photochemical transformation of organic contaminants is not well understood and can arise not only from bond cleavage reactions but also from photophysical processes. In this work, we investigated the photolytic dechlorination of 2-Cl- and 3-Cl-aniline to aminophenols to obtain insights into the impact of substituent position on the apparent ^{13}C and ^{15}N kinetic isotope effects (AKIEs). Laboratory experiments were performed in aerated aqueous solutions at an irradiation wavelength of 254 nm over the pH range 2.0 to 7.0 in the absence and presence of Cs^+ used as excited singlet state quencher. Photolysis of 2-Cl-anilinium cations exhibits normal C and inverse N isotope fractionation while neutral 2-Cl-aniline species shows inverse C and normal N isotope fractionation. In contrast, the photolysis of 3-Cl-aniline was almost insensitive to C isotope composition and the moderate N isotope fractionation points to rate-limiting photophysical processes. ^{13}C- and ^{15}N-AKIE-values of 2-Cl-aniline decreased in the presence of Cs^+ whereas those for 3-Cl-aniline were not systematically affected by Cs^+. Our current and previous work illustrates that photolytic dechlorinations of 2-Cl-, 3-Cl-, and 4-Cl-aniline isomers are each accompanied by distinctly different and highly variable C and N isotope fractionation due to spin selective isotope effects.

3.1 Introduction

The assessment of organic pollutant degradation processes by compound-specific isotope analysis (CSIA) is becoming increasingly popular[38,57,146]. A growing number of studies report fractionation trends for C, H, N, Cl, and S isotopes in organic compounds as well as the corresponding apparent kinetic isotope effects, with which biological and abiotic transformation routes can be characterised[71]. Isotope fractionations from photolytic reactions, however, are currently not well understood and applications of CSIA that include light-induced transformations, for example, of halogenated phenols, anilines, triazines, and diphenylethers,[56,107,117,151,168] are scarce. In contrast to thermal reactions, isotope fractionation in photolytic transformations can originate not only from bond cleavages but also from photophysical processes of excited states such as magnetic interactions of spin carrying nuclei and electrons[18,19,142,148,160]. Isotope effects from photophysical processes are thus more difficult to rationalise and likely more variable because they depend on the population and reactivity of different excited spin states. The latter can be very sensitive to a number of parameters such as the protonation state of the organic pollutant and solution constituents that may act, for example, as singlet or triplet state quenchers. Moreover small differences in molecular structure, for example, aromatic substituent positions, not only alter light absorptivity but can also lead to photolysis through different reaction mechanisms.

We have recently studied the isotope fractionation associated with the photolysis of 4-chloroaniline (4-Cl-aniline)[107] to obtain insights into possible isotope fractionation associated with photolytic dechlorinations of agrochemicals and pharmaceuticals containing reactive chloroaniline substructures[15,20,25,48,69,167,169]. This prior work showed that it is difficult to propose "typical" ranges of kinetic isotope effects for photolytic dechlorination reactions[56,117,151] in a similar way as for microbially mediated dechlorinations, for example, of chlorinated ethenes and chlorobenzenes[3,4,8,29,36,37,50,66,80–82,93,110,111,143]. Photolytic dechlorination of 4-Cl-aniline leads to a carbene intermediate, which reacts to give higher molecular weight coupling products, aniline, and aminophenol[98]. While the apparent ^{13}C-kinetic isotope effects (^{13}C-AKIE) for this dechlorination reaction (1.005 to 1.017) are smaller than for dechlorinations of aromatic and olefinic C–Cl bonds (approx.

1.03, see above refs.), ^{15}N-AKIE-values of up to 1.009 are larger than those reported for thermal reactions in which no N atom is located at the reactive position[107]. Evidence from correlations of ^{13}C-AKIE and ^{15}N-AKIE over the pH range 2.0 to 9.0 and in presence of singlet quenchers suggested that the considerable variability of isotope fractionation was due to reactions from singlet vs. triplet excited states.

Whether the observed spin selectivity of C and N isotope fractionation is indicative for photolytic dechlorinations of other chloroanilines such as the aquatic micropollutant diclofenac, however, is currently unknown. Photolysis of 2-chloroaniline (2-Cl-aniline) and 3-chloroaniline (3-Cl-aniline) also results in dechlorination but current evidence suggests different reaction mechanisms[16,48,94,96,97]. Previous work on the oxidation of *N*-alkylated anilines showed that changes of the type and position of the substituents on the benzene ring can give rise to subtle changes in mechanisms, which result in distinctly different C, H, and N isotope effects[135]. It was the goal of this work to examine the impact of the substituent position on the C and N isotope fractionation for the photolytic dechlorination of (mono-)chloroanilines. Specifically, we aimed at obtaining insights into the diagnostic capabilities of CSIA for photolytic dechlorination of micropollutants with chloroaniline substructures. To this end, we studied the C and N isotope fractionation associated with the direct photolysis of 2-Cl-aniline and 3-Cl-aniline in aerated aqueous solution. Experiments were carried out over the pH range of 2.0 to 7.0 in the absence and presence of CsCl as singlet quencher to account for influence of protonation and spin selectivity on ^{13}C-AKIE and ^{15}N-AKIEs.

3.2 Experimental Section

A list of chemicals including their purities and suppliers can be found in the Supporting Information (SI).

3.2.1 Chemical and isotopic analysis

Concentrations of 2-Cl-aniline, 3-Cl-aniline, 2-aminophenol, and 3-aminophenol were determined by HPLC using a Dionex UltiMate 3000 system equipped with a UV-Vis detector following methods described recently[107,133]. Columns used include

Supelcosil LC-18 (25 cm × 4.6 mm, 5μm) with eluent mixtures of methanol and 1 mM KH_2PO_4 (40/60 vol % for 2-Cl-aniline and 30/70 % vol for 3-Cl-aniline) at a flow rate of 1 mL min^{-1} and a sample injection volume of 20 μL. Polar transformation products were analyzed with LC/MS using a LTQ (Linear Trap Quadrupole) Orbitrap mass spectrometer (Thermo) with electrospray ionization as documented previously[134,135]. Gradient elutions from 90/10 to 5/95 vol % ratios of H_2O/MeOH were run on Atlantis C-18 (15 cm × 3.0 mm, 3 μm) and XBridge C-18 (5 cm × 2.1 mm, 3.5 μm) columns from Waters. Both eluents contained 0.1 vol % formic acid. Qualitative identification of reaction products, such as 2-aminophenoxazin-3-on, was based on the exact masses of tentative molecular structure of expected products as well as MS/MS- fragment spectra[73]. Deuterated aniline concentrations were determined by GC/MS (Ultra Trace GC, DSQII, Thermo) as shown previously[134] using d_5-aniline as external standard. Molecular structures of anticipated products were postulated as shown in the SI.

$^{13}C/^{12}C$ and $^{15}N/^{14}N$ ratios were determined by solid phase microextraction (SPME) using polydimethylsiloxane/divinylbenzene fibers (Supelco) followed by gas chromatography coupled to isotope ratio mass spectrometry[102,103,107,133]. The combustion interface was equipped with a Ni/Pt oxidation reactor[138]. pH values of aqueous samples were adjusted to 7.0 to avoid N isotope fractionation by H^+-exchange reactions[133]. The pK_a of the conjugate acids of 2-Cl- and 3-Cl-aniline are 2.65 and 3.52, respectively[126]. Stable C and N isotope signatures ($\delta^{13}C$ and $\delta^{15}N$) of chloroanilines are given as arithmetic mean ($\pm\sigma$) of triplicate measurements in per mil (‰). Isotopic standard materials purchased from Indiana University were used to report $\delta^{13}C$- and $\delta^{15}N$-values relative to Vienna PeeDee Belemnite and air, respectively. C and N isotope analysis was performed within the method quantification limits of the SPME-GC/IRMS procedure of 1.0 to 2.5 μM for $\delta^{13}C$ and $\delta^{15}N$[72]. Samples were diluted to concentrations yielding peak amplitudes between 0.5 and 3 V. A standard bracketing procedure, referenced to calibrated in-house standards of 2-chloro- and 3-chloroanilines of known $\delta^{13}C$ and $\delta^{15}N$-values, was used to ensure accuracy of the isotope ratio measurements.

3.2.2 Photolysis Experiments

Kinetic and isotopic experiments were carried out in glass-stoppered quartz tubes (OD 18 mm, ID 15 mm) filled with 20 mL of aerated and buffered solution, typically 10 mM phosphate buffer of pH 2.0, 4.0, and 7.0 as shown previously[107]. Quartz tubes were introduced in a DEMA 125 merry-go-round photoreactor (Hans Mangels GmbH, Bornheim-Roidorf, Germany) equipped with a low-pressure mercury (LP Hg) lamp (Heraeus Noblelight model TNN 15/32, nominal power 15 W) and a quartz cooling jacket[24]. A recirculating pure water bath kept the reactor temperature at 25.0 ± 0.2 ℃. Direct photolysis experiments were started by irradiation of monochromatic light at a wavelength of 254 nm and stopped by removing the quartz tubes from the photoreactor. The used Hg lamp enabled us to study the pH-dependence of chloroaniline photolysis within one and four hours for 3-Cl- and 2-Cl-aniline, respectively.

Experiments for the quantification of C and N isotope fractionation were performed at 80 μM initial chloroaniline concentrations. Between 9 and 12 samples consisting of the entire volume of a 20 mL quartz tube were collected at different time points depending on the decay kinetics of 2- and 3-Cl-aniline until fractional conversion exceeded 95%. Samples were split for measurement of substrate concentrations, C and N isotope ratios, identification of reaction products, and UV-vis absorbance on a Cary 100 spectrophotometer.

Experiments for the evaluation of photolysis kinetics were carried out identically using two reactor tubes and initial chloroaniline concentration of only 5 μM. Note that reaction rate constants were independent of the initial substrate concentrations between 5 μM and 80 μM. At predefined time points, samples of 0.5 mL were withdrawn. All kinetic experiments were done in duplicates and rate constants for the direct photolysis of 2- and 3-Cl-aniline were scaled to a constant photon fluence rate of $7.5 \pm 0.8 \cdot 10^{-5}$ einstein m^{-2} s^{-1} using atrazine as a chemical actinometer and corrected for inner-filter light-screening as described by Ratti et al.[107] Direct photolysis of 3-Cl-aniline was also studied in the presence of 1 M d_8-isopropanol at pH 7.0 at initial concentrations of 150 μM[76].

Control experiments for quantification of non-reactive losses and isotope fractionation were set up identically under the experimental conditions described above but without irradiation. Experiments with Cs^+ as a singlet quencher were carried out in 10 mM phosphate buffer containing 1 M CsCl. Reference experiments thereof contained either NaCl or $NaClO_4$ in concentrations from 0.3 to 1.0 M to assess the impact of Cs^+ and Cl^- independently.

3.2.3 Data analysis

A linear regression analysis of δ^{13}C- and δ^{15}N- values, respectively, vs. fractional amount of remaining reactant ratio (C/C_0) as shown in eq. 3.1, was used to derive bulk compound C and N isotope enrichment factors (ϵ_{C}, ϵ_{N}). Based on the assumption that changes in isotope ratios could only occur at the reactive atom positions of the investigated compound, while non-reactive ones remain unchanged, secondary kinetic isotope effects are considered to be negligible. According to this consideration, eq. 3.2 was used to estimate the corresponding apparent ^{13}C- and ^{15}N-kinetic isotope effects (AKIEs).

$$ln\left(\frac{\delta^{\mathrm{h}}\mathrm{E}+1}{\delta^{\mathrm{h}}\mathrm{E}_0+1}\right) = \epsilon_{\mathrm{E}} \cdot ln\left(\frac{C}{C_0}\right) \tag{3.1}$$

$$\mathrm{AKIE}_{\mathrm{E}} = \frac{1}{1+n\cdot\epsilon_{\mathrm{E}}} \tag{3.2}$$

where $\delta^{\mathrm{h}}\mathrm{E}_0$ and $\delta^{\mathrm{h}}\mathrm{E}$ stand for the measured isotope signatures of an element E at time zero and at different time intervals of the reaction. n stands for the number of isotopic atoms and equals 1 for ^{15}N-AKIEs and 6 for ^{13}C-AKIEs derivation.

The kinetics of 2-Cl- and 3-Cl-aniline photolysis to aminophenols and further reaction products were quantified based on a simplified kinetic model (eqs. 3.3-3.5).

$$A \xrightarrow{\gamma \cdot k_1} B \tag{3.3}$$

$$A \xrightarrow{(1-\gamma) \cdot k_1} P_1 \tag{3.4}$$

$$B \xrightarrow{k_2} P_2 \tag{3.5}$$

where A is either 2-Cl- or 3-Cl-aniline, B stands for 2- or 3-aminophenols. P_1 and P_2 stand for further photolysis products of A and B, respectively. k_1 is the pseudo-first order rate constant for photolysis of chloroanilines, whereas k_2 is the rate constant for photolysis of aminophenols. γ quantifies the substrate fraction of chloroaniline that reacts to aminophenol. Reactions 3.3 to 3.5 result in eqs. 3.6 and 3.7 as the integrated rate laws for the concentration dynamics of chloroanilines and aminophenols. Non-linear regression analysis using Igor Pro software (Wavemetrics Inc.) was applied to the data after correction for light attenuation at 254 nm, S_{254}, to account for the light absorption by dissolved species and the geometry of the reactors.[156] First, the fitting of parameter k_1 was obtained from regression of the chloroaniline kinetic data to eq. 3.3, then the determined k_1 was used as fitted parameter to evaluate data for aminophenol concentrations with eq. 3.6, yielding fitting paramaters γ and k_2.

$$[A] = [A_0]\ e^{-k_1 t} \tag{3.6}$$

$$[B] = \gamma \cdot \frac{k_1}{(k_2 - k_1)} \left(e^{-k_1 t} - e^{-k_2 t}\right) [A_0] \tag{3.7}$$

where $[A_0]$ is the initial chloroaniline concentration.

The pH-dependence of observed and photon-fluence based reaction rate constants, k_1 and $k_{E^0_P}$ as well as C and N isotope enrichment factors, ϵ_C and ϵ_N, were calculated using eqs. 3.8 and 3.9.

$$\chi_i = \alpha_{\mathrm{BH^+}} \cdot \chi_i^{\mathrm{BH^+}} + (1 - \alpha_{\mathrm{BH^+}}) \cdot \chi_i^{\mathrm{B}} \tag{3.8}$$

$$\alpha_{\mathrm{BH^+}} = \frac{1}{1 + 10^{\mathrm{pH} - \mathrm{p}K_{\mathrm{BH^+}}}} \tag{3.9}$$

where χ_i stands for the fitted parameters. $\chi_i^{\mathrm{BH^+}}$ and χ_i^{B} are the derived values for the protonated and neutral chloroaniline using ground state acidity constants for the conjugate acids of 2-Cl- and 3-Cl-aniline (2.65 and 3.52)[126]. Note that due to the numerous parameters determined in each experiment, fitting of χ_i was carried out based on only 3 experiments at 3 pH-values. This limitation of experiments, especially at pH-values below p$K_{\mathrm{BH^+}}$ resulted in very small parameter uncertainties (i.e., 95% confidence intervals).

3.3 Results and Discussion

3.3.1 Photolysis of 2-Chloroaniline

The reaction kinetics of the direct photolysis of 2-chloroaniline (2-Cl-aniline, 80 μM) at pH 7.0 and the associated C and N isotope fractionation are shown in Figure 3.1. Disappearance of 2-Cl-aniline followed pseudo-first order kinetics ($k_1 = 4.1 \pm 0.3 \cdot 10^{-4}$ s^{-1}, entry 3a, Table 3.1) with a quantum yield for the neutral species, ϕ^{B}, of 0.05±0.01 mol einstein^{-1}. Photolysis was accompanied by an inverse C and normal N isotope fractionation and the corresponding C and N isotope enrichment factors, ϵ_{C} and ϵ_{N}, were +1.3±0.1‰ and −2.9±0.1‰, respectively. We observed 2-aminophenol (compound **4** in Figure 3.2a) as a transient intermediate (Figure 3.1a). Based on our kinetic analysis, formation of 2-aminophenol at pH 7.0 accounted for more than 50% of 2-Cl-aniline disappearance (eqs. 3.6 and 3.7 with $\gamma = 0.51 \pm 0.08$). Product analyses by high-resolution MS revealed the formation of 2-aminophenoxazin-3-one (**5**, m/z 213.0659).

Photolysis of 2-Cl-aniline in aqueous solution was investigated previously and the typical reaction pathways are summarized in Figure 3.2[16,94,96]. Formation of transient, dechlorinated species (**3**) is speculative due to the low quantum yield or short lifetime of excited state species[96]. Detection of 2-aminophenol and 2-aminophenoxazin-3-one suggest that pathway (i) was operational in our experiments. Moreover, compound **5** was also obtained in irradiation experiments with 2-aminophenol as the substrate suggesting that its disappearance after one hour was at least in part due to formation of the phenoxazine (see SI, Figures S3.1 and S3.3). Neither biphenyl-type coupling products of dechlorinated intermediates with substrate, intermediate, and product molecules (e.g., **7**) nor aniline (**8**) were found in aerated solution experiments, in agreement with the fact that compounds **7** and **8** are reported for deoxygenated solutions only[96]. Because **7** and **8** would have been detected with our analytical procedures,[107] we conclude that pathways (iii) and (iv) were not relevant here for transformation of 2-Cl-aniline. We also did not observe the cyclopentadienecarbonitrile products (**6**), which have been previously reported[96]. Due to the lack of reference material, however, it is more difficult to rule out contributions of pathway (ii) completely.

The combination of inverse C and normal N isotope fractionation is unusual and has not been observed previously for photochemical and thermal reactions of organic pollutants. In contrast, the opposite combination, that is normal C and inverse N isotope fractionation are typical for oxidation reactions of substituted anilines[102,133,134]. Normal ϵ_N-values of smaller magnitude were reported for the direct photolysis of 4-Cl-aniline at pH 7.0 (ϵ_N^{4-Cl} of -1.2 ± 0.2‰ vs. ϵ_N^{2-Cl} of -2.9 ± 0.1‰) where we also assumed that the N atom was not directly involved in the reaction[107]. The ϵ_C for 2-Cl-aniline photolysis (1.3 ± 0.1‰), however, is notably different from the one found for the heterolytic dechlorination of 4-Cl-aniline (-1.2 ± 0.2‰). In analogy to the inverse N isotope fractionation documented for thermal reactions, the inverse C isotope fractionation for 2-Cl-aniline photolysis could be interpreted as evidence for increased bonding to C in the rate-limiting step of the reaction[102,134]. However, inverse C (and N) isotope fractionation, as evidenced for the direct photolysis of atrazine,[56] can also originate from magnetic isotope effects due to interactions of spin carrying nuclei and unpaired electrons. Our recent work on the direct photolysis of 4-Cl-aniline has shown that such magnetic effects, albeit not associated with inverse C isotope fractionation, are very sensitive to changes in solution pH and ionic composition[107].

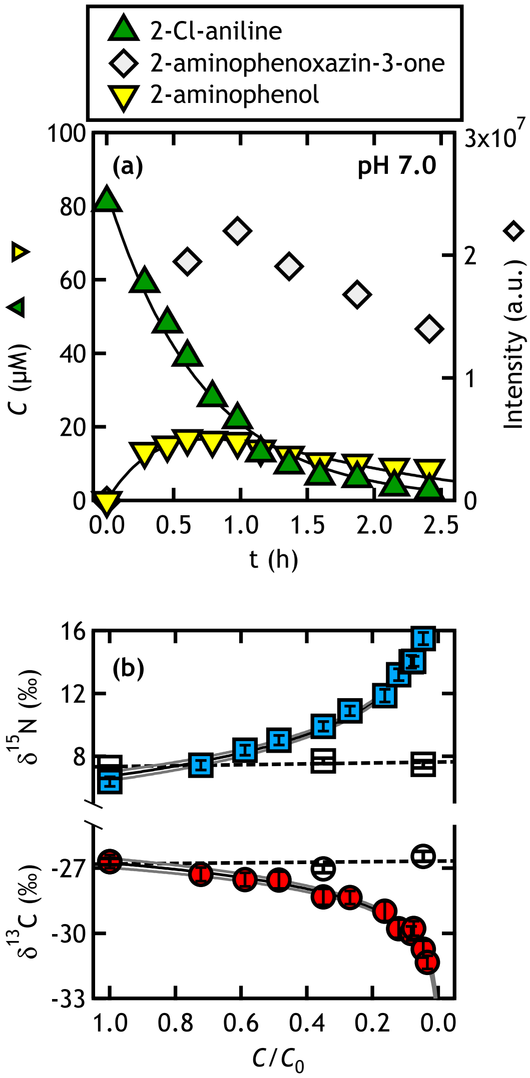

Figure 3.1 (a) 2-Cl-aniline and 2-aminophenol concentrations and signal areas of 2-aminophenoxazin-3-one in photochemical experiments at pH 7.0. Solid lines were calculated with eqs. 3.6-3.7; (b) C and N isotope signatures (δ^{13}C (circles) and δ^{15}N (squares) of 2-Cl-aniline vs. fraction of remaining substrate, C/C_0. Uncertainties represent standard deviations of triplicate measurements. Solid lines correspond to calculated isotope fractionation using eq. 3.1; gray dashed-lines indicate 95% confidence interval of the fit. Empty symbols and dashed lines represent control experiments that were not irradiated.

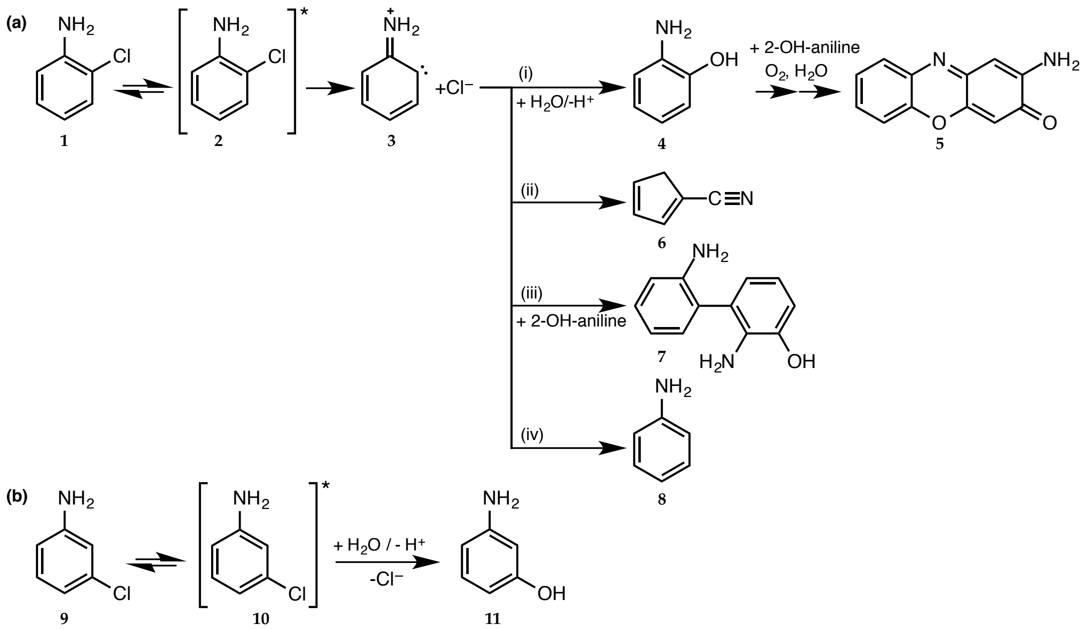

Figure 3.2 (a) Pathways of direct photolysis of 2-Cl-aniline (**1**): Excited species **2** can dechlorinate to a protonated carbene (**3**) and react along four reaction pathways to (i) 2-aminophenol (**4**) and 2-aminophenoxazin-3-one (**5**), (ii) ring-contraction to cyclopenta-1,3-diene-1-carbonitrile (**6**), (iii) biphenyl coupling products (**7**), and aniline (**8**). Compound **7** is an example for different possible molecular structures. (b) Direct photolysis of 3-Cl-aniline **9** to 3-aminophenol **11** through hydrolysis of excited state species **10**.

pH Dependence

We studied the rate constants and isotope enrichment factors of 2-Cl-aniline photolysis at different pH values (2.0, 4.0, 7.0). As shown in Figure 3.3 and in Table 3.1, both the observed and the photon-fluence based photolysis rate constants (k_1 and $k_{\mathrm{E}^0_\mathrm{P}}$) were moderately pH-dependent and differed by only 30% in the studied pH range. While the molar absorption coefficients of the neutral 2-Cl-aniline species ($\epsilon^{\mathrm{B}}_{254} = 56.1 \pm 0.6$ m^2 mol^{-1}) is approximately 3 times larger than that of the protonated species ($\epsilon^{\mathrm{BH}^+}_{254} = 17.8 \pm 0.4$ m^2 mol^{-1}), the reaction quantum yield of the protonated species is twice that of the neutral 2-Cl-aniline ($\phi^{\mathrm{BH}^+} = 0.11 \pm 0.01$ vs. $\phi^{\mathrm{B}} = 0.05 \pm 0.01$, Table S3.1). The combination of higher light absorptivity and lower quantum yield of the neutral 2-Cl-aniline (and *vice versa* for the protonated species) explains the moderate pH-dependence. We successfully quantified the pH-

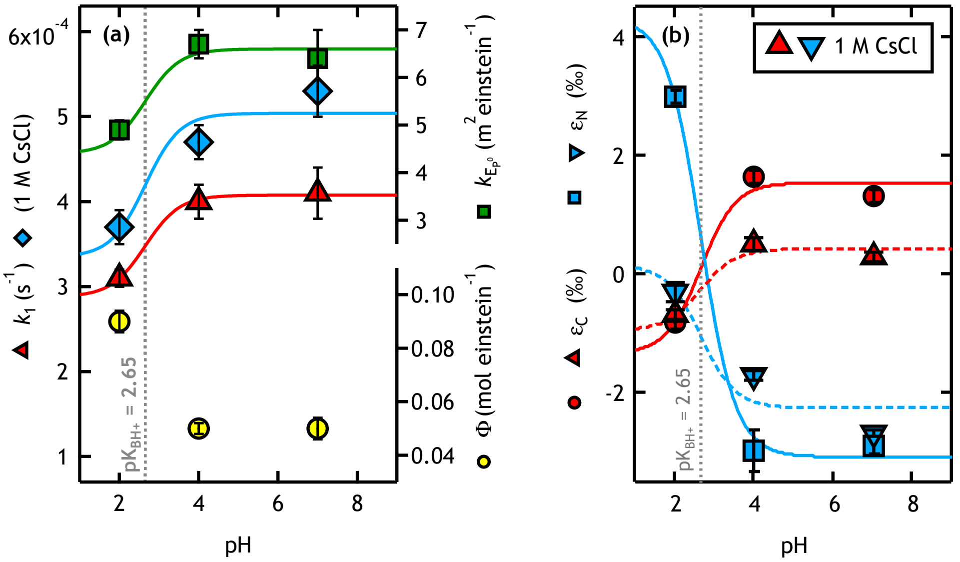

Figure 3.3 (a) Rate constants of 2-Cl-aniline photolysis: k_1 and $k_{\mathrm{E_P^0}}$ are the observed pseudo-first order and photon-fluence based photolysis rate constant; , ϕ is the reaction quantum yield.; (b) C and N isotope enrichment factors, ϵ_{C} and ϵ_{N}, of 2-Cl-aniline photolysis in the presence and absence of 1 M Cs^+ as singlet quencher. Solid lines represent calculated rate constants (eq. 3.8). The vertical dashed lines indicates the $p\mathrm{K}_{\mathrm{BH^+}}$ of ground state 2-Cl-aniline.

dependence of the photolysis rate constants assuming that both protonated and neutral 2-Cl-aniline species reacted independently (solid lines in Figure 3.3a). The assumption is supported by the product analyses. At pH 2.0, 2-aminophenol is formed in smaller amounts (< 20% of the initial 2-Cl-aniline concentration) and the relative peak intensity for 2-aminophenoxazin-3-one decreased by a factor of four compared to experiments at pH 4.0 and 7.0 (Figures S3.1 and 3.1).

We also observed substantial differences in C and N isotope fractionation for the 2-Cl-aniline photolysis of protonated vs. neutral species (Figures S3.1b/d and 3.3b). At solution pH-values of 4.0 and 7.0, C isotope fractionation of the neutral 2-Cl-aniline was inverse while N isotope fractionation was normal. The corresponding ϵ_{C}-values for pH 4.0 and 7.0 are similar (1.7 ± 0.1‰ vs. 1.3 ± 0.1‰) whereas ϵ_{N}-values are identical (-3.0 ± 0.3‰ vs. -2.9 ± 0.1‰, Table 3.1). The good agreement is also shown in Figure 3.4a, where C and N isotope fractionations were correlated and the corresponding slopes $\Delta\delta^{15}\mathrm{N}/\Delta\delta^{13}\mathrm{C}$ are identical within

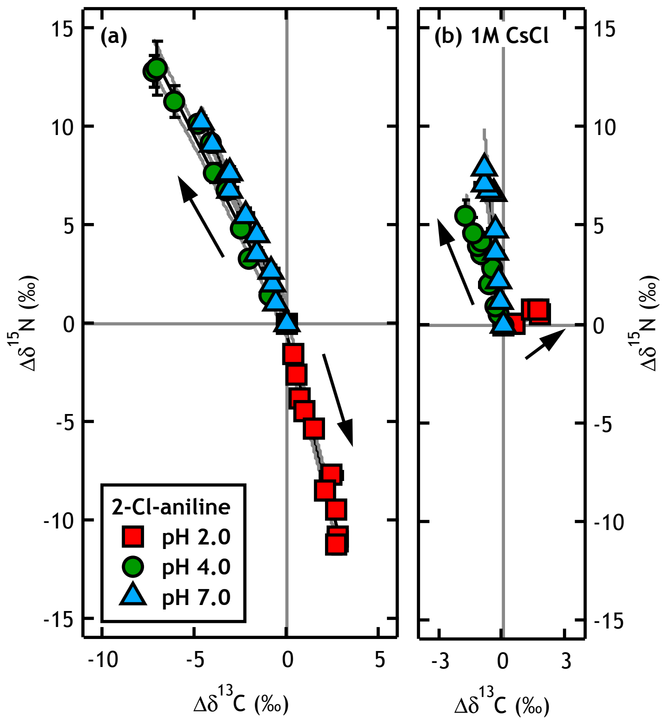

Figure 3.4 Correlation of C and N isotope fractionation ($\Delta\delta^{13}$C, $\Delta\delta^{15}$N) of 2-Cl-aniline for experiments performed at solution pH 2.0, 4.0, and 7.0 in the absence (a) and presence (b) of CsCl as singlet quencher. The grey lines delineate the initial 2-Cl-aniline isotope composition (δ^{13}C $= -26.7‰$, δ^{15}N $= 6.4‰$). Arrows indicate the direction of isotope fractionation with increasing reactant conversion. Error bars are mostly smaller than marker size.

uncertainty (Table 3.1, entries 2a and 3a). At pH 2.0, however, we observed the reversed C and N isotope fractionation trends, that is a normal isotope fractionation for C isotopes and inverse fractionation for N isotopes. The absolute value of ϵ_C for 2-Cl-aniline at pH 2.0 ($|-0.8 \pm 0.1‰|$) is smaller than those measured at pH 4.0 and 7.0, whereas the one for ϵ_N at pH 2.0 is of similar magnitude ($|+3.0 \pm 0.1‰|$) but of opposite sign compared to higher pH. Notice that in this special case, the $\Delta\delta^{15}$N/$\Delta\delta^{13}$C-values (Table 3.1, entries 1a, 2a, 3a) do not fully reflect the substantial difference in C and N isotope fractionation because this parameter cannot account for the direction of isotope fractionation (see arrows in Figure 3.4). The distinctly different C and N isotope fractionation for protonated and neutral 2-Cl-aniline corroborates the above interpretation of photolysis kinetics in that the two species react along independent pathways. We can also exclude the contribution of H^+ exchange reactions to the observed N isotope fractionation at pH 2.0 as in processes, where only the neutral species determines the reactivity of a substituted aniline (e.g., mineral-catalyzed oxidation). Such cases are governed by large normal N isotope fractionation (i.e., $\epsilon_N < 0$[133,134]) in contrast to what is shown in Figure 3.3b.

In analogy to the quantification of the pH-dependence of photolysis rate constants, C and N isotope enrichment factors follow the weighted average of the ϵ_C- and ϵ_N-values for the two species (Figure 3.3b). The C isotope enrichment factors for the photolysis of protonated and neutral species, $\epsilon_C^{BH^+}$ and ϵ_C^{B}, are $-1.4 \pm 0.2‰$ and $1.5 \pm 0.2‰$, respectively (Table 3.1, entries 4a and 5a). An even larger species-dependent difference was found for N isotope fractionation, where $\epsilon_N^{BH^+}$ and ϵ_C^{B} amount to $4.5 \pm 0.1‰$ and $-2.9 \pm 0.3‰$, respectively.

Origin of Isotope Fractionation and Kinetic Isotope Effects

We investigated the C and N isotope fractionation of 2-Cl-aniline photolysis over the pH range of 2.0 to 7.0 in the presence of 1 M CsCl to obtain insights into the contributions of photophysical processes. As shown recently for the photolysis of 4-Cl-aniline,[107] Cs^+ was used to decrease the lifetime of excited singlet states via increased intersystem-crossing and thus increased excited triplet state formation. The corresponding data are shown in Table 3.1, entries "b" and in Figures 3.3b and 3.4b. Addition of Cs^+ led to an increase of reaction rate constants, k_1, by 18% to 30% (Figure 3.3a) and a decrease of isotope fractionation. The differences in measured δ^{13}C-values of 2-Cl-aniline across all experiments were below 4‰ (Figure 3.4b). All ϵ_C- and ϵ_N-values determined from experiments with Cs^+ were smaller than in its absence. The correlation of C and N isotope fractionation (Figure 3.4b) illustrates that the effects of the singlet quencher were more pronounced for protonated than for neutral 2-Cl-aniline species. Note that a quantitative interpretation of the variations of $\Delta\delta^{15}N/\Delta\delta^{13}C$-values is hampered in the present case. The correlations shown in Figure 3 at solution pH 2.0 to 7.0 always reflect the C and N isotope fractionation caused by different combinations isotope effects pertinent to the photolysis of protonated and neutral 2-Cl-aniline species.

$\Delta\delta^{15}N/\Delta\delta^{13}C$-values are thus no longer indicative of a single reaction mechanism and we focus the discussion on pathway-specific parameters ϵ^{BH^+} and ϵ^{B} for C and N isotopes.

The decrease of $\epsilon_N^{BH^+}$ (4.5‰ → 0.3‰, entries 4a/b, Table 3.1) was larger than that for $\epsilon_C^{BH^+}$ (−1.4‰ → −0.9‰) whereas the opposite trend can be observed for neutral 2-Cl-aniline (entries 5a/b, Table 3.1). The sensitivity of both reaction pathways to singlet quenching implies that both dechlorination pathways occur, at least to some extent, from excited singlet states. Previous investigations with laser spectroscopy revealed that the lifetime of transient species was too short to be measured (< 9 ns,[96]) and its spin states are unknown. Our experiments, nevertheless, show that C and N isotope fractionation is susceptible to the population of excited states from which dechlorination happens.

Based on the above observations, we assigned ^{13}C- and ^{15}N-AKIEs to the reaction pathways of protonated and neutral 2-Cl-aniline. Dechlorination of 2-Cl-anilinium cations in the absence of Cs^+ is associated with a normal ^{13}C- and inverse ^{15}N-AKIE$_{BH^+}$ of 1.0084 ± 0.0009 and 0.9955 ± 0.0001, respectively. ^{13}C- and ^{15}N-AKIE$_{BH^+}$ are closer to unity in the presence of the singlet quencher (1.0056 and 0.9997, respectively). This comparison suggests that isotope fractionation originates primarily from singlet state dechlorinations. In the presence of Cs^+, this isotope fractionation could be masked because singlet states are quenched and reaction rates of triplet state dechlorination increase. Alternatively, triplet state dechlorination could exhibit smaller isotope effects. The same interpretation holds for the neutral 2-Cl-aniline even though the mechanisms of reaction is different from that of the of 2-Cl-anilinium cations given that ^{13}C-AKIE$_B$ are inverse and ^{15}N-AKIE$_B$ normal. ^{13}C- and ^{15}N-AKIE$_B$ for dechlorination from singlet states are 0.9909 and 1.0029 and approaching unity in the presence of Cs^+.

3.3.2 Photolysis of 3-Chloroaniline

The concentration as well as the C and N isotope signatures of 3-Cl-aniline during photolysis at pH 7.0 are shown in Figure 3.5 and reveal several differences to the reaction of 2-Cl-aniline under identical conditions. 3-Cl-aniline is photolysed

Table 3.1 C and N isotope enrichment factors (ϵ_C, ϵ_N), apparent ^{13}C-, ^{15}N-kinetic isotope effects (^{13}C and ^{15}N-AKIE), and direct photolysis reaction rate constants, k_1 of 2-Cl-aniline and 3-Cl-aniline in the absence and presence of 1 M CsCl (entries a and b, respectively). [a,b]

Entry	pH	ϵ_C (‰)	ϵ_N (‰)	^{13}C-AKIE [c] (-)	^{15}N-AKIE [c] (-)	k_1 [d] (10^{-4} s^{-1})	$\Delta\delta^{15}N/\Delta\delta^{13}C$ (-)
2-Cl-aniline							
1a	2.0	−0.8 ± 0.1	3.0 ± 0.1	1.0049 ± 0.0007	0.9970 ± 0.0001	3.1 ± 0.1	−3.7 ± 0.5
1b	2.0	−0.7 ± 0.1	−0.3 ± 0.2	1.0040 ± 0.0004	1.0003 ± 0.0002	3.7 ± 0.2	0.5 ± 0.3
2a	4.0	1.7 ± 0.1	−3.0 ± 0.3	0.9902 ± 0.0007	1.0030 ± 0.0003	4.0 ± 0.2	−1.9 ± 0.2
2b	4.0	0.5 ± 0.1	−1.7 ± 0.1	0.9969 ± 0.0007	1.0017 ± 0.0001	4.7 ± 0.2	−3.2 ± 0.7
3a	7.0	1.3 ± 0.1	−2.9 ± 0.1	0.9921 ± 0.0007	1.0029 ± 0.0001	4.1 ± 0.3	−2.2 ± 0.2
3b	7.0	0.3 ± 0.1	−2.7 ± 0.1	0.9982 ± 0.0005	1.0027 ± 0.0001	5.3 ± 0.3	−8.4 ± 2.7
4a	BH^+	−1.4 ± 0.2	4.5 ± 0.1	1.0084 ± 0.0009	0.9955 ± 0.0001	2.9 ± 0.1	
4b	BH^+	−0.9 ± 0.1	0.3 ± 0.2	1.0056 ± 0.0005	0.9997 ± 0.0003	3.4 ± 0.3	
5a	B	1.5 ± 0.2	−2.9 ± 0.3	0.9909 ± 0.0014	1.0029 ± 0.0002	4.1 ± 0.3	
5b	B	0.4 ± 0.2	−2.3 ± 0.3	0.9977 ± 0.0009	1.0023 ± 0.0004	4.9 ± 0.4	
3-Cl-aniline							
6a	2.0	0.3 ± 0.1	1.5 ± 0.1	0.9982 ± 0.0003	0.9985 ± 0.0002	9.2 ± 0.2	4.8 ± 1.0
6b	2.0	−0.1 ± 0.1	1.4 ± 0.2	1.0008 ± 0.0003	0.9986 ± 0.0002	12.6 ± 0.7	−9.1 ± 3.4
7a	4.0	−0.3 ± 0.1	−3.4 ± 0.5	1.0016 ± 0.0006	1.0034 ± 0.0005	30.7 ± 1.7	11.0 ± 3.0
7b	4.0	−0.5 ± 0.1	−5.0 ± 0.1	1.0030 ± 0.0005	1.0050 ± 0.0001	34.6 ± 1.3	10.0 ± 1.7
8a	7.0	−0.4 ± 0.1	−1.7 ± 0.2	1.0024 ± 0.0006	1.0017 ± 0.0002	38.4 ± 1.8	4.1 ± 0.8
8b	7.0	−0.4 ± 0.3	−1.5 ± 0.1	1.0023 ± 0.0018	1.0015 ± 0.0001	48.3 ± 3.8	3.1 ± 1.9
9a	BH^+	0.4 ± 0.1		0.9979 ± 0.0003		7.5 ± 0.2	
9b	BH^+	−0.1 ± 0.1		1.0006 ± 0.0003		11.3 ± 0.7	
10a	B	−0.4 ± 0.1		1.0023 ± 0.0007		36.5 ± 1.5	
10b	B	−0.5 ± 0.1		1.0032 ± 0.0008		40.0 ± 1.9	

[a] All experiments were carried out in 10 mM phosphate buffer adjusted to the given pH
[b] all uncertainties correspond to 95% confidence intervals; [c] calculated from eq. 3.2;
[d] for a LP Hg-lamp with a photon fluence rate of $7.5 \pm 0.8 \cdot 10^{-5}$ einstein m^{-2} s^{-1} and inner filter light-screening factor correction according to Ratti et al.[107]

with a pseudo-first-order rate constant, k_1, of $(3.8 \pm 0.2) \cdot 10^{-3}$ s^{-1} (Table 3.1, entry 8a), that is approximately one order of magnitude faster than for 2-Cl-aniline. 3-Aminophenol was found as the only reaction product accounting for 3-Cl-aniline removal ($\gamma = 0.80 \pm 0.06$ in eq. 3.7; Figures S3.2 and S3.4). Experiments carried out in the presence of d_8-isopropanol used as radical scavenger did not lead to formation of deuterated products (e.g., d-aniline, Figure S3.5). In contrast to 2-Cl-aniline, no high-molecular weight coupling product could be detected. Finally, C and N isotope fractionation of 3-Cl-aniline is normal and the magnitude of isotope fractionation is smaller (ϵ_C and ϵ_N-values of -0.4 ± 0.1‰ and -1.7 ± 0.2‰). Our observations agree with previous work, which suggested that excited 3-Cl-aniline is hydrolysed to 3-aminophenol (Figure 3.2b)[16,97] without formation of long-lived radical species. A comparison of isotope fractionation with other photochemical hydrolysis reactions that could confirm this hypothesis, however, is hampered by the lack of adequate data.

pH Dependence and Influence of Singlet Quencher and Dissolved Ions on Reaction Rates

We studied the kinetics of 3-Cl-aniline photolysis at pH 2.0, 4.0, and 7.0 as well as in the presence of Na^+, Cs^+, Cl^-, and ClO_4^- in concentrations of 0, 0.33, 0.67, and 1.0 M. The results are illustrated in Figure 3.6a. Pseudo-first-order rate constants, k_1, photon-fluence based rate constants, $k_{E_P^0}$, and quantum yields follow the identical qualitative trends observed for 2-Cl-aniline, which suggest that protonated and neutral species reacted in separate, independent reactions. The observed rates can be rationalized by the rate constants for each species and their fractional abundance as in eq. 3.8. Despite smaller quantum yields, ϕ, neutral 3-Cl-aniline reacts approximately 4.5 times faster than the anilinium cation because photon-fluence based rate constants, $k^B_{E_P^0}$, and absorption coefficients, ϵ^B_{254}, exceed that of protonated 3-Cl-aniline by factors of 4.1 and 6.5, respectively (Table S3.1). We observed that only the presence of 1 M Cs^+ increased k_1 by 26% and thus beyond experimental uncertainty at solution pH 7.0 (see inset in Figure 3.6a). At this pH and at constant ionic strength of 1 M, none of the other ions exhibited any measurable effect on k_1. The lack of effect of a singlet quencher at all solution

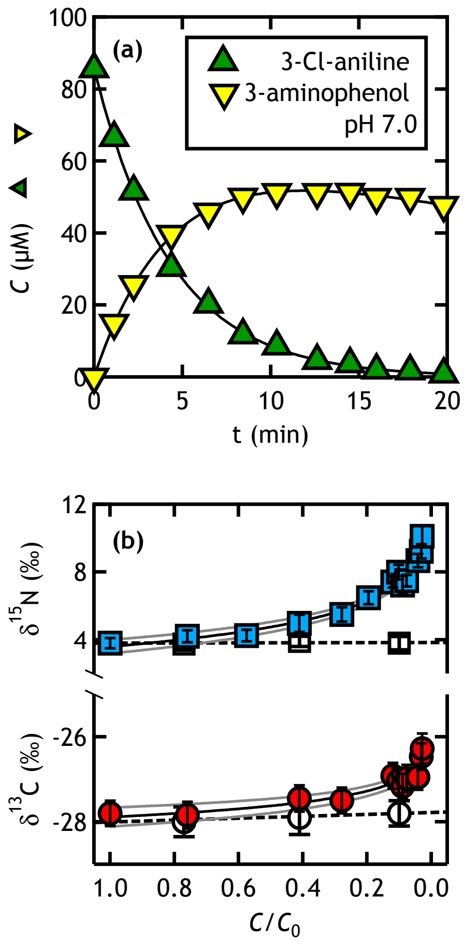

Figure 3.5 (a) 3-Cl-aniline and 3-aminophenol concentrations in photochemical experiments at pH 7.0. Solid lines were calculated with eqs. 3.6-3.7; (b) C and N isotope signatures (δ^{13}C (circles) and δ^{15}N (squares) of 3-Cl-aniline vs. fraction of remaining substrate, C/C_0. Uncertainties represent standard deviations of triplicate measurements. Solid lines correspond to calculated isotope fractionation using eq. 3.1; gray dashed-lines indicate 95% confidence interval of the fit. Empty symbols and dashed lines represent control experiments that were not irradiated.

pH-values implies the photolysis of 3-Cl-aniline happened primarily from excited triplet states. Moreover, because we did not observe an impact of varying concentrations of Cl^-or ClO_4^- on k_1, we conclude that Cl^--elimination during hydrolysis of excited state species may not have been rate-limiting or did not happen through a heterolytic pathway.

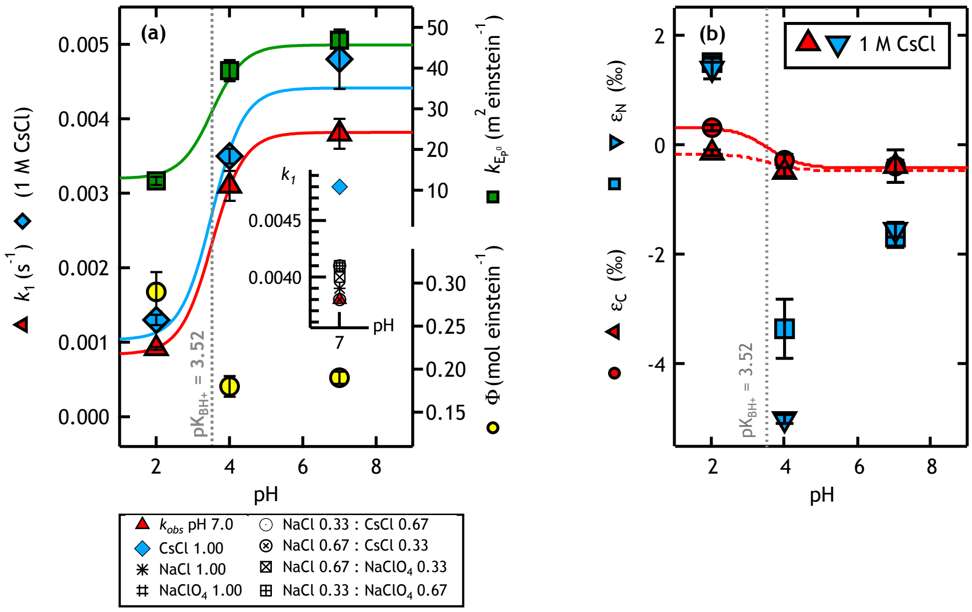

Figure 3.6 (a) Rate constants of 3-Cl-aniline photolysis: k_1 and $k_{E_P^0}$ are the observed pseudo-first order and photon-fluence based photolysis rate constants, respectively, ϕ is the reaction quantum yield. The inset shows k_1-values at pH 7.0 for different NaCl, CsCl, and $NaClO_4$ combinations at a total ionic strength of 1.0 M; (b) C and N isotope enrichment factors, ϵ_C and ϵ_N, of 3-Cl-aniline photolysis in the presence and absence of 1 M Cs^+ as singlet quencher. Solid lines represent calculated rate constants (eq. 3.8). The vertical dashed lines indicates the $p\mathrm{K}_{\mathrm{BH}^+}$ of ground state 3-Cl-aniline.

Isotope Fractionation and Kinetic Isotope Effects

Isotopic analysis shown in Figure 3.7a of experiments performed at three different solution pH confirms the kinetic analysis in that protonated 3-Cl-aniline species exhibit inverse C and N isotope fractionation, whereas the opposite trend was found for neutral species. C isotope fractionation, however, was only very minor and the magnitude of the calculated ϵ_C-values did not exceed 0.5‰ in either normal or inverse direction (Table 3.1). N isotope fractionation was larger than that for C isotopes even though no N atom is involved in the hypothesized hydrolysis reaction. In contrast to ϵ_C-values, those for ϵ_N shown in Figure 3.6b did not follow a weighted average of ϵ_N-values for protonated and neutral 3-Cl-aniline species, respectively (eq. 3.8), which made it impossible to quantify reliable $\epsilon_N^{\mathrm{BH}^+}$ and ϵ_N^{B} values.

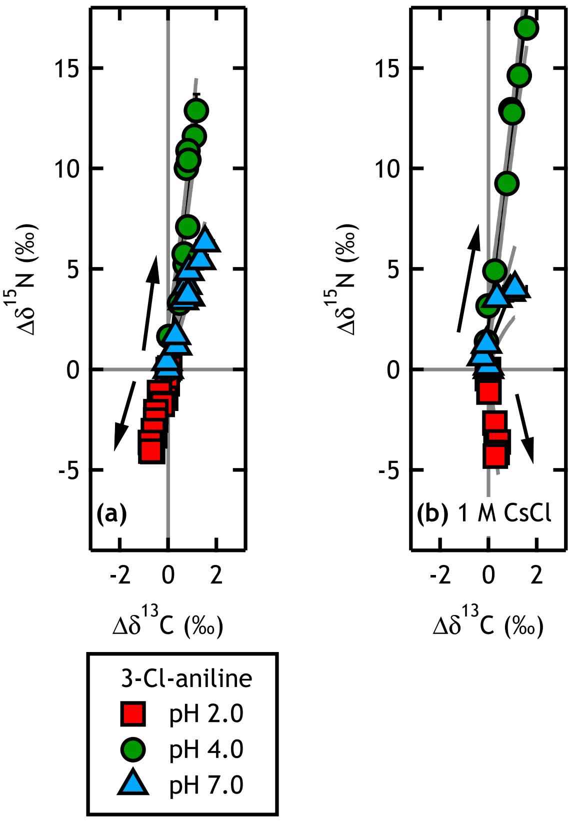

Figure 3.7 Correlation of C and N isotope fractionation ($\Delta\delta^{13}$C, $\Delta\delta^{15}$N) of 3-Cl-aniline for experiments performed at solution pH 2.0, 4.0, and 7.0 in the absence (a) and presence (b) of CsCl as singlet quencher. The grey lines delineate the initial 3-Cl-aniline isotope composition (δ^{13}C $= -27.8$‰, δ^{15}N $= 3.8$‰). Arrows indicate the direction of isotope fractionation with increasing reactant conversion. Error bars are smaller than marker size.

The inverse ϵ_N-values at pH 2.0 rule out contributions from equilibrium isotope effects associated with N-atom deprotonation, which would have caused measurable normal N isotope fractionation (i.e., $\epsilon_N < 0$). The presence of the singlet quencher Cs^+ did not affect C and N isotope fractionation except for experiments made at pH 4.0, where ϵ_N increased from -3.4 ± 0.5‰ to -5.0 ± 0.1‰ (Table 3.1, entries 7a,b). We have recently found that the pH-dependent N isotope fractionation associated with the direct photolysis of 4-Cl-aniline also resulted in ^{15}N-AKIEs, which did not follow from separate contributions of different 4-Cl-aniline species[107].

Instead, we hypothesized that pH-dependent isotope fractionation originated from spin selective photophysical processes, whose pH-dependence cannot be assessed based on ground state acidity constants. We conclude that such processes may have also been involved in the photolysis of 3-Cl-aniline at pH 4.0 with and without Cs^+. At pH 2.0 and 7.0, however, where ϵ_N-values were identical with and without Cs^+, dechlorination is not spin-selective and assumed to occur from excited triplet states. The ^{15}N-AKIEs of 3-Cl-aniline photolysis from 0.9985 to 1.005 compiled in Table 3.1 therefore reflect data for spin- and pH-dependent processes that cannot be extrapolated to other experimental conditions.

3.4 Implications

The position of aromatic Cl substitution in chloroanilines gives rise to subtle differences in photolysis mechanisms, which are related to the formation and reactivity of different excited state (radical) species. Our work illustrates that substituent positions also modulate the C and N isotope fractionation associated with photochemical dechlorinations. (i) The photolysis of 2-Cl-aniline to 2-aminophenol and products thereof exhibits a combination of normal ^{13}C- and inverse ^{15}N-AKIEs for the 2-Cl-anilinium cation whereas the neutral species react with inverse ^{13}C- and normal ^{15}N-AKIEs. Because isotope effects for dechlorination of both species were sensitive to the presence of a singlet quencher and therefore spin selective, we conclude that the ^{13}C- and ^{15}N-AKIEs originate from magnetic interactions. Based on the current knowledge, however, it is not possible to identify the processes leading to inverse vs. normal isotope fractionation. (ii) Even though the photolysis of 3-Cl-aniline also results in the formation of the corresponding aminophenol, the reaction is almost insensitive to C isotope composition. The observation that this reaction nevertheless exhibits moderate ^{15}N-kinetic isotope effects, which were partly spin- and pH dependent, suggests that the hydrolysis at the C-3 position was not rate-limiting and that photophysical processes may have determined isotope sensitivity. (iii) Our data for 2-Cl- and 3-Cl-aniline contrasts the C and N isotope fractionation trends associated with the photolysis of 4-Cl-aniline under identical experimental conditions. The latter reacts via excited state carbene species, and 4-Cl-aniline photolysis exhibited larger, highly pH-dependent, and exclusively normal ^{13}C- and ^{15}N-AKIEs up to 1.017 and 1.009, respectively. Experiments carried out with 4-Cl-aniline in presence and absence of Cs^{+} implied that photolysis happened from both excited singlet and triplet states whereas our data suggest that 2-Cl-aniline reacted predominantly from excited singlet states.

The comparison of ^{13}C- and ^{15}N-kinetic isotope effects shows that isotope fractionation in photochemical dechlorination reactions of organic water pollutants needs to be considered differently from that of thermal dechlorinations. C (and Cl) isotope fractionation associated, for example, with the reductive dechlorination of chlorohydrocarbons can be interpreted in terms of the kinetics of dissociative electron transfer reactions and the extent of C–Cl-bonding changes[36]. The understanding of C and Cl isotope effects therefore enables one to assess if, to what extent, and by which reaction pathway chlorohydrocarbons are degraded in the environment based on the observed C and Cl isotope fractionation. An interpretation of isotope fractionation trends of organic micropollutants exhibiting chloroaniline substructures (e.g., diclofenac), which may undergo photochemical transformations, however, requires a careful evaluation of reaction conditions. Given that C and N isotope fractionation of chloroanilines was highly variable with pH and position of Cl substitution, an extrapolation of the ^{13}C- and ^{15}N-AKIEs presented here to reactions in surface water requires a careful comparison of reaction conditions. On the other hand, the insights into the variability of isotope fractionation provided here offer new opportunities for fingerprinting photochemical dechlorination processes. Probing for the sensitivity of isotope fractionation through changes of water chemistry may provide an additional option to track photolytic dechlorinations.

Acknowledgement

This work was supported by the EU Initial Training Network CSI:Environment (Grant agreement no. 264'329). We thank an anonymous reviewer for valuable comments.

Supporting Information to Chapter 3

S3.1 Chemicals

Chemicals and gases were purchased from various manufacturers and used without further treatment. A list of compound names, purities, and suppliers follows. 2-Chloroaniline (≥99.5%), 3-chloroaniline (99%), cesium chloride (99.9%) and potassium phosphate monobasic (>99%) were purchased from Sigma-Aldrich (Buchs SG, Switzerland); hydrochloric acid (32%) and sodium hydroxide (98%), sodium chloride (>99%) were from Merck (Dietikon, Switzerland); methanol (for HPLC gradient) from Acros Organics (Geel, Belgium); All aqueous solutions were prepared in nanopure water (18.2 MΩ-cm, Barnstead NANOpure Diamond Water Purification System).

The carrier and reference gases for GC and GC/IRMS included helium (He, 99.999%), N_2 (99.9999%), CO_2 (99.999%), H_2 (99.999%), synthetic air (20 ± 1% O_2 in N_2, 99.9995%), O_2 (99.9995%) and, N_2 (99.9995%) from Carbagas (Rümlang, Switzerland).

S3.2 Tables

Table S3.1 Photon-fluence based, pseudo-first order reaction rate constants for the neutral ($k^{\mathrm{B}}_{\mathrm{E}^0_P}$) and conjugated acidic ($k^{\mathrm{BH}^+}_{\mathrm{E}^0_P}$) form of 2-, 3-Cl-aniline, measured at constant photon fluence rate at $\lambda = 254$nm. $\varepsilon^{\mathrm{B}}_{254}$ and $\varepsilon^{\mathrm{BH}^+}_{254}$ are the molar absorption coefficients while ϕ^{B} and ϕ^{BH^+} are the quantum yields obtained for 2-, 3-Cl-aniline in its neutral and conjugated acidic form. Uncertainties correspond to $\pm 1\sigma$.

Compound	$k^{\mathrm{B}}_{\mathrm{E}^0_P}$ (m^2 einstein^{-1})	$\varepsilon^{\mathrm{B}}_{254}$ (m^2 mol^{-1})	ϕ^{B} (mol einstein^{-1})	$k^{\mathrm{BH}^+}_{\mathrm{E}^0_P}$ (m^2 einstein^{-1})	$\varepsilon^{\mathrm{BH}^+}_{254}$ (m^2 mol^{-1})	ϕ^{BH^+} (mol einstein^{-1})
2-Cl-aniline	6.6 ± 0.5	56.1 ± 0.6	0.051 ± 0.004	4.5 ± 0.3	17.8 ± 0.4	0.109 ± 0.008
3-Cl-aniline	47.6 ± 1.8	111.9 ± 9.4	0.185 ± 0.017	11.5 ± 1.1	17.1 ± 5.5	0.292 ± 0.098

S3.3 Figures

S3.3.1 Direct photolysis of 2-Cl-aniline

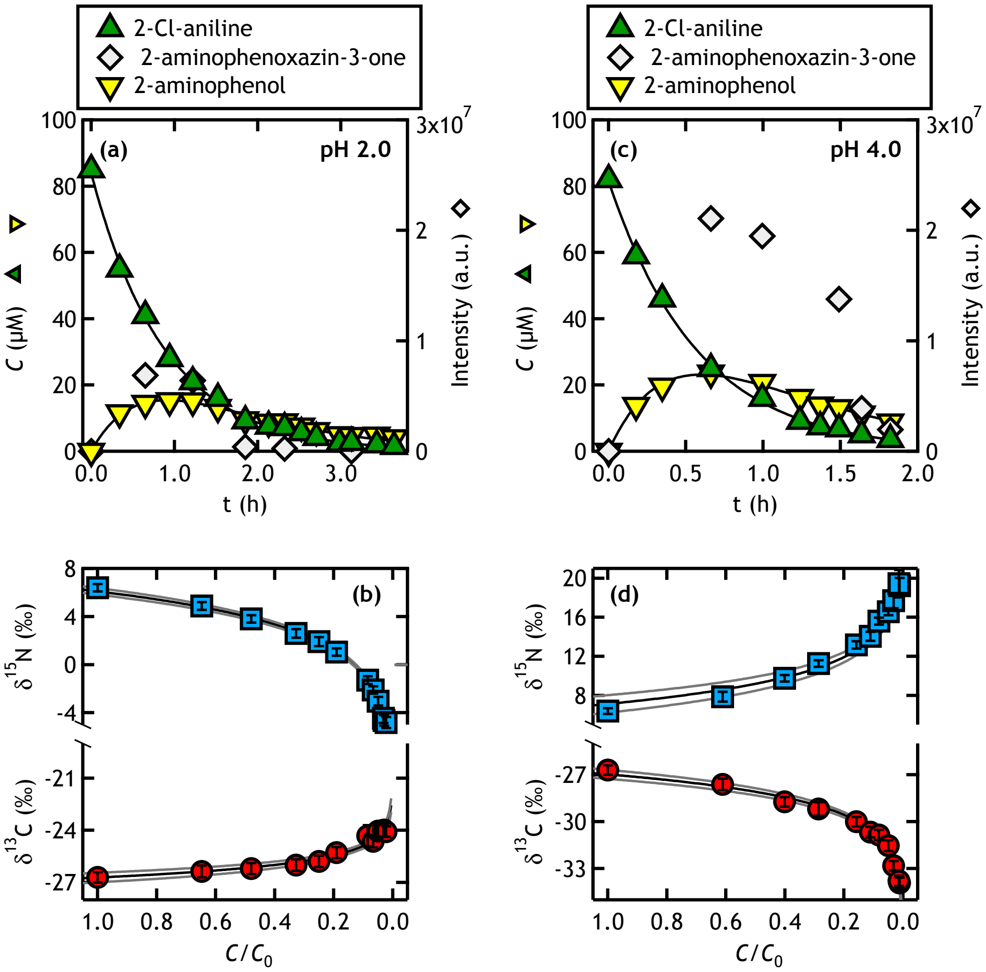

Figure S3.1 Direct photolysis of 2-Cl-aniline at pH 2.0 (panels a and b) and at pH 4.0 (panels c and d). (a, c) Concentration profiles of 2-Cl-aniline decay and 2-aminophenol ($\gamma^{2-\mathrm{Cl-aniline}}_{\mathrm{pH}=2.0} = 0.48 \pm 0.04$, $\gamma^{2-\mathrm{Cl-aniline}}_{\mathrm{pH}=4.0} = 0.53 \pm 0.06$) and signal areas of 2-aminophenoxazin-3-one ($C_{12}H_8N_2O_2$; m/z = 213.0659). Solid lines were calculated according to eqs. 3.6-3.7. (b, d) N and C isotope signatures (δ^{15}N (squares) and δ^{13}C (circles)) vs. fraction of the remaining substrate, C/C_0. Uncertainties represent standard deviations of triplicate measurements. Solid lines correspond to the calculated isotope fractionation according to eq. 3.1; gray-dashed lines indicate 95% confidence interval of the non-linear regression fit.

S3.3.2 Direct photolysis of 3-Cl-aniline

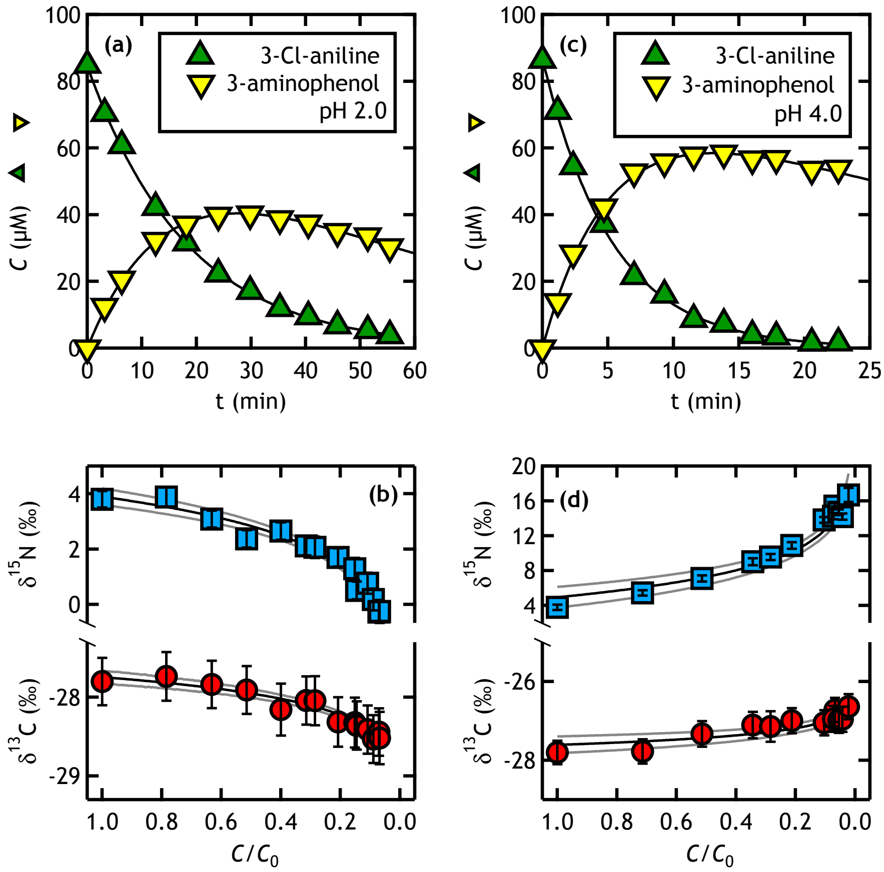

Figure S3.2 Direct photolysis of 3-Cl-aniline at pH 2.0 (panels a and b) and at pH 4.0 (panels c and d). (a, c) Concentration profiles of 3-Cl-aniline decay and 3-aminophenol ($\gamma_{\mathrm{pH=2.0}}^{\mathrm{3-Cl-aniline}} = 0.88 \pm 0.02$, $\gamma_{\mathrm{pH=4.0}}^{\mathrm{3-Cl-aniline}} = 0.90 \pm 0.03$). Solid lines were calculated according to eqs. 3.6-3.7. (b, d) N and C isotope signatures (δ^{15}N (squares) and δ^{13}C (circles)) vs. fraction of the remaining substrate, C/C_0. Uncertainties represent standard deviations of triplicate measurements. Solid lines correspond to the calculated isotope fractionation according to eq. 3.1; gray-dashed lines indicate 95% confidence interval of the non-linear regression fit.

S3.4 Product analysis

S3.4.1 Direct photolysis of 2-Cl-aniline and 2-aminophenol

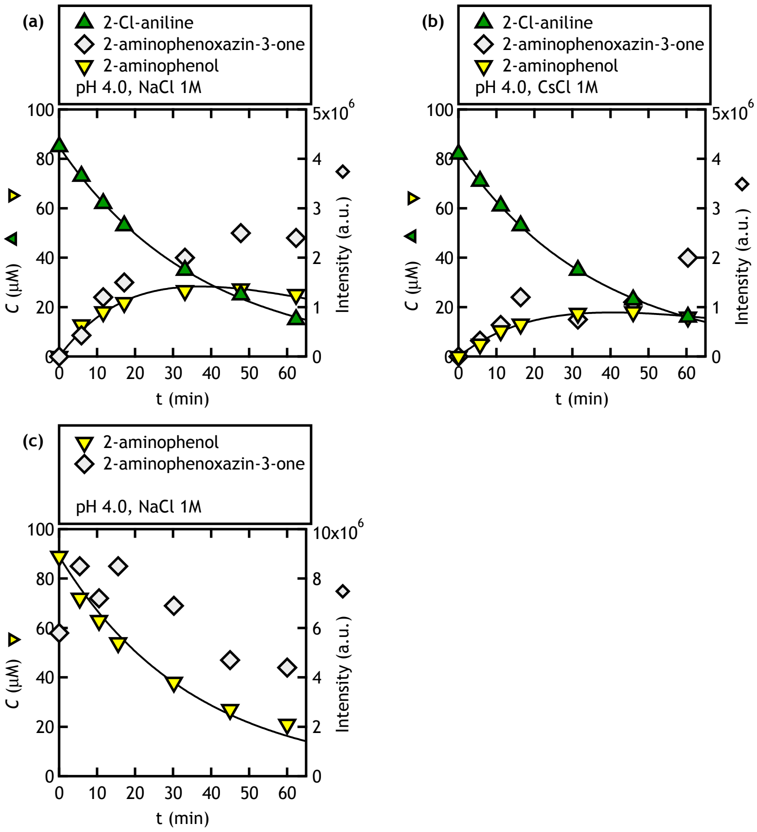

Figure S3.3 Direct photolysis of 2-Cl-aniline in the presence of 1.0 M NaCl (a) and 1.0 M CsCl (b) at pH 4.0. Direct photolysis of 2-aminophenol (c) in solutions containing 1.0 M NaCl. Grey diamonds show the signal area of 2-aminophenoxazin-3-one ($C_{12}H_8N_2O_2$; m/z = 213.0659). Solid lines were calculated according eqs. 3.6-3.7.

S3.4.2 Direct photolysis of 3-Cl-aniline

Formation of 3-aminophenol at different solution pH-values and different concentration of dissolved ions ($I = 1$ M).

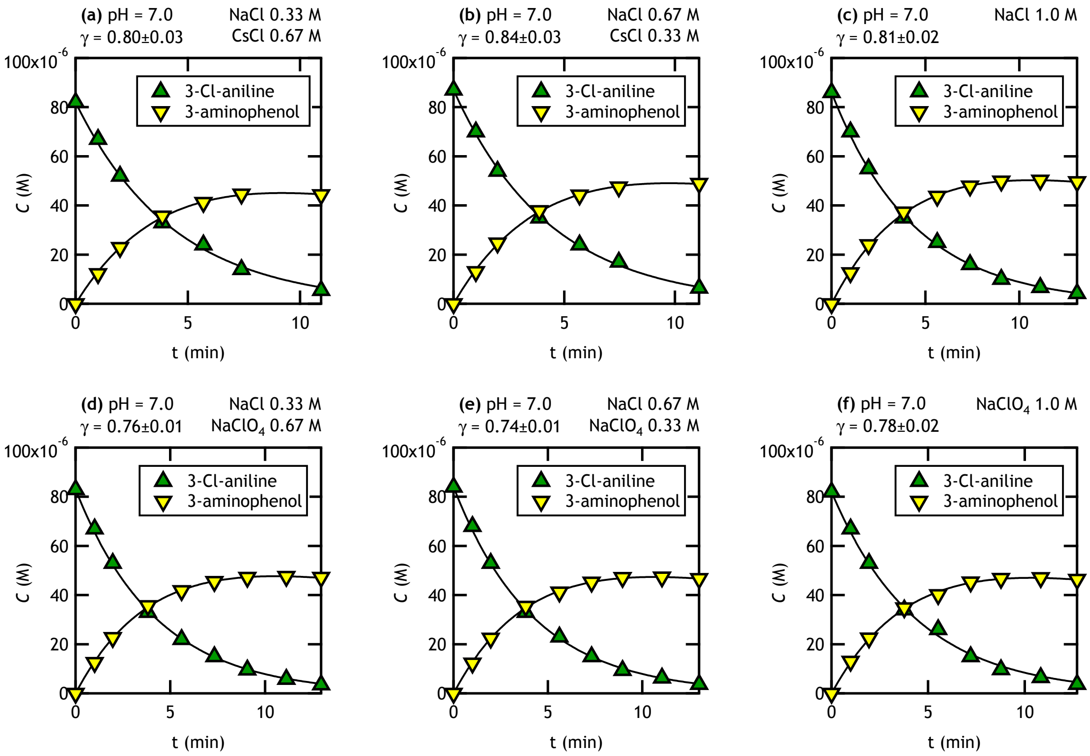

Figure S3.4 Direct photolysis of 3-Cl-aniline at pH 7.0 in the presence of different concentrations of Na^{+}, Cs^{+}, Cl^{-}, and ClO_4^{-} at constant ionic strength I of 1.0 M. Solid lines were calculated according eqs. 3.6-3.7.

Formation of deuterated aniline

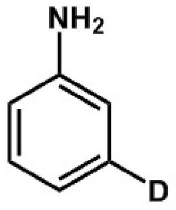

(i)

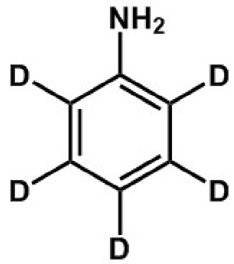

(ii)

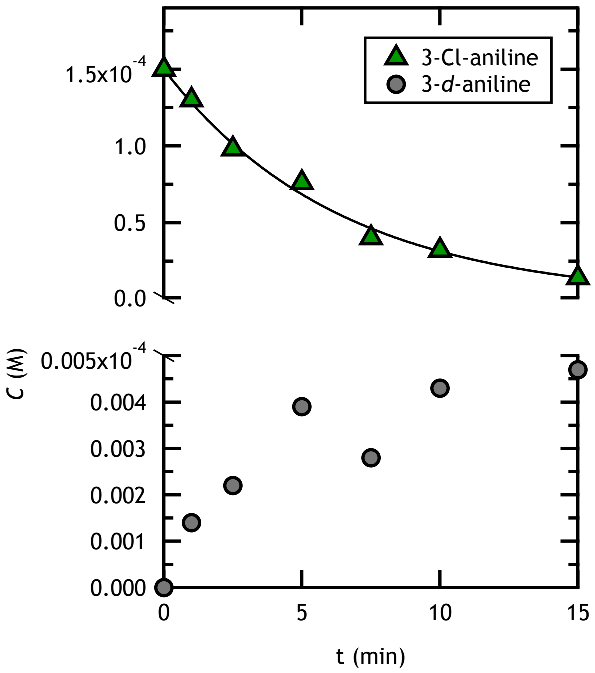

Figure S3.5 Direct photolysis of 3-Cl-aniline in an aerated solution at pH 7.0 containing 1.0 M d_8-isopropanol. Concentration profiles of 3-Cl-aniline and 3-D-aniline (i, C_6DH_6N; m/z = 94). d_5-Aniline (ii, $C_6D_5H_2N$; m/z = 98) was used as analytical standard for the calibration of 3-D-aniline. The solid line was calculated according to eq. 3.6.

S3.5 Inner filter light-screening factors (S_{254})

S3.5.1 Direct photolysis of 2-Cl-aniline

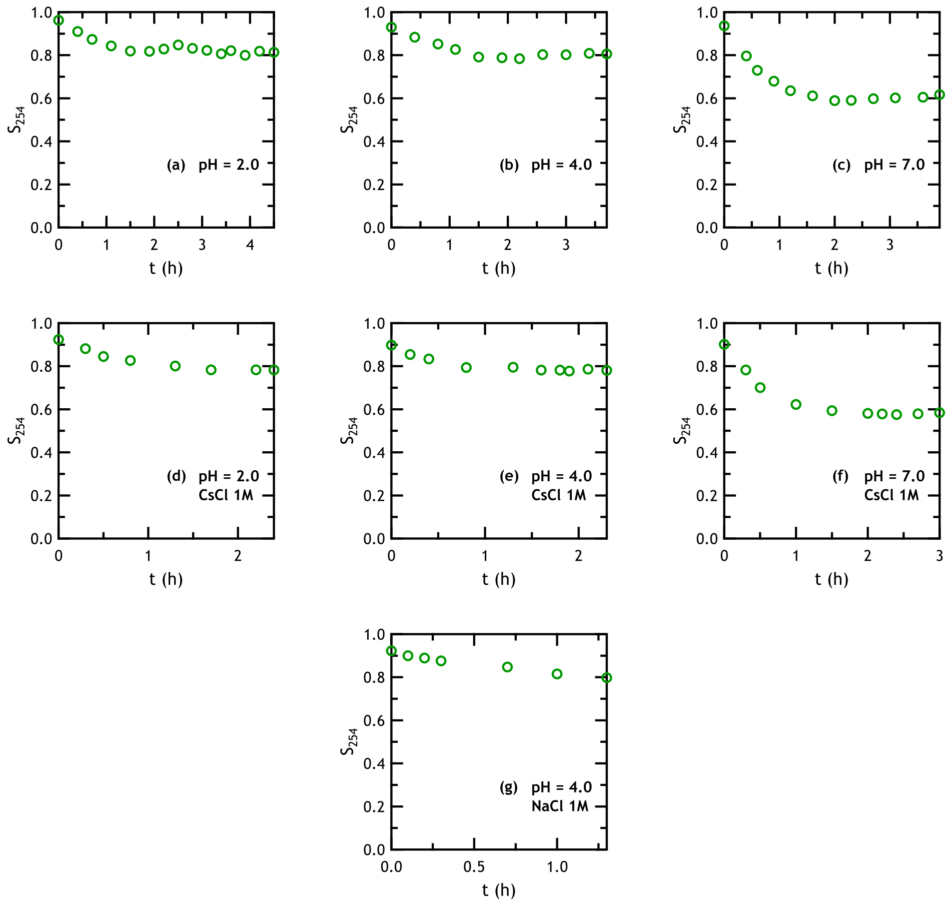

Figure S3.6 Inner-filter light screening factors (S_{254}) calculated at $\lambda = 254$ nm vs. irradiation time according to Ratti et al. [107] for the direct photolysis of 2-Cl-aniline over a pH range from 2.0 to 7.0 without addition of NaCl (panels a-c) , in the presence of 1.0 M CsCl (panels d-f) or 1.0 M NaCl (panel g).

S3.5.2 Direct photolysis of 3-Cl-aniline

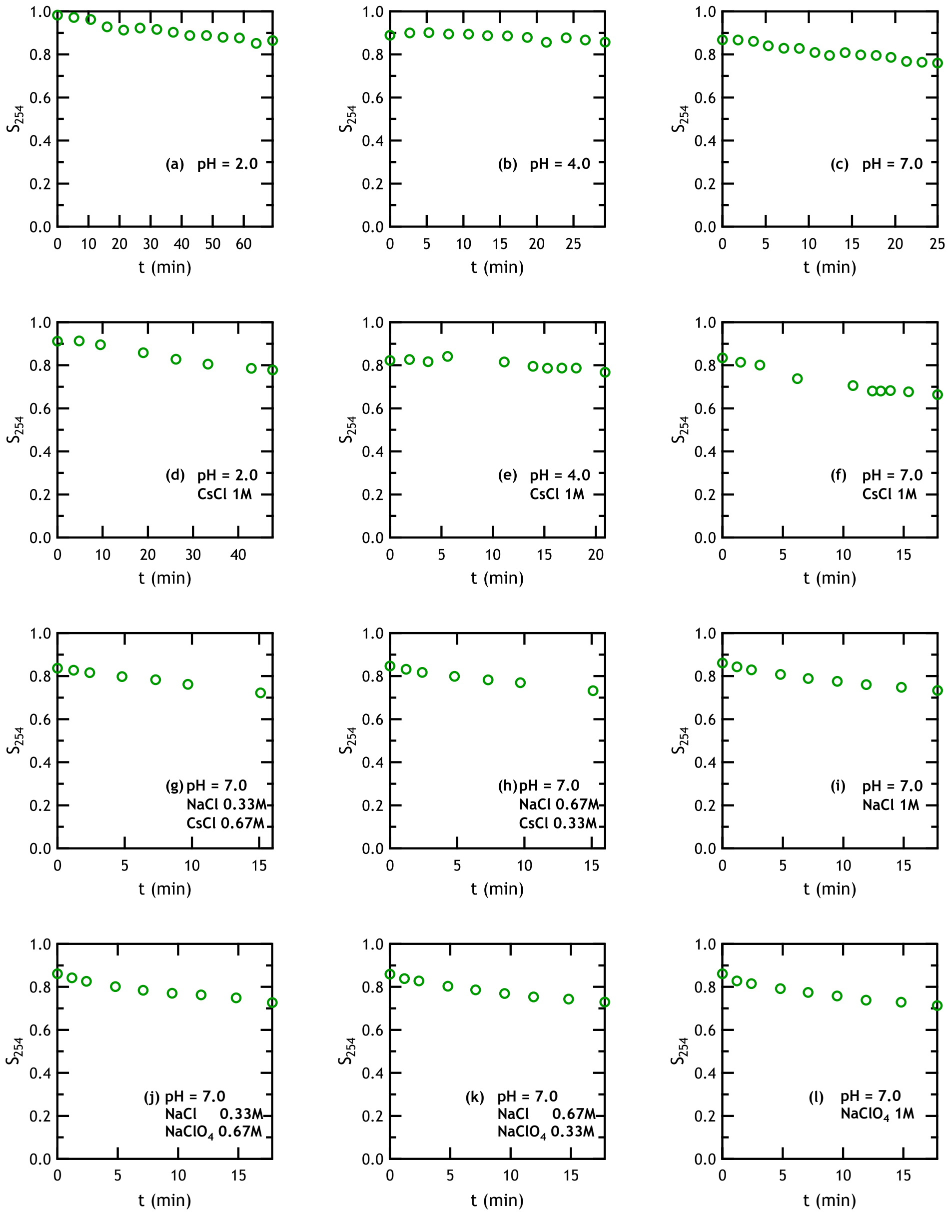

Figure S3.7 Inner-filter light screening factors (S_{254}) calculated at $\lambda = 254$ nm vs. irradiation time according to Ratti et al.[107] for the direct photolysis of 3-Cl-aniline over a pH range from 2.0 to 7.0 without addition of NaCl (panels a-c), in the presence of CsCl 1.0 M at pH 7.0 (panels d-f), and at pH = 7.0 at variable NaCl, $NaClO_4$ and CsCl concentration (panels g-l) with constant ionic strength of 1.0 M.

S3.6 UV-vis absorption spectra

S3.6.1 Direct photolysis of 2-Cl-aniline

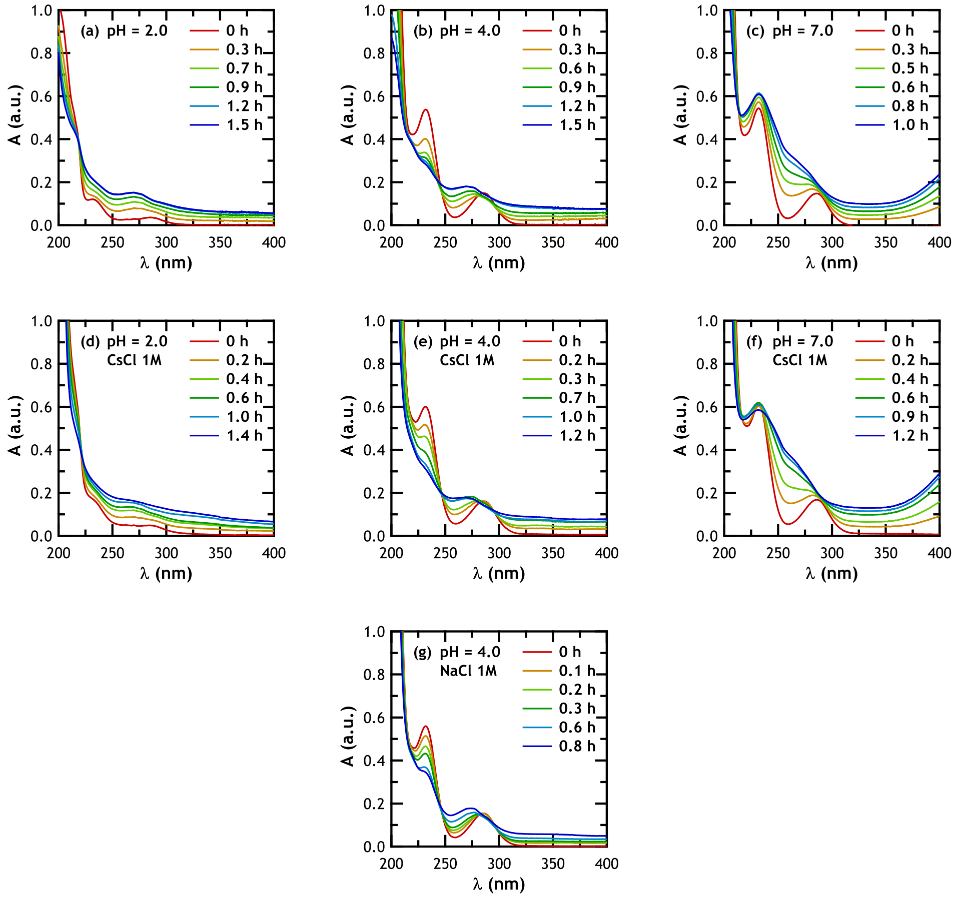

Figure S3.8 Evolution of UV-vis absorption spectra during direct photolysis of 2-Cl-aniline over a pH range from 2.0 to 7.0 without added salts (panels a-c) and in the presence of 1.0 M concentrations of CsCl (panels d-f) and NaCl (panel g), respectively. Optical path length was 1 cm, initial 2-Cl-aniline concentration $= 80\mu$M.

S3.6.2 Direct photolysis of 3-Cl-aniline

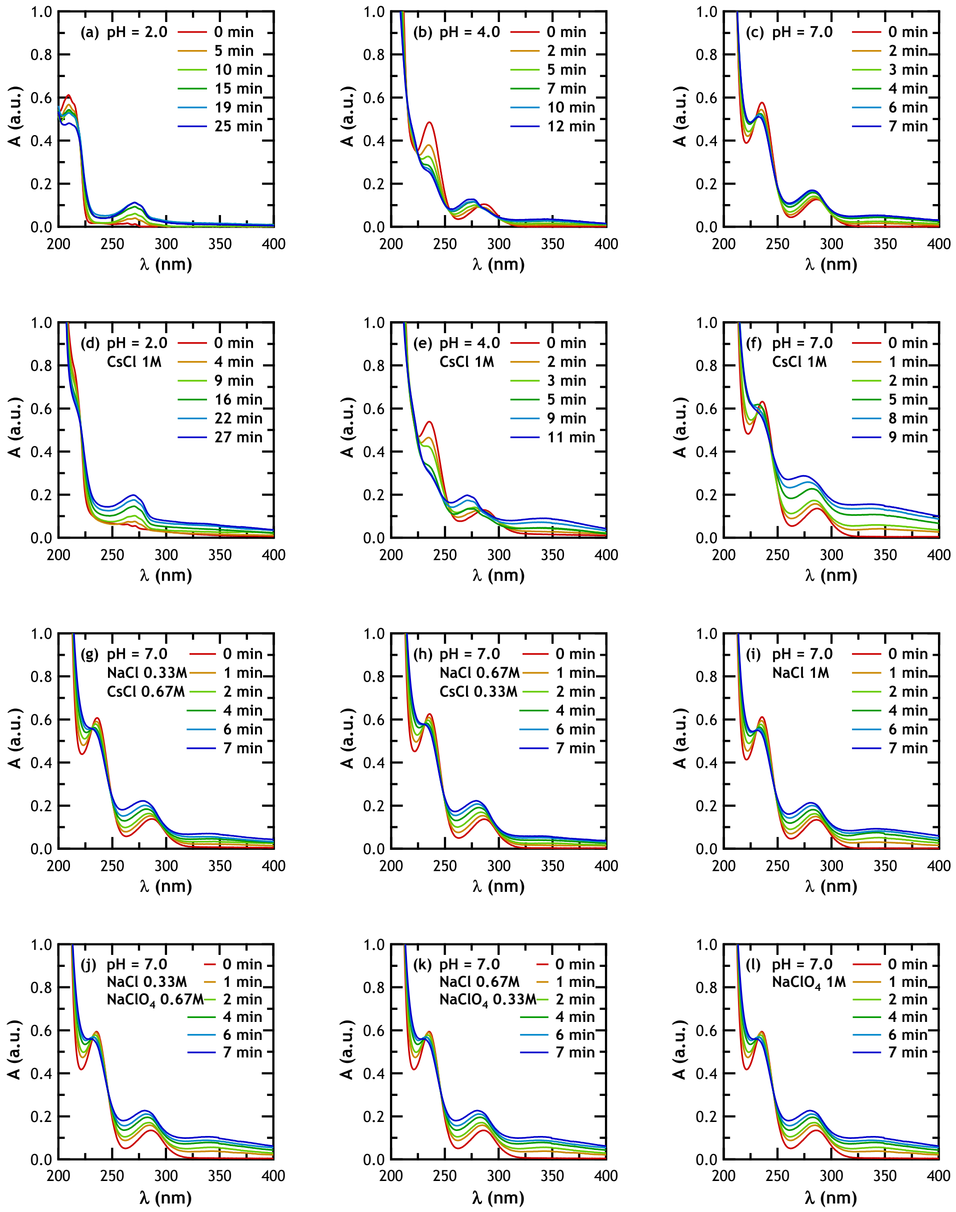

Figure S3.9 Evolution of UV-vis absorption spectra during direct photolysis of 3-Cl-aniline over a pH range from 2.0 to 7.0 without added salts (panels a-c), in the presence of 1.0 M concentrations of CsCl at pH 7.0 (panels d-f). Panels g-l show UV-vis spectra at pH 7.0 at different concentrations of NaCl, $NaClO_4$ and CsCl. Optical path length was 1 cm, initial 3-Cl-aniline concentration $= 80\mu$M.

Chapter 4

Isotope Fractionation Associated with the Indirect Photolysis of Substituted Anilines in Aqueous Solution

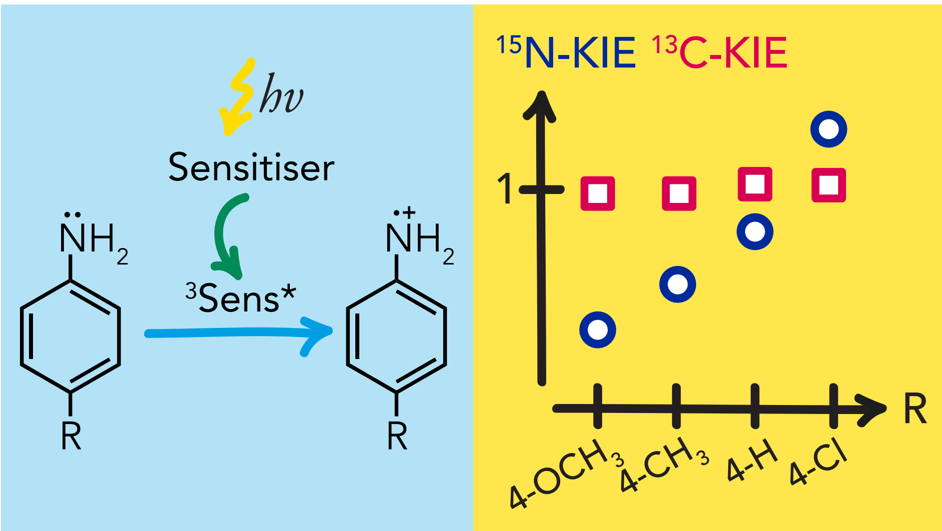

M. Ratti, S. Canonica, K. McNeill, J. Bolotin and T. B. Hofstetter. Isotope fractionation associated with the indirect photolysis of substituted anilines in aqueous solution. *submitted to Environ. Sci. Technol.*

Abstract

Organic micropollutants containing aniline substructures are susceptible to different light-induced transformation processes in aquatic environments and water treatment processes. Here, we investigated magnitude and variability of C and N isotope fractionation of four *para*-substituted anilines associated with the indirect photolysis to support the elucidation of aromatic amine transformation pathways in sunlit surface waters. Experiments were conducted in aerated aqueous solutions at irradiation wavelengths $\geq$ 400 nm, which contained model photosensitizers for excited triplet states of dissolved organic matter, namely anthraquinone disulfonate ($^3AQDS^{2-*}$) and methylene blue ($^3MB^{+*}$). Transformation of aniline, 4-CH_3-, 4-OCH_3- and 4-Cl-aniline by ($^3AQDS^{2-*}$) and methylene blue ($^3MB^{+*}$) was associated with inverse and normal N isotope fractionation whereas C isotope fractionation was negligible. The apparent ^{15}N-kinetic isotope effects (AKIE) were almost identical for both photosensitizers, increased from 0.9958 ± 0.0013 for 4-OCH_3-aniline to 1.0035 ± 0.0006 for 4-Cl-aniline, and correlated well with the electron donating properties of aromatic substituent. N isotope fractionation is pH-dependent in that it is dominated by H^+ exchange reactions below and N atom oxidation processes above the pK_a-value of the substituted aniline's conjugate acid. Our data show that the correlation of C and N isotope fractionation for direct and indirect photolysis is different to distinguish the two degradation pathways if they occurred simultaneously.

4.1 Introduction

Numerous organic micropollutants contain aniline substructures, which are often responsible for the initial steps of degradation in aquatic environments as well as in water treatment processes[126]. Such reactions include oxidations by dissolved, particle-bound oxidants, and enzymes, additions to electrophilic sites of organic matter, as well as direct photolysis[21,23,24,27,40,48,64,75,79,95,112,120,145,154]. In addition to adverse effects caused by the parent compound, an identification of the predominant transformation pathways is essential for the assessment of risks for human health and the environment because these processes can give rise to products of equal or even greater (eco)toxicity[127]. However, products of such reactions (e.g., high molecular weight radical coupling products) are numerous and usually difficult to analyse quantitatively for example, when bound to organic matter. We have therefore proposed to use compound-specific isotope analysis (CSIA[35,38,57,61]) and quantify the share of different degradation reactions from the change in stable C, H, and N isotope ratios in the residual contaminants containing aromatic amine moieties[102,107,133–135].

Stable isotope based approaches for organic micropollutants offer interesting possibilities to assess the fate of N-containing contaminants, even if competing reaction pathways occur and reaction products are partially unknown[89,103,104,107,139 67,88,125,162–164]. Depending on the chemical bond(s) broken or formed, stable isotope compositions measured in the remaining fraction of a contaminant molecule change over time and distance from the pollution source due to kinetic and equilibrium isotope effects[166]. Examples of redox reactions of triazine and phenylurea herbicides, nitroaromatic explosives show that especially the combination of N isotope fractionation with that for C and H are indicative for the ongoing transformation processes and, in many instances, also enable the quantification of the extent of degradation[56,88,104,108,163]. An application of CSIA-based procedures for micropollutants with aromatic amine functional groups is currently hampered because the isotope effects associated with the important degradation routes are not fully known.

In aerobic surface waters, direct photolysis as well as enzymatic, mineral-catalyzed, and photochemical oxidations are considered as major elimination routes.

Some of these processes were shown to cause substantial C and N isotope fractionation which originates from isotope effects of different reaction mechanisms. For example, the direct photolysis of chlorinated anilines is subject to C and N isotope fractionation from photophysical processes during dechlorination of excited state species[106,107]. Enzymatic oxidations in metabolic reactions, on the other hand, involve dioxygenation of the aromatic ring[102] while cometabolic oxidations have been proposed to be initiated by single electron transfer at the N atom[84,135]. The latter is also the predominant pathway of MnO_2-catalyzed oxidations of aromatic amines[134,135]. The apparent kinetic isotope effects (AKIEs) of oxidative degradation routes originate predominantly from the change of bonding to N atom. We have proposed that an increase in C–N bond strength in the resulting imine bonds was responsible for the often observed inverse N isotope fractionation[102,134,135]. Even though the understanding of KIEs requires further investigation, current evidence suggest that thermal reactions lead to only minor C isotope fractionation as opposed to direct photolysis, where both C and N isotope fractionation matter. However, it is currently unclear, whether oxidations caused by dissolved oxidants, for example those generated in the presence of light (e.g., excited triplet states of dissolved organic matter) also follow the trends found for mineral-catalyzed oxidations.

The goal of the present work was therefore to investigate the C and N isotope effects associated with the sensitised photolysis of aromatic amines and to evaluate whether the resulting C and N isotope fractionation trends enable the elucidation of aromatic amine transformation pathways in sunlit surface waters. To this end, we studied ^{13}C- and ^{15}N-AKIEs pertinent to the oxidation of substituted anilines by triplet states of transient photooxidants generated through light absorption of dissolved organic matter (^{3}DOM). Laboratory experiments were carried out with anthraquinonesulfonates and methylene blue as model compounds for ^{3}DOM. We illustrate the typical C and N isotope fractionation trends associated with the indirect photolysis of substituted anilines and its pH dependence with 4-methylaniline as example. For the discussion of isotope effects from different photooxidants as well as those from mineral-catalyzed oxidations, we compare data from experiments with aniline and three *para*-substituted anilines, namely, 4-methyl-, 4-methoxy-, and 4-chloroaniline with regard to their substituent effects on the observable C and N isotope fractionation.

4.2 Experimental Section

A list of chemicals including their purities and suppliers can be found in the Supporting Information (SI).

4.2.1 Chemical Analysis

We measured the concentrations of aniline, 4-methylaniline (4-CH_3-aniline), 4-methoxyaniline (4-OCH_3-aniline) and 4-chloroaniline (4-Cl-aniline) with reversed-phase HPLC and UV-vis detection (Dionex UltiMate 3000). Two different eluent compositions (40/60 vol % and 30/70 % vol) of methanol and 1 mM KH_2PO_4 buffered at pH 7.0 were used with a flow rate of 1 mL min^{-1} and a sample injection volume of 20 μL on a Supelcosil LC-18 (25 cm $\times$4.6 mm, 5μm)[107,134]. Transformation products were analysed by LC-MS/MS in positive ion mode using an LTQ (Linear Trap Quadrupole) Orbitrap mass spectrometer (Thermo) with electrospray ionization as documented previously[134,135]. Gradient elutions were run from 90/10 to 5/95 vol % ratios of H_2O/MeOH (containing 0.1 vol % formic acid) on Atlantis C-18 (15 cm $\times$ 3.0 mm, 3 μm) and XBridge C-18 (5 cm $\times$ 2.1 mm, 3.5 μm) columns from Waters. Identification of the products was based on exact mass and fragmentation patterns due to the lack of standard reference material. The postulated molecular structures are shown in the SI.

4.2.2 Stable Isotope Analysis

C and N isotope ratios of substituted anilines were measured by gas chromatography coupled to isotope ratio mass spectrometry (GC/IRMS) after solid-phase microextraction (SPME) with polydimethylsiloxane/divinylbenzene (PDMS/DVB, Supelco) fibers as described previously[107,133]. The combustion interface of the GC/IRMS was equipped with a Ni/Pt oxidation reactor[138]. Due to pK_a-values of the substituted aniline's conjugate acid between 4.0 and 5.3,[126] we adjusted pH-values of aqueous samples to pH 7.0 and 7.5 to avoid isotope fractionation from

H^+-exchange reactions.

C and N isotope signatures, $\delta^{13}C$ and $\delta^{15}N$, are given as arithmetic mean of triplicate measurements ($\pm\sigma$) in per mil (‰). Isotopic standard materials purchased from Indiana University were used to report $\delta^{13}C$- and $\delta^{15}N$-values relative to Vienna PeeDee Belemnite and air, respectively. C and N isotope analysis was performed within the method quantification limits (MQLs) of the SPME-GC/IRMS procedure[72]. MQLs for $\delta^{13}C$ and $\delta^{15}N$ amounted to 1.0 and 2.5 μM for 4-Cl-aniline, 2.0 μM and 3.5 μM for aniline and 4-CH_3-aniline, as well as 4.0 μM to 25.0 μM for 4-OCH_3-aniline. Samples were diluted to concentrations yielding peak amplitudes between 0.5 and 3 V. A standard bracketing procedure, referenced to a calibrated in-house standards of aniline, 4-Cl-aniline, 4-CH_3-aniline and 4-OCH_3-aniline of known $\delta^{13}C$ and $\delta^{15}N$-values, was used to ensure accuracy of the isotope ratio measurements.

4.2.3 Photochemical experiments

Batch experiments were carried out with aniline, 4-CH_3-aniline, 4-OCH_3-aniline, and 4-Cl-aniline and two photosensitizers, that is 9,10-anthraquinone-1,5-disulfonate (AQDS) and methylene blue (MB), respectively. For experiments with AQDS, 20 mL reactors typically contained 1 mM of the photosensitizer, 10 mM phosphate buffer (pH 7.0), and 100 μM of initial concentration of the substituted aniline. Due to the low extraction efficiency of 4-OCH_3-aniline with solid-phase microextraction (see below), experiments with this substrate were carried out with initial concentrations of 800 μM at pH 7.5. Experiments with MB were carried identically except for the lower photosensitizer concentrations of 30 μM (100 μM with 4-OCH_3-aniline). The pH dependence of the sensitized photolysis of substituted anilines was studied in reactors containing 1 mM of AQDS and 100 μM of 4-CH_3-aniline in the pH range between 2.0 to 7.0. Control experiments were carried out identically except for the addition of the photo-sensitizers.

All solutions were irradiated in glass-stoppered quartz tubes (OD 18 mm, ID 15 mm) equipped with magnetic stirring bars filled with 20 mL of reaction solution after introducing them into a DEMA 125 merry-go-round photoreactor (Hans Mangels GmbH, Bornheim-Roidorf, Germany) equipped with a Heraeus Noblelight model TQ 718 medium-pressure mercury (MP Hg) lamp operating at 500 W[156]. A borosilicate glass cooling jacket and a combination of 0.25 M sodium nitrate and 0.05 M sodium nitrite filter solutions restricted transmission of wavelengths to $\geq$ 400 nm. A recirculating pure water bath kept the reaction temperature at 25.0 ± 0.2 ℃. Production of excited triplet states of the photosensitizer was initiated by irradiation of polychromatic light at wavelengths above 400 nm, where the investigated substituted anilines did not absorb light. Reactions were stopped by removing the quartz tubes from the light source. Experiments with AQDS as photosensitizer required between 2.5 and 20 hours whereas those with MB could be carried out within 6 to 60 minutes.

At predefined time points, which we evaluated in test experiments, reactions were stopped and the entire volume of the quartz tube was used for concentration and isotope ratio analysis. Reactors from experiments with AQDS were also subject to product analysis by high-resolution mass spectrometry as described earlier[107,134]. Typically, 9 to 15 samples were generated with fractional substrate conversion of up to 95% out of which at least 8 reactors were processed further. Only in experiments with 4-OCH_3-aniline, fractional conversion was lower. The pH-values of aqueous samples were adjusted to 7.0 and 7.5 to avoid N isotope fractionation by H^+-exchange reactions[133]. UV-vis absorption spectra were acquired on a Cary 100 spectrophotometer, to verify photosensitizer decay. While MB concentration dropped during the experiments, that of AQDS remained constant.

4.2.4 Data evaluation

A linear regression analysis of δ^{13}C- and δ^{15}N- values, respectively, vs. fractional amount of remaining reactant ratio (C/C_0) (eq. 4.1) was used to derive bulk compound C and N isotope enrichment factors (ϵ_C, ϵ_N). Based on the assumption that oxidation occur exclusively at the N atom, we derived apparent ^{13}C- and ^{15}N-kinetic isotope effects (AKIEs) with eq. 4.2. ^{13}C-AKIEs thus represent the weighted average of secondary isotope effects of all C atoms.

$$ln\left(\frac{\delta^{\mathrm{h}}\mathrm{E}+1}{\delta^{\mathrm{h}}\mathrm{E}_0+1}\right)=\epsilon_{\mathrm{E}}\cdot ln\left(\frac{C}{C_0}\right) \tag{4.1}$$

$$\mathrm{AKIE_E}=\frac{1}{1+\epsilon_{\mathrm{E}}} \tag{4.2}$$

where $\delta^{\mathrm{h}}\mathrm{E}_0$ and $\delta^{\mathrm{h}}\mathrm{E}$ stand for the measured isotope signatures of an element E at time zero and at different amounts of fractional conversion, respectively.

We accounted for contributions of primary ^{15}N and secondary ^{13}C equilibrium isotope effects from H^+ exchange on the observable N and C isotope fractionation assuming a sequential reaction as in eqs. 4.3 and 4.4.

$$\mathrm{BH^+} \underset{k_2}{\overset{k_1}{\rightleftharpoons}} \mathrm{B}+\mathrm{H^+} \xrightarrow{k_3} \mathrm{P} \tag{4.3}$$

$$k_{\mathrm{obs}}=\frac{k_1\times k_3}{k_2[\mathrm{H^+}]+k_3} \tag{4.4}$$

where k_1 and k_2 are reaction rate constants of H^+ exchange at the aromatic amino group, k_3 stands for the oxidation of the neutral species to radical products (P), and k_{obs} is the overall rate constant of product formation. As shown by Skarpeli-Liati et al.[134], isotope fractionation on k_{obs} reflect the isotope fractionation of the protonated and neutral species as in eq. 4.5.

$$\epsilon_{\mathrm{E}}=\frac{1}{\alpha_{\mathrm{BH^+}}\cdot \mathrm{EIE_E^{BH^+}}\cdot \mathrm{AKIE_E^B}+\left(1-\alpha_{\mathrm{BH^+}}\right)\cdot \mathrm{AKIE_E^B}}-1 \tag{4.5}$$

where E stands for either N or C isotopes and $\alpha_{\mathrm{BH^+}}$ is the fraction of protonated substituted aniline corresponding to $\left(1+10^{\mathrm{pH}-\mathrm{p}K_{\mathrm{BH^+}}}\right)^{-1}$. $\mathrm{EIE_E^{BH^+}}$ are the ^{15}N and ^{13}C equilibrium isotope effect for the deprotonation of BH^+, $\mathrm{AKIE_E^B}$ are the apparent ^{15}N and ^{13}C kinetic isotope effects of the oxidation reaction of B.

4.3 Results and Discussion

4.3.1 Oxidation of substituted anilines by excited triplet states of anthraquinonedisulfonate ($^3AQDS^{2-*}$)

Isotope fractionation of 4-CH_3-aniline

The transformation of 4-methylaniline (4-CH_3-aniline) in irradiated solutions containing 1 mM of 9,10-anthraquinone-1,5-disulfonate (AQDS) at pH 7.0 is shown in Figure 4.1a. The disappearance of 4-CH_3-aniline was accompanied by the formation of products of higher molecular weight, typically di- and trimers of partially reacted substrate (Figure S4.3, Supporting Information). The products are indicative of coupling reactions of radical intermediates formed through N atom oxidation[134,135]. Transformation of substituted anilines by such oxidative processes have been observed not only after irradiation of aqueous solutions containing photosensitizers but also in mineral- and enzyme catalyzed reactions[32,75,109].

Oxidation of 4-CH_3-aniline by excited triplet states of AQDS ($^3AQDS^{2-*}$) resulted in inverse N isotope fractionation corresponding to a N isotope enrichment factor, ϵ_N, of $3.6 \pm 0.9‰$ (entry 3a in Table 4.1). C isotope fractionation associated with 4-CH_3-aniline oxidation was also inverse ($\epsilon_C = 0.9 \pm 0.4‰$) but almost negligible, that is $\delta^{13}C$ only decreased by 2‰ after more than 95% of substrate conversion (Figure 4.1b). We did not observe changes in C and N isotope ratios in irradiated solutions that did not contain AQDS. The observed combination of inverse N and negligible C isotope fractionation for the oxidation of 4-CH_3-aniline by $^3AQDS^{2-*}$ matches previous observations where N atom oxidation lead to the formation of radical intermediates[102,134,135]. The aromatic amino group in radical intermediates was suggested to exhibit partial imine character in the transition state and thus stronger C–N bonds. C isotope fractionation partly reflects this partial imine bonding to a minor extent because none of the C atom is directly involved in the reaction. The apparent primary ^{15}N- and secondary ^{13}C-kinetic isotope effects calculated with eq. 4.2 amount to 0.9960 ± 0.0009 and 0.9991 ± 0.0004, respectively (Table 4.1).

Note that the disappearance kinetics of 4-CH_3-aniline were slightly biphasic and included fast initial transformation followed by a decreasing reaction rate.

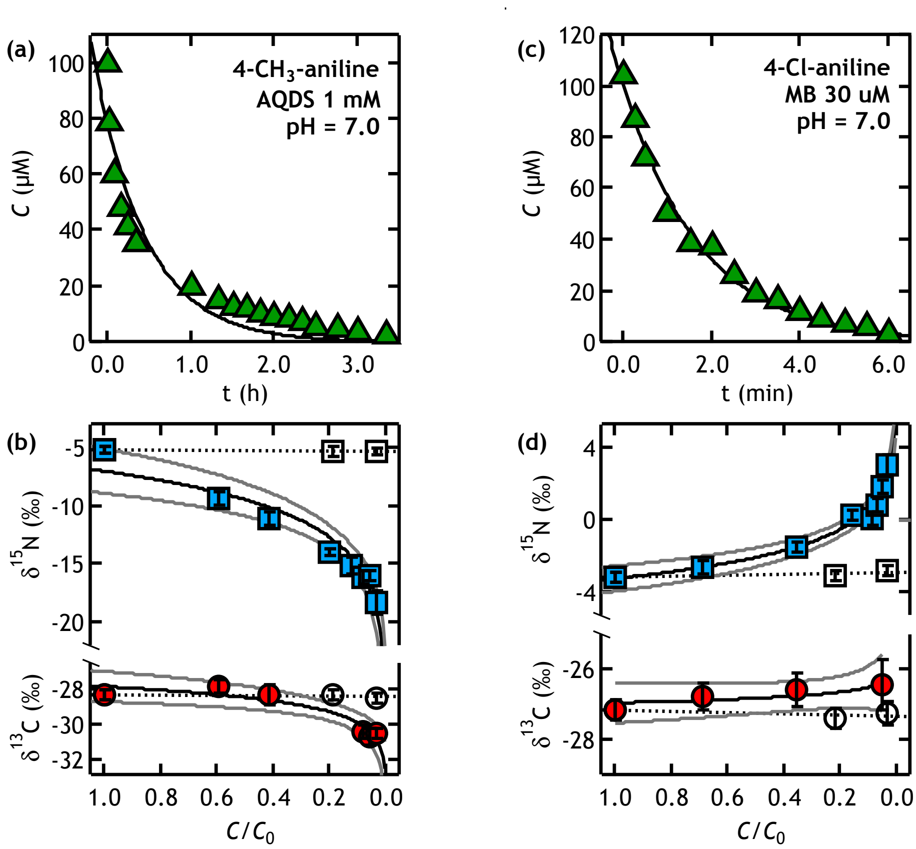

Figure 4.1 Transformation of 4-CH_3-aniline (panels a, b) by $^3AQDS^{2-*}$ and of 4-Cl-aniline (panels c, d) by $^3MB^{+*}$ at pH 7.0. Panels (a) and (c): substituted aniline concentrations. Solid lines show pseudo-first-order decay kinetics. Panels (b) and (c): C and N isotope signatures (δ^{13}C, circles, δ^{15}N, squares) vs. fraction of remaining substrate (C/C_0). Uncertainties represent standard deviations of triplicate measurements. Solid lines were calculated with eq. 4.1; gray-dashed lines are 95% confidence interval. Control experiments were treated identically but reactors did not contain photosensitizers (empty symbols, dashed lines).

The latter could have been due to quenching of $^3AQDS^{2-*}$, light screening by reaction products, and a reduction of the partial intermediates to the parent compound[21,23,155–157]. Because the C and N isotope fractionation trends remained constant throughout the reaction, none of the processes seemed to impact the isotope fractionation behaviour from the oxidation reaction.

Table 4.1 C and N isotope enrichment factors (ϵ_C, ϵ_N), apparent ^{13}C-, ^{15}N-kinetic isotope effects (^{13}C and ^{15}N-AKIE), as well as isotope fractionation slopes $\Delta\delta^{15}N/\Delta\delta^{13}C$ of experiments with irradiated solution containing anthraquinone disulfonate (AQDS) and methylene blue (MB), respectively. [a,b]

Entry	Compound	pH	ϵ_C (‰)	ϵ_N (‰)	^{13}C-AKIE [c] (-)	^{15}N-AKIE [c] (-)	$\Delta\delta^{15}N/\Delta\delta^{13}C$ (-)
$^3AQDS^{2-*}$							
1	Aniline	7.0	−1.4 ± 0.5	1.3 ± 0.2	1.0014 ± 0.0005	0.9987 ± 0.0002	−0.8 ± 0.3
2	4-Cl-aniline	7.0	−1.0 ± 0.1	−3.5 ± 0.6	1.0010 ± 0.0001	1.0035 ± 0.0006	3.3 ± 0.5
3a	4-CH_3-aniline	7.0	0.9 ± 0.4	3.6 ± 0.9	0.9991 ± 0.0004	0.9965 ± 0.0009	3.8 ± 0.4
3b	4-CH_3-aniline	6.0	−0.1 ± 0.6	4.0 ± 0.9	1.0001 ± 0.0006	0.9960 ± 0.0009	−12.3 ± 3.5
3c	4-CH_3-aniline	5.3	1.4 ± 0.8	1.3 ± 0.4	0.9986 ± 0.0008	0.9988 ± 0.0004	1.0 ± 0.4
3d	4-CH_3-aniline	4.0	0.4 ± 1.3	−3.4 ± 0.6	0.9996 ± 0.0013	1.0034 ± 0.0006	−4.0 ± 1.6
3e	4-CH_3-aniline	2.0	−0.2 ± 0.2	−5.2 ± 0.6	1.0002 ± 0.0002	1.0052 ± 0.0006	16.7 ± 1.9
4	4-OCH_3-aniline	7.5	−0.2 ± 0.4	4.2 ± 1.4	1.0002 ± 0.0004	0.9958 ± 0.0013	-11.0 ± 8.4
$^3MB^{+*}$							
5	Aniline	7.0	0.7 ± 1.1	2.1 ± 0.7	0.9993 ± 0.0011	0.9979 ± 0.0007	2.0 ± 1.2
6	4-Cl-aniline	7.0	−0.2 ± 0.4	−1.7 ± 0.3	1.0002 ± 0.0004	1.0017 ± 0.0003	4.2 ± 3.5
7	4-CH_3-aniline	7.0	0.5 ± 1.0	2.3 ± 0.6	0.9995 ± 0.0010	0.9977 ± 0.0006	1.7 ± 0.7
8	4-OCH_3-aniline	7.5	−1.4 ± 2.3	4.2 ± 1.3	1.0014 ± 0.0023	0.9958 ± 0.0012	-2.4 ± 1.6

[a] All experiments were carried out in 10 mM phosphate buffer adjusted to the given pH
[b] all uncertainties correspond to 95% confidence intervals; [c] calculated with eq. 4.2;

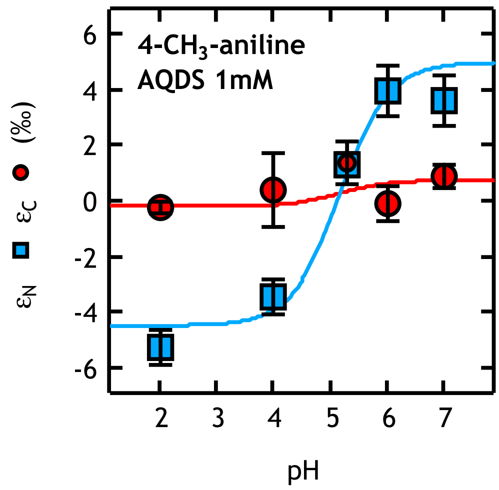

Figure 4.2 N anc C isotope enrichment factors, ϵ_{N} and ϵ_{C}, for 4-CH_3-aniline oxidation by ^{3}AQDS^{2-*} in the pH-range 2.0 to 7.0. The solid line corresponds to ϵ-values calculated from eq. 4.5 with $\mathrm{p}K_{\mathrm{BH^+}} = 5.17$[126] and the following isotope effects: ^{15}N-EIE$^{\mathrm{BH^+}} = 1.0095 \pm 0.0008$, ^{15}N-AKIE$^{\mathrm{B}} = 0.9950 \pm 0.0005$, ^{13}C-EIE$^{\mathrm{BH^+}} = 1.0009 \pm 0.0004$, ^{13}C-AKIE$^{\mathrm{B}} = 0.9992 \pm 0.0003$.

pH dependence

4-CH_3-aniline was also used as model compound to probe for the pH dependence of C and N isotope fractionation during the oxidation of by ^{3}AQDS^{2-*}. ϵ_{N}-values derived in the pH range 2.0 to 7.0 (Table 4.1, entries 3a-e) were fit well with eq. 4.5 as shown in Figure 4.2 assuming that only the neutral 4-CH_3-species react with ^{3}AQDS^{2-*} and that deprotonation precedes this oxidation step. The resulting ^{15}N-equilibrium isotope effect, ^{15}N-EIE, for the deprotonation of the 4-CH_3-anilinium cation amounted to 1.0095 ± 0.0008, which is slightly smaller than previous ^{15}N-EIEs derived from the pH-dependent oxidation of 4-CH_3-aniline by MnO_2 (1.015 ± 0.004,[134]). Regardless of this differences, the ^{15}N-EIE larger than unity adequately describe the phenomenon that ^{15}N is found preferentially in the protonated organic N species[43,125,133]. The calculated ^{15}N-AKIE for the oxidation of the neutral species of 0.9950 ± 0.0005 matches the values from experiments performed at solution pH 6.0 and 7.0, where this species predominates. The agreement with the ^{15}N-AKIE for the oxidation of 4-CH_3-aniline by MnO_2 of 0.9941 ± 0.0003 suggest that the N isotope fractionation may not be modulated by the type of oxidant (see further discussion below). We also derived the corresponding data for C isotope fractionation associated with deprotonation and substituted aniline oxidation, which had so far not been determined. The ^{13}C-EIE$^{BH^+}$ of 1.0009 ± 0.0004 and ^{13}C-AKIE^{B} of 0.9992 ± 0.0003 confirm the small secondary isotope effects on C in agreement with earlier findings[133,134].

Substituent effects

Following the procedures discussed above for 4-CH_3-aniline, we investigated the transformation of aniline, 4-OCH_3-, and 4-Cl-aniline by $^3AQDS^{2-*}$. Note that experiments with 4-OCH_3-aniline were carried out at pH 7.5 and at higher initial concentrations (a) to avoid contributions of H^+-exchange reactions on the measured isotope fractionation and (b) because of a smaller extraction efficiency by SPME. Pseudo-first order substrate disappearance kinetics, C and N isotope fractionation, as well as evidence for formation of radical coupling products are shown in the SI (Figures S4.1-S4.5) and Table 4.1. N isotope fractionation was larger than that for C and we observed both normal and inverse fractionation for the two elements. ϵ_N- and the corresponding ^{15}N-AKIE-values of the four substituted anilines correlated with the electronic properties of the aromatic substituents as quantified in σ_p^--substituent constants[54] (Figure 4.3). The most electron-donating substituent (4-OCH_3) led to the most inverse N isotope fractionation whereas that of 4-Cl-aniline was even normal.

This type of correlation was observed previously[134] for the oxidation of substituted anilines in MnO_2-containing suspensions and the data are also shown in Figure 4.3. The similarity of the correlations imply the same N-atom oxidation mechanism regardless of the oxidant. However, we hypothesized earlier that N-atom oxidations are associated with the formation of partial iminie bonds after the first electron transfer and that N isotope fractionation was always inverse due to stronger C–N bonds[134,135]. This assumption regarding the origin of N isotope fractionation no longer holds. The ^{15}N-AKIEs measured for the oxidation of 4-Cl-aniline by $^3AQDS^{2-*}$ is normal (1.0035 ± 0.0006, Table 4.1, entry 2) but we have no evidence that 4-Cl-aniline was transformed in by an alternative mechanism.

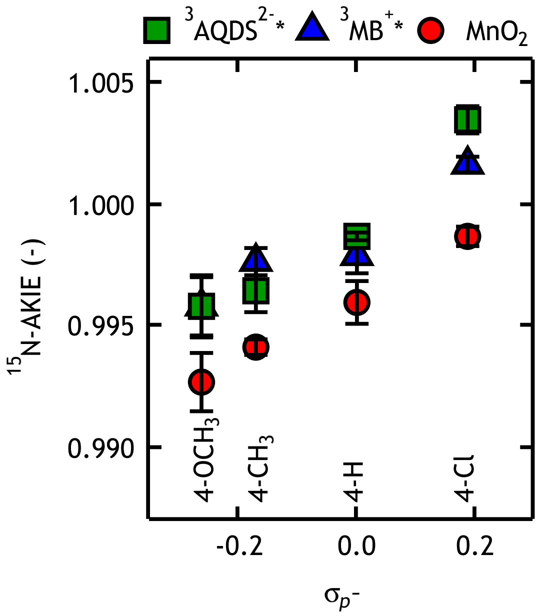

Figure 4.3 Correlation of ^{15}N-AKIE-values for the oxidation of aniline (4-H), 4-CH$_3$-, 4-OCH$_3$-, and 4-Cl-aniline by excited triplet states of two photosensitziers ($^3AQDS^{2-*}$, $^3MB^{+*}$) and suspensions of MnO_2[134] with σ_p^- substituent constants[54]. Note that the ^{15}N-AKIEs for oxidation of 4-OCH$_3$-aniline by $^3AQDS^{2-*}$ and $^3MB^{+*}$ are identical.

4.3.2 Oxidation of substituted anilines by excited triplet states of methylene blue ($^3MB^{+*}$)

The transformation of four substituted anilines from irradiated solutions containing methylene blue ($^3MB^{+*}$) at pH 7.0 is shown exemplarily for 4-Cl-aniline in Figure 4.1c/d and the data for the other compounds can be found in the SI (section S4.3). Note that the kinetics of 4-CH$_3$- and 4-OCH$_3$-aniline oxidation by $^3MB^{+*}$ was biphasic in contrast to its reaction with aniline and 4-Cl-aniline as well as oxidation of the four substituted anilines by $^3AQDS^{2-*}$. Biphasic kinetics (and incomplete oxidation) can be attributed to the fast oxidation of 4-CH$_3$- and 4-OCH$_3$-aniline oxidation by $^3MB^{+*}$ and a quenching of $^3MB^{+*}$ by radical coupling products. Compared to reactors with AQDS, the total concentration of MB was > 30 times smaller. The oxidation of substituted anilines by $^3MB^{+*}$ was accompanied with measurable N isotope fractionation with ϵ_N-values ranging from

$-1.7 \pm 0.3‰$ to $+4.2 \pm 1.3‰$ (Table 4.1, entries 5-8). δ^{13}C-values changed only to a minor extent and none of the ϵ_C-values is significantly different from zero. The ^{15}N-AKIEs for oxidation by $^3MB^{+*}$ are largely identical to those found with $^3AQDS^{2-*}$ as oxidant except for 4-Cl-aniline, which differ by only 0.0015 AKIE units. The oxidation of substituted anilines by $^3MB^{+*}$ also show the same substituent effects on ^{15}N-AKIE-values (Figure 4.3) suggesting that the mechanisms of initial electron transfer form the substrates to the two triplet photosensitizers were identical.

The factors controlling the rates of substituted aniline oxidation by $^3MB^{+*}$ were investigated recently in detail by Erickson et al.[40]. Rates of electron transfer from substituted anilines to $^3MB^{+*}$ increase with the electron donating properties of the substituent of the aromatic amines. Bimolecular rate constants for quenching of $^3MB^{+*}$ exceeding $4.0 \cdot 10^9$ M^{-1} s^{-1} indicated that oxidation of 4-CH_3- and 4-OCH_3-aniline is diffusion controlled whereas aniline and 4-Cl-aniline reacted one order of magnitude slower. However, we do not have any evidence that diffusion control would limit the extent of isotope fractionation. ^{15}N-AKIEs were even more inverse for the two fast reacting substituted anilines. This finding implies that the electron transfer reaction alone was not responsible for N isotope fractionation but that the latter is also determined by the bonding changes associated with the formation of the radical intermediates[134,135]. This interpretation is consistent with the results from experiments with $^3AQDS^{2-*}$. The bimolecular rate constants for oxidation of substituted anilines by $^3AQDS^{2-*}$ are not known, but the reduction potential of $^3AQDS^{2-*}$ exceeds that of $^3MB^{+*}$ ($E_H^{0\prime}(^3AQDS^{2-*}/AQDS^{3-})$ of 1.86 V[83] vs. $E_H^{0\prime}(^3MB^{+*}/MB^{\bullet})$ of 1.43 V[40]). Because of the even larger driving force of electron transfers from substituted anilines to $^3AQDS^{2-*}$, we assume that the latter also happens at diffusion controlled rates. Nevertheless, we observe N isotope fractionation and the ^{15}N-AKIE values for oxidation by $^3AQDS^{2-*}$ closely follow those where $^3MB^{+*}$ was the oxidant.

Note that the very similar results for the two photo-oxidants also provide indirect evidence that singlet oxygen, $^1O_2$, did not contribute to the transformation and thus isotope fractionation of substituted anilines in our experiments. $^1O_2$ can be formed in aqueous solution from reactions of dissolved O_2 with $^3MB^{+*}$ and $^3AQDS^{2-*}$. The limited available data suggest that more $^1O_2$ could be formed from $^3MB^{+*}$ due to its longer triplet lifetime compared to $^3AQDS^{2-*}$[40,90,165]. Assuming that $^1O_2$ reacted by a different mechanisms with substituted anilines than the two photosensitizers, we would expect that a reaction of substituted anilines with $^1O_2$ leads to a distinctly different C and N isotope fractionation in experiments with MB. As shown in Figure 4.3 and Table 4.1, however, we cannot observe such trends.

Origin of N isotope fractionation

Figure 4.3 compiles the currently available ^{15}N-AKIEs for the transformation of substituted anilines through N atom oxidation by excited triplet states of two photosensitizers and MnO_2 minerals. While N atoms oxidation exhibit rather small ^{15}N-AKIEs compared to aniline dioxygenation[102] or N atom reduction,[46,63,163] we observe consistent substituent effects effects. Changes of the electron donor (or acceptor) properties of aromatic substituent lead to a very similar change in ^{15}N-AKIEs regardless of the oxidant. Despite this correlation, however, ^{15}N-AKIE values for indirect photolysis are offset relative to those for MnO_2 suspensions by approximately 0.003 to 0.005 AKIE units. We cannot explain this offset with different rate-limiting steps of photochemical vs. mineral-catalyzed reactions, which, in the present case, would lead to a partial masking of isotope effects in reactions with $^3AQDS^{2-*}$ and $^3MB^{+*}$. This scenario would require that ^{15}N-AKIEs for 4-Cl-aniline approach unity. Instead, ^{15}N-AKIEs switch from inverse to normal implying that one can no longer invoke a tightening of N bonding as exclusive origin of N isotope fractionation. Normal ^{15}N-AKIEs were found for the oxidation of 4-Cl-*N*-methyl- and 4-Cl-*N,N*-dimethylanilines by horseradisch peroxidase in presence of H_2O_2[135]. Substituted *N*-alkyl-anilines, however, are subject to oxidative *N*-dealkylation and the data of Skarpeli-Liati et al.[135] suggest that this reaction pathways was responsible for ^{15}N-AKIEs larger than unity rather than N atom oxidation. Even though the results presented in this study enable one to delineate typical ^{15}N-AKIEs for oxidation of substituted anilines, we cannot rationalize the origin of N isotope fractionation for all compounds.

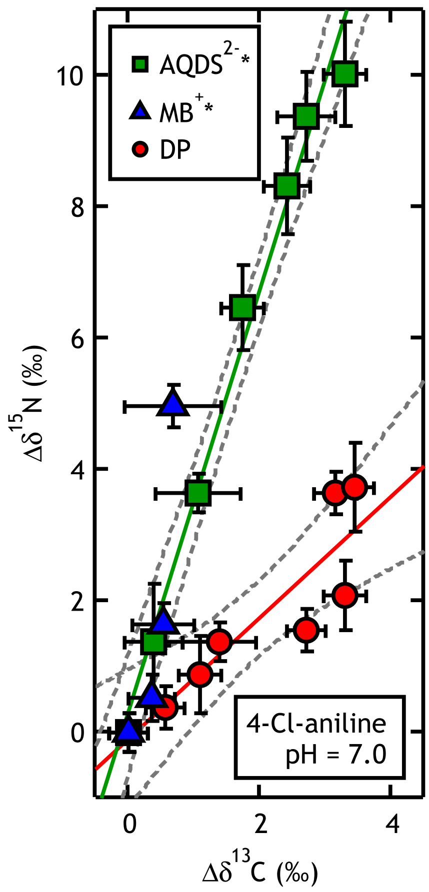

Figure 4.4 Correlation of C and N isotope fractionation ($\Delta\delta^{13}$C, $\Delta\delta^{15}$N) of 4-Cl-aniline for direct photolysis (DP) and indirect photolysis experiments, by using AQDS and MB as photosensitizers, at pH = 7.0. The grey lines delineate the initial 4-Cl-aniline isotope composition ($\delta^{13}\text{C} = -27.1‰$, $\delta^{15}\text{N} = -3.1‰$).

4.4 Environmental Significance

With the data presented in this and earlier work[106,107] it is, for the first time, possible to assess the diagnostic power of CSIA for photochemical transformation of aromatic amines in contaminated surface waters. In Figure 4.4, we have compiled the C and N isotope signature trends of 4-Cl-aniline associated with its direct photolysis at 254 nm as well as the oxidation by the two photosensitizers discussed above at pH 7.0. Slopes of the correlation of $\Delta\delta^{15}\text{N}/\Delta\delta^{13}\text{C}$ are equivalent to the ratio $\epsilon_{\text{N}}/\epsilon_{\text{C}}$. The ratios reflect the mechanisms of 4-Cl-aniline transformation regardless of whether isotope fractionation is masked or not[35]. $\Delta\delta^{15}N/\Delta\delta^{13}C$-values for direct and indirect photolysis are 0.9 ± 0.3[107] and 3.3 ± 0.5 (Table 4.1, entry 2), respectively, and thus sufficiently different to distinguish the two degradation pathways if they occurred simultaneously. Notice that data for $^3MB^{+*}$ follow the same trend as for $^3AQDS^{2-*}$ but is uncertain here due to the limited number of $\delta^{13}C$ measurements (see entry 6 in Table 4.1). The combined C and N isotope fractionation analysis reveals isotopic fingerprints with which transformation of 4-Cl-aniline through N atom oxidation or photolytic dechlorination can be tracked. In contrast to this kind of data treatment for non-photochemical degradation processes of other organic contaminants,[8,34,67,70,85,100,103,110,116,125,162–164] however, the correlations of $\delta^{15}N$ vs. $\delta^{13}C$ of photolytic processes are quite variable due to the spin sensitivity of kinetic isotope effects for changes in solution pH and ionic composition and require a thorough consideration of reaction conditions.

Acknowledgement

This work was supported by the EU Initial Training Network CSI:Environment (Grant agreement no. 264'329).

Supporting Information to Chapter 4

S4.1 Chemicals

Chemicals and gases were purchased from various manufacturers and used without further treatment. A list of compound names, purities, and suppliers follows. Aniline (≥99.5%), *p*-toluidine (99.6%), 4-chloroaniline (98%), *p*-anisidine (≥99%), methylene blue (certified by the Biological Stain Commission) and potassium phosphate monobasic (>99%) were purchased from Sigma-Aldrich (Buchs SG, Switzerland); anthraquinone-1,5-disulfonic acid disodium salt (98%) was from ABCR GmbH & CO. KG (Karlsruhe, Deutschland); hydrochloric acid (32%) and sodium hydroxide (98%), sodium chloride (>99%) were from Merck (Dietikon, Switzerland); methanol (for HPLC gradient) from Acros Organics (Geel, Belgium). All aqueous solutions were prepared in nanopure water (18.2 MΩ-cm, Barnstead NANOpure Diamond Water Purification System).

The carrier and reference gas for GC and GC/IRMS included helium (He, 99.999%), N_2 (99.9999%), CO_2 (99.999%), H_2 (99.999%), synthetic air (20 ± 1% O_2 in N_2, 99.9995%), O_2 (99.9995%) and, N_2 (99.9995%) from Carbagas (Rümlang, Switzerland). All aqueous solutions were prepared in nanopure water (18.2 MΩ-cm, Barnstead NANOpure Diamond Water Purification System).

S4.2 Tables

Table S4.1 Pseudo-first order reaction rate constants for the indirect photolysis of aniline and 4-Cl-, 4-CH_3-, 4-OCH_3-aniline, by using AQDS and MB as photo-sensitizer. Uncertainties are 95% confidence intervals.

Compound (-)	pH (-)	k_{obs} (h^{-1})
AQDS		
aniline	7.0	0.6 ± 0.2
4-Cl-aniline	7.0	1.7 ± 0.3
4-CH_3-aniline	7.0	1.6 ± 0.6
4-OCH_3-aniline	7.5	0.14 ± 0.02
MB		
aniline	7.0	31 ± 6
4-Cl-aniline	7.0	34 ± 3
4-CH_3-aniline	7.0	n.d.
4-OCH_3-aniline	7.5	n.d.

S4.3 Figures

S4.3.1 Photosensitizer: AQDS

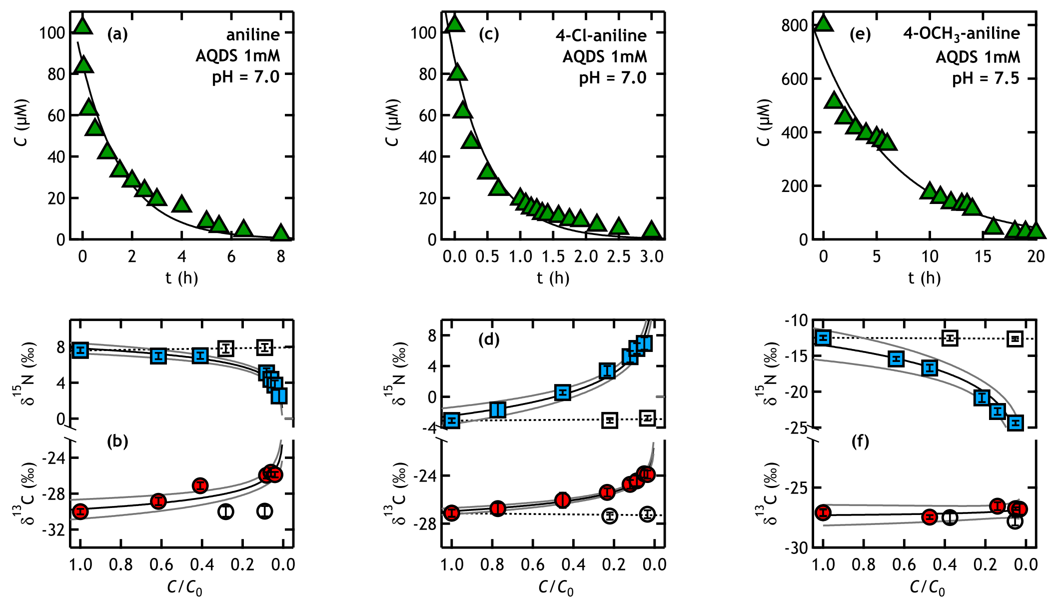

Figure S4.1 Indirect photolysis of aniline (panels a,b), 4-Cl-aniline (panels c,d) and 4-OCH_3-aniline (panels e, f) by using AQDS as photosensitizer. Substrate's concentration profiles (triangles) over irradiation time (panels a, c, e). Solid lines were calculated according to a pseudo-first-order decay kinetic. Gray-dashed lines indicate 95% confidence interval for the fit. (b, d, f) N and C isotope signatures (δ^{15}N (squares) and δ^{13}C (circles)) are represented versus the remaining substrate fraction (C/C_0). Uncertainties represent standard deviations of triplicate measurements. Solid lines correspond to the calculated isotope fractionation according to eq. 4.1; gray-dashed lines indicate 95% confidence interval of the fit. Control experiments (empty symbols, dashed lines) didn't show C and N isotope fractionation.

S4.3.2 Photosensitizer: MB

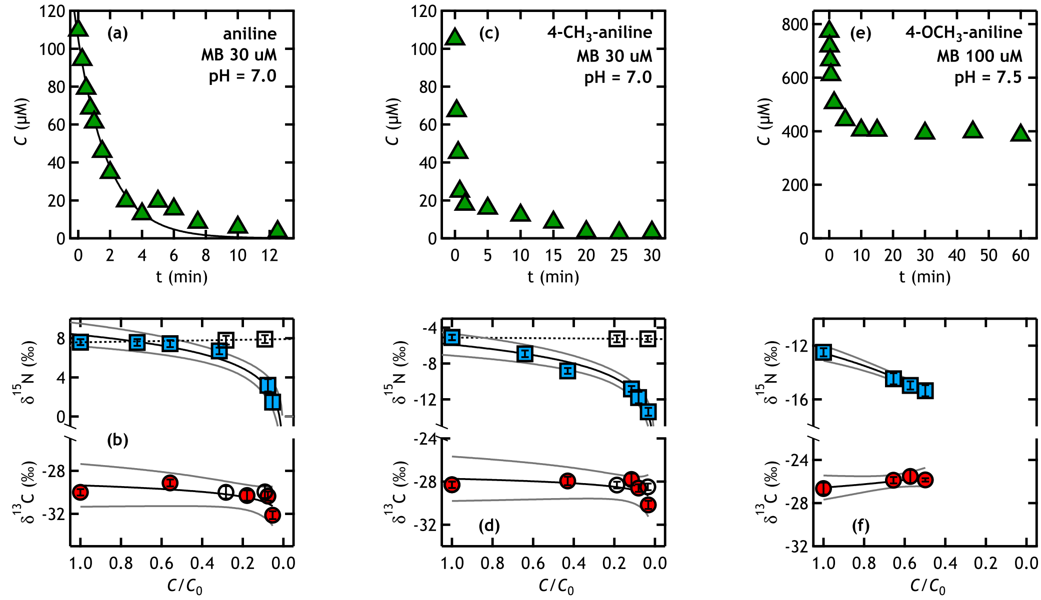

Figure S4.2 Indirect photolysis of aniline (panels a, b), 4-CH_3-aniline (panels c, d) and 4-OCH_3-aniline (panels e,f) by using MB as photosensitizer. Substrate's concentration profiles (triangles) over irradiation time (panels a, c, e). Solid lines were calculated according to a pseudo-first-order decay kinetic. Gray-dashed lines indicate 95% confidence interval for the fit. (b, d, f) N and C isotope signatures (δ^{15}N (squares) and δ^{13}C (circles)) are represented versus the remaining substrate fraction (C/C_0). Uncertainties represent standard deviations of triplicate measurements. Solid lines correspond to the calculated isotope fractionation according to eq. 4.1; gray-dashed lines indicate 95% confidence interval of the fit. Control experiments (empty symbols, dashed lines) didn't show C and N isotope fractionation.

S4.4 Product analysis

S4.4.1 Indirect Photolysis of 4-CH_3-aniline

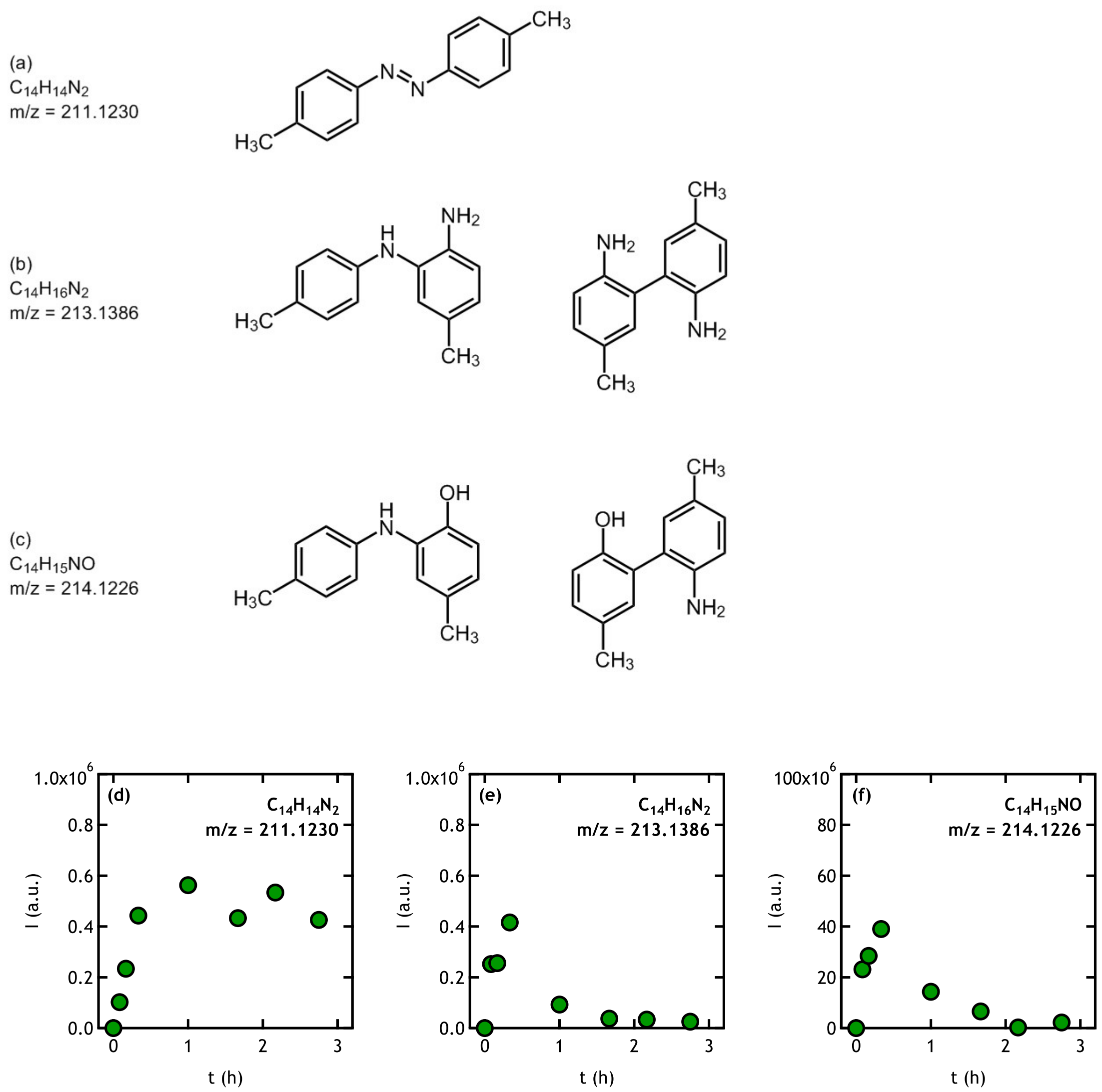

Figure S4.3 4-CH_3-aniline batch reaction experiment at pH = 7.0 in the presence of AQDS 1mM. Representation of the possible identified structures and their isomers (a-c). Signal areas of the investigated mass-to-charge (m/z) are represented over irradiation time (d-f).

S4.4.2 Indirect Photolysis of aniline

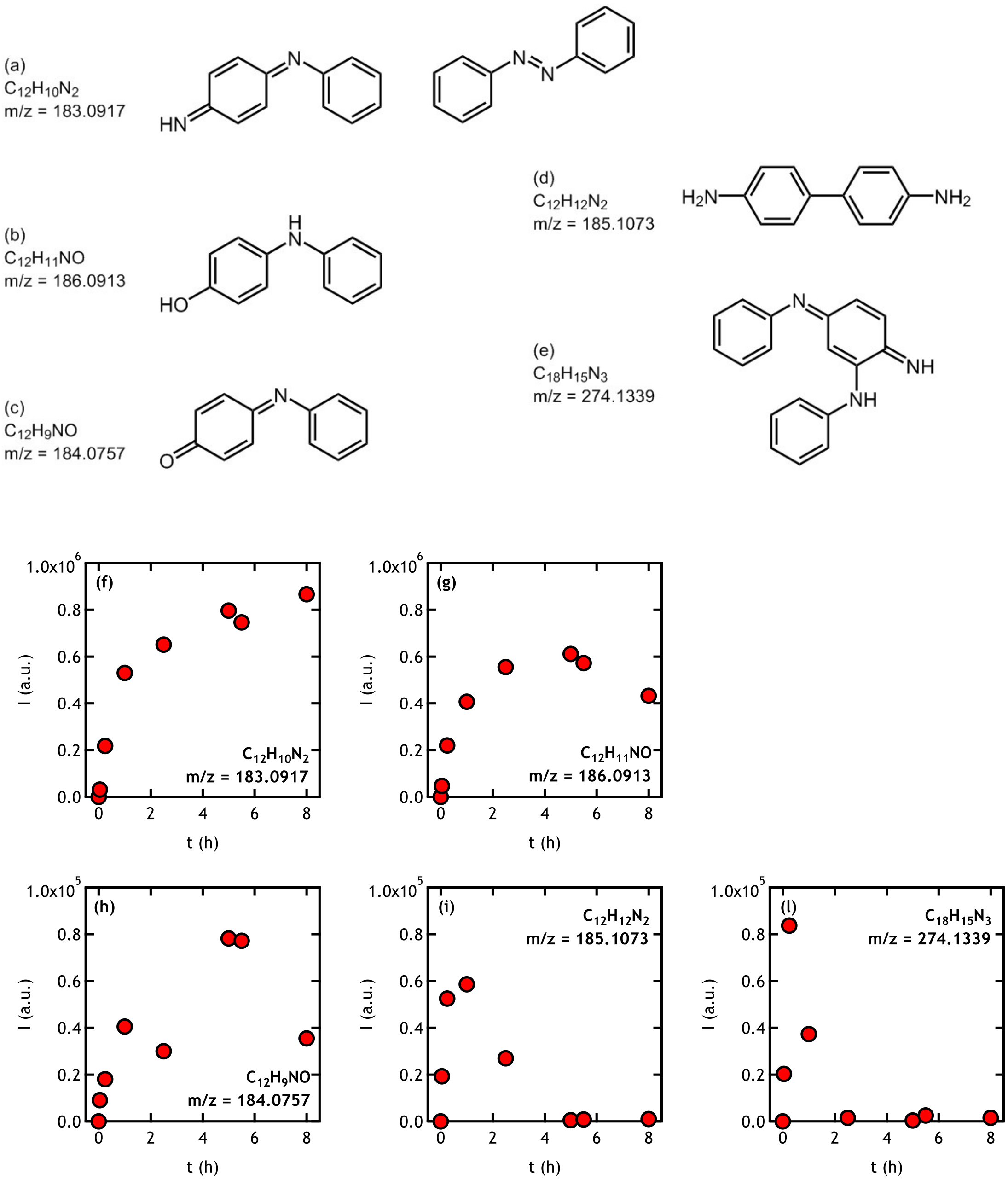

Figure S4.4 Aniline batch reaction experiment at pH = 7.0 in the presence of AQDS 1mM. Representation of the possible identified structures and their isomers (a-e). Signal areas of the investigated mass-to-charge ratio (m/z) are represented over irradiation time (f-l).

S4.4.3 Indirect Photolysis of 4-Cl-aniline

(a)
$C_{12}H_8Cl_2N_2$
m/z = 251.0137

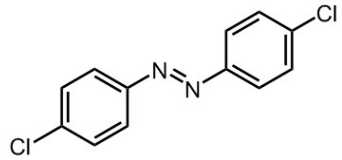

(b)
$C_{12}H_{11}ClN_2$
m/z = 219.0684

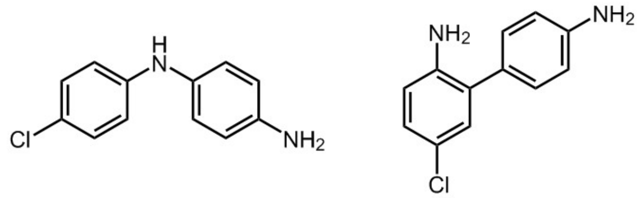

(c)
$C_{12}H_8ClNO$
m/z = 218.0367

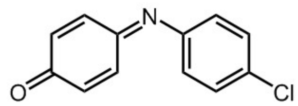

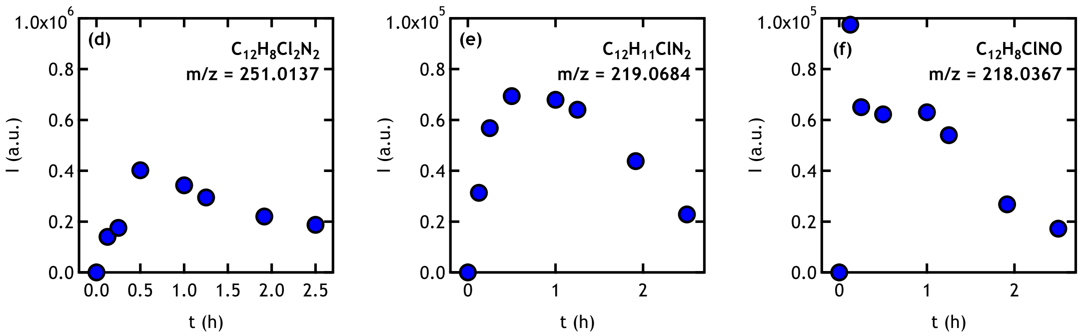

Figure S4.5 4-Cl-aniline batch reaction experiment at pH = 7.0 in the presence of AQDS 1mM. Representation of the possible identified structures and their isomers (a-c). Signal areas of the investigated mass-to-charge (m/z) are represented over irradiation time (d-f).

Chapter 5

Conclusions and Outlook

5.1 Assessing direct and indirect photolysis of aromatic amines by CSIA

The findings presented in this study show that the direct and indirect light-induced transformations of a few substituted anilines can be associated with distinctly different C and N isotope fractionation that could be detected in sunlit surface waters. Because direct and indirect photo-transformations of many aromatic amines are potentially competing reactions, the identification of specific C and N isotope fractionation patterns trends is of great importance to a more widespread application of CSIA and require further study.

Our results for the indirect photolysis of substituted anilines by transient triplet excited states oxidants revealed trends in ^{15}N-AKIEs that could be rationalized in terms of electron donating and accepting properties of the aromatic substituents. Assuming that the same N atom oxidation mechanism holds for other aromatic amines and DOM-derived photooxidants, out data offers a basis for the estimates of N isotope enrichment factors in the absence of measured data. However, we have not studied indirect photolyses of *ortho*- and *meta*-substituted anilines. In earlier work with MnO_2 as oxidant, it was shown that substituent effects on ^{15}N-AKIEs followed the trends that substituent exerted on radical stability. Preferential radical localization in *ortho*- and *para*-position explained why very similar substituent effects on ^{15}N-AKIEs were only observed for these substituent positions but not for *meta*-substitution. We would thus hypothesize that *meta*-substituted anilines all show a similar ^{15}N-AKIE of 0.997, regardless of the photooxidant. ^{15}N-AKIE of *ortho*-substituted anilines, in contrast, should be comparable to those of the *para*-substituted isomer.[134]

Isotope effects from the direct photolysis of organic pollutants are currently more difficult to interpret, because of the lack in a qualitative understanding of the factors that govern the isotope fractionation.[148] In this study, we investigated aromatic dechlorinations from excited states as model reactions. Our data for 3-Cl- and 4-Cl-aniline suggest that bond cleavages going through radical intermediates enable spin-dependent reactions, whose isotope effects likely originate from magnetic interactions. Photolysis of 4-Cl-aniline occur with concomitant formation of a radical intermediate (i.e., carbene), whereas the carbene is not formed in the direct photolysis of 3-Cl-aniline. C isotope fractionation was measurable only in the case of 4-Cl-aniline, whereas the change of δ^{13}C of 3-Cl-aniline did not exceeded 0.5‰. Because the population of excited states is sensitive to pH and ionic solution composition of aqueous media, isotope effects were also very variable. It is thus not straightforward to compare KIEs among different compounds in photolytic reactions. One should also keep in mind that the concept for derivation of AKIE for thermal reactions explicitly neglects secondary isotope effect. Whether this approximation is valid for magnetic isotope effects is less likely because light-absorption processes involve electronic transitions that depend on the structure of the entire molecule.

5.2 Magnetic isotope effects in direct photolysis reactions of organic micropollutants

Even though a systematic evaluation of direct photolysis reactions for their potential to exhibit magnetic isotope effects is beyond the scope of this work, there are interesting examples that suggest that this phenomenon may be encountered frequently, if the photolysis of contaminants exhibiting such molecular structures were investigated by CSIA. Current understanding suggest that photolysis reactions that lead to radical intermediates may potentially show magnetic isotope effects but it is unknown which other properties of the reactions may also be prerequisite. Examples include the photolytic aromatic dechlorination of 2,4-dichloroaniline,[95] 2,6-dichlorophenylamine,[48] diclofenac,[39] atrazine[56] and 2-chloropyridine.[140] Radical intermediates are also formed through hydrogen abstraction and homolytic C-N bond scissions in the case of direct photolysis reactions of non-chlorinated aromatic amines, like 4-CH_3-aniline[5] and N-(triphenylmethyl)aniline.[132] Carbenes were formed during the direct photolysis of *ortho*- and *para*-substituted phenolic compounds.[13,49,113] Radical formation through an homolytic scission of a C-C bond (Norrish type I) and through an hydrogen abstraction process (Norrish II), was reported for the excited states of carbonyl[149] and nitroaromatic[33] compounds.

The latter is one of the few examples, for which some of the principles of magnetic isotope effects were elucidated.[148] Upon light absorption, dibenzyl ketone undergoes a Norrish type I reaction with formation of a radical pair, which recombine only in spin-selective cage reactions. Only singlet radical pairs recombinations are allowed, whereas recombinations from triplets are not. In addition, triplet-singlet conversion is faster for the radical pair holding a magnetic nucleus (e.g. ^{13}C), due to induced hyperfine coupling between magnetic moments of unpaired electron and ^{13}C. Recombinations of radical pairs with a magnetic nucleus (^{13}C, ^{14}N and ^{15}N) are faster compared to those holding a non-magnetic nucleus (^{12}C) and will thus affect reaction rates and potentially lead to measurable isotope fractionation.[18,148]

5.3 Next steps towards an application of CSIA of aromatic amines in aquatic systems

This study is a first step towards application of CSIA to study transformation of aromatic amines in sunlit surface waters. An identification of transformation processes can be accomplished from the correlation of C and N isotope fractionation, that is from $\Delta\delta^{15}N/\Delta\delta^{13}C$-values, which can be directly compared to results from laboratory studies. Such data is now, for the first time, available for direct photolysis of chloroanilines and their oxidation by surrogates for excited triplet states of dissolved organic matter. While data for 4-Cl-aniline has been shown in Chapter 4 for pH 7.0, we need to speculate regarding the C and N isotope fractionation of 2-Cl- and 3-Cl-aniline during indirect photolysis based on *ortho*- and *meta*-substituent effects (see above). Assuming the $\Delta\delta^{15}N/\Delta\delta^{13}C$-values for sensitized photolysis of 2-Cl-aniline follows the trends established for 4-Cl-aniline at neutral pH, these processes can also easily be distinguished from the direct photolysis of 2-Cl-aniline (Figure 5.1). The latter showed a unique combination of inverse C and normal N isotope fractionation. As illustrated in Figure 5.1, this approach is less promising for 3-Cl-aniline, if we hypothesize that C and N isotope fractionation for indirect photoysis is similar to those reported for the indirect photolysis of aniline (Figure S4.1-S4.2). To test the above hypothesis in applications of CSIA to environmental samples, some open questions need to be resolved regarding the understanding of isotope fractionation and with respect to analytical

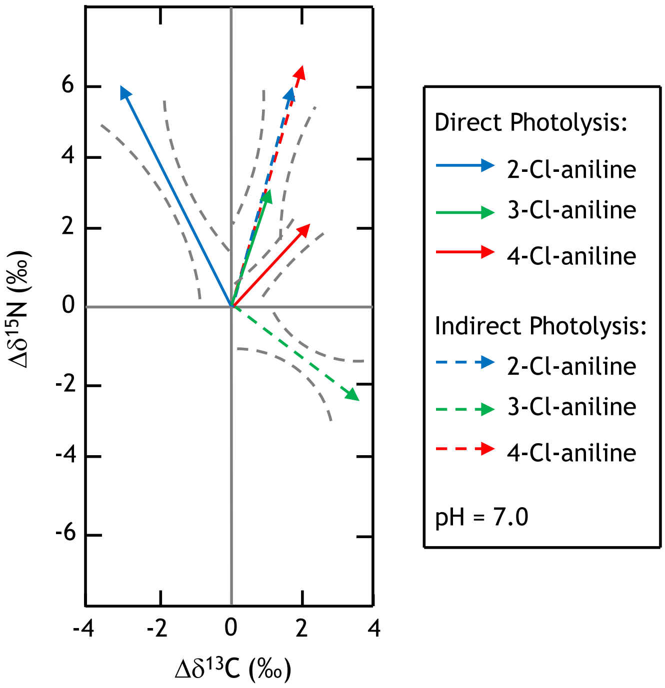

Figure 5.1 Direct photolysis of 4-Cl-aniline lead to a $\Delta\delta^{15}$N/$\Delta\delta^{13}$ value of 0.9 ± 0.3 with as reported in Table 2.1 in Chapter 2. Direct photolysis of 2- and 3-Cl-aniline lead to $\Delta\delta^{15}$N/$\Delta\delta^{13}$ values of -2.2 ± 0.2 and 4.1 ± 0.8 respectively, as shown in Table 3.1 in Chapter 3. Indirect photolysis of 2- is assumed to give the same $\Delta\delta^{15}$N/$\Delta\delta^{13}$ value reported for the indirect photolysis of 4-Cl-aniline which correspond to 3.3 ± 0.5 as shown in Table 4.1 in Chapter 4. The indirect photolysis of 3-Cl-aniline is assumed to give a $\Delta\delta^{15}$N/$\Delta\delta^{13}$ value of -0.8 ± 0.3 as reported for the indirect photolysis of aniline in Table 4.1 in Chapter 4. The length of the arrows indicates C and N isotope enrichment factors (ϵ_C, ϵ_N) observed for the different substrates during their direct and indirect photodegradation. Grey dashed lines represent the confidence interval.

approaches to CSIA.

As mentioned in Chapter 4, we do not yet know the possible isotope fractionation trends and kinetic isotope effects of the transformation of aromatic amines by other transient photooxidants such as reactive oxygen species including singlet oxygen $^1O_2$, hydroxyl radicals ($^\bullet$OH), and peroxides.[31,91,119] In contrast to excited triplet states of dissolved organic matter, reactive oxygen species will not only react at the N but also with aromatic and aliphatic C atoms and therefore generate smaller $\Delta\delta^{15}N/\Delta\delta^{13}C$-trend lines than the ones shown in Chapter 4. More quantitative estimates, however, require further experiments under well controlled conditions.

Finally, new approaches are needed to enable the isotopic analysis of aromatic amines from natural water samples. Current method quantification limits by solid-phase microextraction coupled to GC/IRMS enable measurements of low μM concentrations in samples of a few milliliters.[133] Larger water samples of a few liters can indeed be treated by solid-phase extraction and enabled one to lower current quantification limits by one to two orders of magnitude. As shown by Schreglmann et al.[124], for the analysis of triazine herbicides in the low μg/L-range of groundwater samples, however, such an approach also requires additional treatment steps for the removal of the accumulated organic matrix.

References

[1] Y. Abe, R. Aravena, J. Zopfi, O. Shouakar-Stash, E. Cox, J. D. Roberts, and D. Hunkeler. Carbon and chlorine isotope fractionation during aerobic oxidation and reductive dechlorination of vinyl chloride and cis-1,2-dichloroethene. *Environ. Sci. Technol.*, 43:101–107, 2009.

[2] M. C. Aelion, P. Höhener, D. Hunkeler, and R. Aravena, editors. *Environmental Isotopes in Biodegradation and Bioremediation.* 450 pp. CRC Press, Boca Raton, 2010.

[3] C. Aeppli, M. Berg, O. A. Cirpka, C. Holliger, R. P. Schwarzenbach, and T. B. Hofstetter. Influence of mass-transfer limitations on carbon isotope fractionation during microbial dechlorination of trichloroethene. *Environ. Sci. Technol.*, 43:8813–8820, 2009.

[4] C. Aeppli, T. B. Hofstetter, H. I. F. Amaral, R. Kipfer, R. P. Schwarzenbach, and M. Berg. Quantifying *in-situ* transformation rates of chlorinated ethenes by combining compound-specific stable isotope analysis, groundwater dating, and carbon isotope mass balances. *Environ. Sci. Technol.*, 44:3705–3711, 2010.

[5] N. Akai, H. Yoshida, K. Ohno, and M. Aida. Photochemistry of *p*-toluidine in a low-temperature argon matrix. Infrared spectrum and geometrical structure of 4-methylanilino radical. *Chem. Phys. Lett.*, 403:390–395, 2005.

[6] T. A . Albanis, T. G. Danis, and M. K. Kourgia. Transportation of pesticides in estuaries of the Axios, Loudias and Aliakmon rivers (Thermaikos Gulf), Greece. *Sci. Total Envrion.*, 156:11–22, 1994.

[7] R. Andreozzi, R. Marotta, and N. Paxéus. Pharmaceuticals in STP effluents and their solar photodegradation in aquatic environment. *Chemosphere*, 50: 1319–1330, 2003.

[8] A. Badin, G. Buttet, J. Maillard, C. Holliger, and D. Hunkeler. Multiple dual C–Cl isotope patterns associated with reductive dechlorination of tetrachloroethene. *Environ. Sci. Technol.*, 48:9179–9186, 2014.

[9] S. Bahnmüller, U. Von Gunten, and S. Canonica. Sunlight-induced transformation of sulfadiazine and sulfamethoxazole in surface waters and wastewater effluents. *Water research*, 57:183–192, 2014.

[10] R. Bartha and D. Pramer. Pesticide transformation to aniline and azo compounds in soil. *Science*, 156:1617–1618, 1967.

[11] B. A. Bergquist and J. D. Blum. Mass-dependent and -independent fractionation of Hg isotopes by photoreduction in aquatic systems. *Science*, 318: 417–420, 2007.

[12] S. Bondarenko and J. Gan. Degradation and sorption of selected organophosphate and carbamate insecticides in urban stream sediments. *Environ. Toxicol. Chem.*, 23:1809–1814, 2004.

[13] F. Bonnichon, C. Richard, and G. Grabner. Formation of an alphaketocarbene by photolysis of aqueous 2-bromophenol. *Chem. Commun.*, pages 73–74, 2001.

[14] F. Bonvin, J. Omlin, R. Rutler, W. B. Schweizer, P. J. Alaimo, T. J. Strathmann, K. McNeill, and T. Kohn. Direct photolysis of human metabolites of the antibiotic sulfamethoxazole: Evidence for abiotic back-transformation. *Environ. Sci. Technol.*, 47:6746–6755, 2013.

[15] A. L. Boreen, W. A. Arnold, and K. McNeill. Photodegradation of pharmaceuticals in the aquatic environment: A review. *Aquat. Sci.*, 65:320–341, 2003.

[16] P. Boule, K. Othmen, C. Richard, B. Szczepanik, and G. Grabner. Phototransformation of halogenoaromatic derivatives in aqueous solution. *Int. J. Photoenergy*, 1:6, 1999.

[17] A. Buchachenko. MIE versus CIE - Comparative analysis of magnetic and classical isotope effects. *Chem. Rev.*, 95:2507–2528, 1995.

[18] A. Buchachenko. Magnetic isotope effect: Nuclear spin control of chemical reactions. *J. Phys. Chem. A*, 105:9995–10011, 2001.

[19] A. Buchachenko. Mass-independent isotope effects. *J. Phys. Chem. B*, 117: 2231–2238, 2013.

[20] J. M. Buth, P. O. Steen, C. Sueper, D. Blumentritt, P. J. Vikesland, W. A. Arnold, and K. McNeill. Dioxin photoproducts of triclosan and its chlorinated derivatives in sediment cores. *Environ. Sci. Technol.*, 44:4545–4551, 2010.

[21] S. Canonica and H. Laubscher. Inhibitory effect of dissolved organic matter on triplet-induced oxidation of aquatic contaminants. *Photochem. Photobiol. Sci.*, 7:547–551, 2008.

[22] S. Canonica, U. Jans, K. Stemmler, and J. Hoigne. Transformation kinetics of phenols in water - Photosensitization by dissolved natural organic material and aromatic ketones. *Environ. Sci. Technol.*, 29:1822–1831, 1995.

[23] S. Canonica, T. Kohn, M. Mac, F. J. Real, J. Wirz, and U. Von Gunten. Photosensitizer method to determine rate constants for the reaction of carbonate radical with organic compounds. *Environ. Sci. Technol.*, 39:9182–9188, 2005.

[24] S. Canonica, L. Meunier, and U. Von Gunten. Phototransformation of selected pharmaceuticals during UV treatment of drinking water. *Water Res.*, 42:121–128, 2008.

[25] J. K. Challis, M. L. Hanson, K. J. Friesen, and C. S. Wong. A critical assessment of the photodegradation of pharmaceuticals in aquatic environments: Defining our current understanding and identifying knowledge gaps. *Environ. Sci.: Processes Impacts*, 16:672–696, 2014.

[26] C. C. H. Chan, S. O. C. Mundle, T. Eckert, X. Liang, S. Tang, G. Lacrampe-Couloume, E. A. Edwards, and B. Sherwood Lollar. Large carbon isotope fractionation during biodegradation of chloroform by *Dehalobacter* cultures. *Environ. Sci. Technol.*, 46:10154–10160, 2012.

[27] D. Colon, E. J. Weber, and G. L. Baughman. Sediment-associated reactions of aromatic amines. 2. QSAR development. *Environ. Sci. Technol.*, 36:2443–2450, 2002.

[28] E. H. Cordes and W. P. Jencks. Mechanism of hydrolysis of Schiff bases derived from aliphatic amines. *J. Am. Chem. Soc.*, 85:2843–2848, 1963.

[29] S. Cretnik, A. Bernstein, O. Shouakar-Stash, F. Loffler, and M. Elsner. Chlorine isotope effects from isotope ratio mass spectrometry suggest intramolecular C-Cl bond competition in trichloroethene (TCE) reductive dehalogenation. *Molecules*, 19:6450–6473, 2014.

[30] M. T. D. Cronin, Y. H. Zhao, and R. L. Yu. pH-dependence and QSAR analysis of the toxicity of phenols and anilines to *Daphnia magna*. *Environ. Toxicol.*, 15:140–148, 2000.

[31] A. P. Darmanyan, W. S. Jenks, and P. Jardon. Charge-transfer quenching of singlet oxygen O_2 ($^1\Delta_g$) by amines and aromatic hydrocarbons. *J. Phys. Chem. A*, 102:7420–7426, 1998.

[32] J. Dec and J. Bollag. Effect of various factors on dehalogenation of chlorinated phenols and anilines during oxidative coupling. *Environ. Sci. Technol.*, 29:657–663, 1995.

[33] D. Döpp. Reactions of aromatic nitro compounds via excited triplet states. In *Triplet States II*, pages 49–85. Springer, 1975.

[34] C. Dorer, C. Vogt, S. Kleinsteuber, A. J. M. Stams, and H. Richnow. Compound-specific isotope analysis as a tool to characterize biodegradation of ethylbenzene. *Environ. Sci. Technol.*, 48:9122–9132, 2014.

[35] M. Elsner. Stable isotope fractionation to investigate natural transformation mechanisms of organic contaminants: Principles, prospects and limitations. *J. Environ. Monit.*, 12:2005–2031, 2010.

[36] M. Elsner and T. B. Hofstetter. Current perspectives on the mechanisms of chlorohydrocarbon degradation in subsurface environments: Insight from kinetics, product formation, probe molecules, and isotope fractionation. In P. G. Tratnyek, T. J. Grundl, and S. B. Haderlein, editors, *Aquatic Redox Chemistry*, volume 1071 of *ACS Symposium Series*, pages 407–439. American Chemical Society, 2011.

[37] M. Elsner, L. Zwank, D. Hunkeler, and R. P. Schwarzenbach. A new concept linking observable stable isotope fractionation to transformation pathways of organic pollutants. *Environ. Sci. Technol.*, 39:6896–6916, 2005.

[38] M. Elsner, M. A. Jochman, T. B. Hofstetter, D. Hunkeler, A. Bernstein, T. C. Schmidt, and A. Schimmelmann. Current challenges in compound-specific stable isotope analysis of environmental organic contaminants. *Anal. Bioanal. Chem.*, 403:2471–2491, 2012.

[39] S. Encinas, F. Bosca, and M. A. Miranda. Phototoxicity associated with diclofenac: A photophysical, photochemical, and photobiological study on the drug and its photoproducts. *Che. Res. Toxicol.*, 11:946–952, 1998.

[40] P. R. Erickson, N. Walpen, J. J. Guerard, S. N. Eustis, J. S. Arey, and K. McNeill. Controlling factors in the rates of oxidation of anilines and phenols by triplet methylene blue in aqueous solution. *J. Phys. Chem. A*, 119:3233–3243, 2015.

[41] D. Fabbri, M. Minella, V. Maurino, C. Minero, and D. Vione. Photochemical transformation of phenylurea herbicides in surface waters: A model assessment of persistence, and implications for the possible generation of hazardous intermediates. *Chemosphere*, 119:601–607, 2015.

[42] B. Ferrari, N. Paxeus, R. L. Giudice, A. Pollio, and J. Garric. Ecotoxicological impact of pharmaceuticals found in treated wastewaters: Study of carbamazepine, clofibric acid, and diclofenac. *Ecotoxicol. Environ. Saf.*, 55: 359–370, 2003.

[43] P. F. Fitzpatrick. Oxidation of amines by flavoproteins. *Arch. Biochem. Biophys.*, 493:13–25, 2010.

[44] A. M. Fogarty and O. H. Tuovinen. Microbiological degradation of pesticides in yard waste composting. *Microbiol. Rev.*, 55:225–233, 1991.

[45] M. Freccero, M. Fagnoni, and A. Albini. Homolytic vs heterolytic paths in the photochemistry of haloanilines. *J. Am. Chem. Soc.*, 125:13182–13190, 2003.

[46] C. A. Gorski, J. T. Nurmi, P. G. Tratnyek, T. B. Hofstetter, and M. M. Scherer. Redox behavior of magnetite: Implications for contaminant reduction. *Environ. Sci. Technol.*, 44:55–60, 2010.

[47] F. Gosetti, M. Bottaro, V. Gianotti, E. Mazzucco, P. Frascarolo, D. Zampieri, C. Oliveri, A. Viarengo, and M. C. Gennaro. Sun light degradation of 4-chloroaniline in waters and its effect on toxicity. A high performance liquid chromatography - Diode array - Tandem mass spectrometry study. *Environ. Pollut.*, 158:592–598, 2010.

[48] G. Grabner and C. Richard. Mechanisms of direct photolysis of biocides based on halogenated phenols and anilines. *Handbook of Environmental Chemistry*, 2:161–192, 2005.

[49] G. Grabner, C. Richard, and G. Kohler. Formation and reactivity of 4-oxocyclohexa-2,5-dienylidene in the photolysis of 4-chlorophenol in aqueous-solution at ambient-temperature. *J. Am. Chem. Soc.*, 116:11470–11480, 1994.

[50] C. Griebler, L. Adrian, R. U. Meckenstock, and H. Richnow. Stable carbon isotope fractionation during aerobic and anaerobic transformation of trichlorobenzene. *FEMS Microbiol. Ecol.*, 48:313–321, 2004.

[51] A. Grirrane, A. Corma, and H. García. Gold-catalyzed synthesis of aromatic azo compounds from anilines and nitroaromatics. *Science*, 322:1661–1664, 2008.

[52] F. P. Guengerich, C. H. Yun, and T. L. Macdonald. Evidence for a 1-electron oxidation mechanism in *N*-dealkylation of *N,N*-dialkylanilines by cytochrome P450 2B1 - Kinetic hydrogen isotope effects, linear free energy relationships, comparisons with horseradish peroxidase, and studies with oxygen surrogates. *J. Biol. Chem.*, 271:27321–27329, 1996.

[53] B. Guizzardi, M. Mella, M. Fagnoni, M. Freccero, and A. Albini. Generation and reactivity of the 4-aminophenyl cation by photolysis of 4-chloroaniline. *J. Org. Chem.*, 66:6353–6363, 2001.

[54] C. Hansch, A. Leo, and R. W. Taft. A survey of Hammett substituent constants and resonance and field parameters. *Chem. Rev.*, 91:165–195, 1991.

[55] A. E. Hartenbach, T. B. Hofstetter, M. Aeschbacher, M. Sander, D. Kim, T. J. Strathmann, W. A. Arnold, C. J. Cramer, and R. P. Schwarzenbach. Variability of nitrogen isotope fractionation during the reduction of nitroaromatic compounds with dissolved reductants. *Environ. Sci. Technol.*, 42: 8352–8359, 2008.

[56] A. E. Hartenbach, T. B. Hofstetter, P. R. Tentscher, S. Canonica, M. Berg, and R. P. Schwarzenbach. Carbon, hydrogen, and nitrogen isotope fractionation during light-induced transformations of atrazine. *Environ. Sci. Technol.*, 42:7751–7756, 2008.

[57] T. B. Hofstetter and M. Berg. Assessing transformation processes of organic contaminants by compound-specific stable isotope analyses. *TrAC, Trends in Anal. Chem.*, 30:618–627, 2011.

[58] T. B. Hofstetter, C. G. Heijman, S. B. Haderlein, C. Holliger, and R. P. Schwarzenbach. Complete reduction of TNT and other (poly)nitroaromatic compounds under iron reducing subsurface conditions. *Environ. Sci. Technol.*, 33:1479–1487, 1999.

[59] T. B. Hofstetter, A. Neumann, and R. P. Schwarzenbach. Reduction of nitroaromatic compounds by Fe(II) species associated with iron-rich smectites. *Environ. Sci. Technol.*, 40:235–242, 2006.

[60] T. B. Hofstetter, C. M. Reddy, L. J. Heraty, M. Berg, and N. C. Sturchio. Carbon and chlorine isotope effects during abiotic reductive dechlorination of polychlorinated ethanes. *Environ. Sci. Technol.*, 41:4662–4668, 2007.

[61] T. B. Hofstetter, R. P. Schwarzenbach, and S. M. Bernasconi. Assessing transformation processes of organic compounds using stable isotope fractionation. *Environ. Sci. Technol.*, 42:7737–7743, 2008.

[62] T. B. Hofstetter, J. C. Spain, S. F. Nishino, J. Bolotin, and R. P. Schwarzenbach. Identifying competing aerobic nitrobenzene biodegradation pathways using compound-specific isotope analysis. *Environ. Sci. Technol.*, 42:4764–4770, 2008.

[63] T. B. Hofstetter, J. Bolotin, S. G. Pati, M. Skarpeli-Liati, S. Spahr, and R. S. Wijker. Isotope effects as new proxies for organic pollutant transformation. *Chimia*, 68:788–792, 2014.

[64] H. Huang, D. Sommerfeld, B. C. Dunn, C. R. Lloyd, and E. M. Eyring. Ferrate(VI) oxidation of aniline. *J. Chem. Soc.-Dalton Trans.*, pages 1301–1305, 2001.

[65] K. Hunger. *Industrial dyes: chemistry, properties, applications.* John Wiley & Sons, 2007.

[66] D. Hunkeler and M. Elsner. Principles and mechanisms of isotope fractionation. In *Environmental Isotopes in Biodegradation and Bioremediation*, pages 43–78. CRC Press, 2010.

[67] S. Huntscha, T. B. Hofstetter, E. L. Schymanski, S. Spahr, and J. Hollender. Biotransformation of benzotriazoles: Insights from transformation product identification and compound-specific isotope analysis. *Environ. Sci. Technol.*, 48:4435–4443, 2014.

[68] O. S. Jacobsen and R. Bossi. Degradation of ethylenethiourea (ETU) in oxic and anoxic sandy aquifers. *FEMS Microbiol. Rev.*, 20:539–544, 1997.

[69] J. T. Jasper and D. L. Sedlak. Phototransformation of wastewater-derived trace organic contaminants in open-water unit process treatment wetlands. *Environ. Sci. Technol.*, 47:10781–10790, 2013.

[70] S. Jeannottat and D. Hunkeler. Chlorine and carbon isotopes fractionation during volatilization and diffusive transport of trichloroethene in the unsaturated zone. *Environ. Sci. Technol.*, 46:3169–3176, 2012.

[71] M. A. Jochmann and T. C. Schmidt. *Compound-specific Stable Isotope Analysis.* 376 pp. The Royal Society of Chemistry, 2012.

[72] M. A. Jochmann, M. Blessing, S. B. Haderlein, and T. C. Schmidt. A new approach to determine method detection limits for compound-specific isotope analysis of volatile organic compounds. *Rapid Commun. Mass Spectrom.*, 20: 3639–3648, 2006.

[73] S. Kern, K. Fenner, H. P. Singer, R. P Schwarzenbach, and J. Hollender. Identification of transformation products of organic contaminants in natural waters by computer-aided prediction and high-resolution mass spectrometry. *Environ. Sci. Technol.*, 43:7039–7046, 2009.

[74] P. Klan and J. Wirz. *Photochemistry of organic compounds: From concepts to practice.* 563 pp. John Wiley & Sons, Ltd., 2009.

[75] J. Klausen, S. B. Haderlein, and R. P. Schwarzenbach. Oxidation of substituted anilines by aqueous MnO_2: Effect of co-solutes on initial and quasi steady state kinetics. *Environ. Sci. Technol.*, 31:2642–2649, 1997.

[76] S. Kliegman and K. McNeill. Reconciling disparate models of the involvement of vinyl radicals in cobalamin-mediated dechlorination reactions. *Environ. Sci. Technol.*, 43:8961–8967, 2009.

[77] E. P. Kuhn and J. M. Suflita. Anaerobic biodegradation of nitrogen-substituted and sulfonated benzene aquifer contaminants. *Hazardous waste and hazardous materials*, 6:121–133, 1989.

[78] S. Laha and R. G. Luthy. Oxidation of aniline and other primary aromatic amines by manganese dioxide. *Environ. Sci. Technol.*, 24:363–373, 1990.

[79] Y. Lee and U. Von Gunten. Oxidative transformation of micropollutants during municipal wastewater treatment: Comparison of kinetic aspects of selective (chlorine, chlorine dioxide, ferrate(VI), and ozone) and non-selective oxidants (hydroxyl radical). *Water Res.*, 44:555–566, 2010.

[80] X. Liang, M. R. Howlett, J. L. Nelson, G. Grant, S. Dworatzek, G. Lacrampe-Couloume, S. H. Zinder, E. A. Edwards, and B. Sherwood Lollar. Pathway-dependent isotope fractionation during aerobic and anaerobic degradation of monochlorobenzene and 1,2,4-trichlorobenzene. *Environ. Sci. Technol.*, 45: 8321–8327, 2011.

[81] X. Liang, C. E. Devine, J. Nelson, B. Sherwood Lollar, S. Zinder, and E. A. Edwards. Anaerobic conversion of chlorobenzene and benzene to CH_4 and

CO_2 in bioaugmented microcosms. *Environ. Sci. Technol.*, 47:2378–2385, 2013.

[82] X. Liang, S. O. C. Mundle, J. L. Nelson, E. Passeport, C. C. H. Chan, G. Lacrampe-Couloume, S. H. Zinder, and B. Sherwood Lollar. Distinct carbon isotope fractionation during anaerobic degradation of dichlorobenzene isomers. *Environ. Sci. Technol.*, 48:4844–4851, 2014.

[83] I. Loeff, J. Rabani, A. Treinin, and H. Linschitz. Charge transfer and reactivity of $n-\pi^*$ and $\pi-\pi^*$ organic triplets, including anthraquinonesulfonates, in interactions with inorganic anions: A comparative study based on classical marcus theory. *J. Am. Chem. Soc.*, 115:8933–8942, 1993.

[84] M. P. Maier, S. De Corte, S. Nitsche, T. Spaett, N. Boon, and M. Elsner. C & N isotope analysis of diclofenac to distinguish oxidative and reductive transformation and to track commercial products. *Environ. Sci. Technol.*, 48:2312–2320, 2014.

[85] J. R. McKelvie, M. R. Hyman, M. Elsner, C. Smith, D. M. Aslett, G. Lacrampe-Couloume, and B. Sherwood Lollar. Isotopic fractionation of methyl tert-butyl ether suggests different initial reaction mechanisms during aerobic biodegradation. *Environ. Sci. Technol.*, 43:2793–2799, 2009.

[86] L. Melander and W. H. Saunders. *Reaction Rates of Isotopic Molecules.* 331 pp. John Wiley & Sons; Wiley Interscience Publication, 1980.

[87] H. Mestankova, B. Escher, K. Schirmer, U. Von Gunten, and S. Canonica. Evolution of algal toxicity during (photo) oxidative degradation of diuron. *Aquat. Toxicol.*, 101:466–473, 2011.

[88] A. H. Meyer and M. Elsner. $^{13}C/^{12}C$ and $^{15}N/^{14}N$ isotope analysis to characterize degradation of atrazine: Evidence from parent and daughter compound values. *Environ. Sci. Technol.*, 47:6884–6891, 2013.

[89] A. H. Meyer, A. Dybala-Defratyka, P. J. Alaimo, I. Geronimo, A. D. Sanchez, C. J. Cramer, and M. Elsner. Cytochrome P_{450}-catalyzed dealkylation of atrazine by *Rhodococcus* sp strain N186/21 involves hydrogen atom transfer rather than single electron transfer. *Dalton Trans.*, 43:12175–12186, 2014.

[90] J. N. Moore, D. Phillips, N. Nakashima, and K. Yoshihara. Photophysics and photochemistry of sulphonated derivatives of 9, 10-anthraquinone."strong" versus "weak" sensitisers. *J. Chem. Soc. Faraday Trans.*, 83:1487–1508, 1987.

[91] P. Neta and R. W. Fessenden. Hydroxyl radical reactions with phenols and anilines as studied by electron spin resonance. *J. Phys. Chem.*, 78:523–529, 1974.

[92] A. Neumann, T. B. Hofstetter, M. Skarpeli-Liati, and R. P. Schwarzenbach. Reduction of polychlorinated ethanes and carbon tetrachloride by structural Fe(II) in smectites. *Environ. Sci. Technol.*, 43:4082–4089, 2009.

[93] I. Nijenhuis, N. Stelzer, M. Kästner, and H. Richnow. Sensitive detection of anaerobic monochlorobenzene degradation using stable isotope tracers. *Environ. Sci. Technol.*, 41:3836–3842, 2007.

[94] K. Othmen and P. Boule. Phototransformation of 2-chloroaniline in aqueous solution. *Bull. Environ. Contam. Toxicol.*, 59:924–927, 1997.

[95] K. Othmen and P. Boule. Photochemical behaviour of dichloroanilines in water and formation of aminochlorophenoxazones. *J. Photochem. Photobiol. A Chem.*, 121:161–167, 1999.

[96] K. Othmen and P. Boule. Photochemical behaviour of 2-halogenoanilines in aqueous solution. *J. Photochem. Photobiol., A*, 136:79–86, 2000.

[97] K. Othmen, P. Boule, and C. Richard. Mechanism of 3-halogenoaniline photolysis in methanol. *New J. Chem.*, 23:857–861, 1999.

[98] K. Othmen, P. Boule, B. Szczepanik, K. Rotkiewicz, and G. Grabner. Photochemistry of 4-chloroaniline in solution. formation and kinetic properties of a new carbene, 4-iminocyclohexa-2,5-dienylidene. *J. Phys. Chem. A*, 104: 9525–9534, 2000.

[99] J. L. Packer, J. J. Werner, D. E. Latch, K. McNeill, and W. A. Arnold. Photochemical fate of pharmaceuticals in the environment: Naproxen, diclofenac, clofibric acid, and ibuprofen. *Aquatic Sciences*, 65:342–351, 2003.

[100] J. Palau, S. Cretnik, O. Shouakar-Stash, M. Höche, M. Elsner, and D. Hunkeler. C and Cl isotope fractionation of 1,2-dichloroethane displays unique $\delta^{13}C/\delta^{37}Cl$ patterns for pathway identification and reveals surprising C–Cl bond involvement in microbial oxidation. *Environ. Sci. Technol.*, 48:9430–9437, 2014.

[101] G. Palma, A. Sánchez, Y. Olave, F. Encina, R. Palma, and R. Barra. Pesticide levels in surface waters in an agricultural–forestry basin in southern Chile. *Chemosphere*, 57:763–770, 2004.

[102] S. G. Pati, K. A. Shin, M. Skarpeli-Liati, J. Bolotin, S. N. Eustis, J. C. Spain, and T. B. Hofstetter. Carbon and nitrogen isotope effects associated with the dioxygenation of aniline and diphenylamine. *Environ. Sci. Technol.*, 46: 11844–11853, 2012.

[103] S. G. Pati, H. E. Kohler, J. Bolotin, R. E. Parales, and T. B. Hofstetter. Isotope effects of enzymatic dioxygenation of nitrobenzene and 2-nitrotoluene by nitrobenzene dioxygenase. *Environ. Sci. Technol.*, 48:10750–10759, 2014.

[104] H. Penning, S. R. Sorensen, A. H. Meyer, J. Aamand, and M. Elsner. C, N, and H isotope fractionation of the herbicide isoproturon reflects different microbial transformation pathways. *Environ. Sci. Technol.*, 44:2372–2378, 2010.

[105] E. Pines. The kinetic isotope effect in the photo-dissociation reaction of excited-state acids in aqueous solutions. In A. Kohen and H. Limbach, editors, *Isotope Effects in Chemistry and Biology*, pages 451–464. CRC Press / Taylor & Francis, New York, 2006.

[106] M. Ratti, S. Canonica, K. McNeill, J. Bolotin, and T. B. Hofstetter. Isotope fractionation associated with the photochemical dechlorination of chloroanilines. *Environ. Sci. Technol.*, 49:9797–9806, 2015.

[107] M. Ratti, S. Canonica, K. McNeill, P. R. Erickson, J. Bolotin, and T. B. Hofstetter. Isotope fractionation associated with the direct photolysis of 4-chloroaniline. *Environ. Sci. Technol.*, 49:4263–4273, 2015.

[108] S. Reinnicke, A. Simonsen, S. R. Sørensen, J. Aamand, and M. Elsner. C and N isotope fractionation during biodegradation of the pesticide metabolite 2,6-dichlorobenzamide (BAM): Potential for environmental assessments. *Environ. Sci. Technol.*, 46:1447–1454, 2012.

[109] C. K. Remucal and M. Ginder-Vogel. A critical review of the reactivity of manganese oxides with organic contaminants. *Environ. Sci. Technol.*, 16: 1247–1266, 2014.

[110] J. Renpenning, S. Keller, S. Cretnik, O. Shouakar-Stash, M. Elsner, T. Schubert, and I. Nijenhuis. Combined C and Cl isotope effects indicate differences between corrinoids and enzyme (*Sulfurospirillum multivorans* PceA) in reductive dehalogenation of tetrachloroethene, but not trichloroethene. *Environ. Sci. Technol.*, 48:11837–11845, 2014.

[111] J. Renpenning, I. Rapp, and I. Nijenhuis. Substrate hydrophobicity and cell composition influence the extent of rate limitation and masking of isotope fractionation during microbial reductive dehalogenation of chlorinated ethenes. *Environ. Sci. Technol.*, 49:4293–4301, 2015.

[112] C. Richard and S. Canonica. Aquatic phototransformation of organic contaminants induced by coloured dissolved natural organic matter. In P. Boule, D. W. Bahnemann, and K. L. Robertson, editors, *Environmental Photochemistry Part II*, volume 2, pages 299–323. Springer, Heidelberg, 2005.

[113] C. Richard and G. Grabner. Mechanism of phototransformation of phenol and derivatives in aqueous solution. In *Environmental photochemistry*, pages 217–239. Springer, 1999.

[114] S. D. Richardson and T. A. Ternes. Water analysis: Emerging contaminants and current issues. *Anal. Chem.*, 83(12):4614–4648, 2011.

[115] M. A. Rishavy and W. W. Cleland. ^{13}C, ^{15}N, and ^{18}O equilibrium isotope effects and fractionation factors. *Can. J. Chem.*, 77:967–977, 1999.

[116] M. Rosell, R. Gonzaez-Olmos, T. Rohwerder, K. Rusevova, A. Georgi, F. D. Kopinke, and H. Richnow. Critical evaluation of the 2D-CSIA scheme for distinguishing fuel oxygenate degradation reaction mechanisms. *Environ. Sci. Technol.*, 46:4757–4766, 2012.

[117] N. Rosenfelder, P. Bendig, and W. Vetter. Stable carbon isotope analysis (δ^{13}C values) of polybrominated diphenyl ethers and their UV-transformation products. *Environ. Pollut.*, 159:2706–2712, 2011.

[118] F. Saito, S. Tobita, and H. Shizuka. Photoionization mechanism of aniline derivatives in aqueous solution studied by laser flash photolysis. *J. Photochem. Photobiol., A*, 106:119–126, 1997.

[119] I. Saito, T. Matsuura, and K. Inoue. Formation of superoxide ion via one-electron transfer from electron donors to singlet oxygen. *J. Am. Chem. Soc.*, 105:3200–3206, 1983.

[120] J. Sarasa, S. Cortes, P. Ormad, R. Gracia, and J. L. Ovelleiro. Study of the aromatic by-products formed from ozonation of anilines in aqueous solution. *Water Res.*, 36:3035–3044, 2002.

[121] J. M. Sayer and P. Conlon. The timing of the proton-transfer process in carbonyl additions and related reactions. General acid-catalyzed hydrolysis of imines and *N*-acylimines of benzophenone. *J. Am. Chem. Soc.*, 102:3592–3600, 1980.

[122] T. C. Schmidt, L. Zwank, M. Elsner, M. Berg, R. U. Meckenstock, and S. B. Haderlein. Compound-specific stable isotope analysis of organic contaminants in natural environments: A critical review of the state of the art, prospects, and future challenges. *Anal. Bioanal. Chem.*, 378:283–300, 2004.

[123] S. Schnell and B. Schink. Anaerobic aniline degradation via reductive deamination of 4-aminobenzoyl-CoA in *Desulfobacterium anilini*. *Arch. Microbiol.*, 155:183–190, 1991.

[124] K. Schreglmann, M. Hoeche, S. Steinbeiss, S. Reinnicke, and M. Elsner. Carbon and nitrogen isotope analysis of atrazine and desethylatrazine at sub-microgram per liter concentrations in groundwater. *Anal. Bioanal. Chem.*, 405:2857–2867, 2013.

[125] H. K. V. Schürner, J. L. Seffernick, A. Grzybkowska, A. Dybala-Defratyka, L. P. Wackett, and M. Elsner. Characteristic isotope fractionation patterns in *s*-triazine degradation have their origin in multiple protonation options in the *s*-triazine hydrolase TrzN. *Environ. Sci. Technol.*, 49:3490–3498, 2015.

[126] R. P. Schwarzenbach, P. M. Gschwend, and D. M. Imboden. *Environmental Organic Chemistry.* 1311 pp. John Wiley & Sons, 2^{nd} edition, 2003.

[127] R. P. Schwarzenbach, B. I. Escher, K. Fenner, T. B. Hofstetter, C. A. Johnson, U. Von Gunten, and B. Wehrli. The challenge of micropollutants in aquatic systems. *Science*, 313:1072–1077, 2006.

[128] R. P. Schwarzenbach, T. Egli, T. B. Hofstetter, U. Von Gunten, and B. Wehrli. Global water pollution and human health. *Annu. Rev. Environ. Resour.*, 35:109–36, 2010.

[129] K. M. Scott, X. Lu, C. M. Cavanaugh, and J. S. Liu. Optimal methods for estimating kinetic isotope effects from different forms of the Rayleigh distillation equation. *Geochim. Cosmochim. Acta*, 68:433–442, 2004.

[130] K. A. Shin and J. C. Spain. Pathway and evolutionary implications of diphenylamine biodegradation by *Burkholderia* sp. Strain JS667. *Appl. Environ. Microbiol.*, 75:2694–2704, 2009.

[131] K. E. Simmons, R. D. Minard, and J. M. Bollag. Oligomerization of 4-chloroaniline by oxidoreductases. *Environ. Sci. Technol.*, 21:999–1003, 1987.

[132] M. G. Siskos, A. K. Zarkadis, S. Steenken, N. Karakostas, and S. K. Garas. Photodissociation of *N*-(triphenylmethyl) anilines: A laser flash photolysis, ESR, and product analysis study. *J. Org. Chem.*, 63:3251–3259, 1998.

[133] M. Skarpeli-Liati, W. A. Arnold, A. Turgeon, C. J. Cramer, and T. B. Hofstetter. pH-dependent equilibrium isotope fractionation associated with compound-specific nitrogen and carbon isotope analysis by SPME-GC/IRMS. *Anal. Chem.*, 83:1641–1648, 2011.

[134] M. Skarpeli-Liati, M. Jiskra, A. Turgeon, A. N. Garr, W. A. Arnold, C. J. Cramer, R. P. Schwarzenbach, and T. B. Hofstetter. Using nitrogen isotope fractionation to assess the oxidation of substituted anilines by manganese oxide. *Environ. Sci. Technol.*, 45:5596–5604, 2011.

[135] M. Skarpeli-Liati, S. G. Pati, J. Bolotin, S. N. Eustis, and T. B. Hofstetter. Carbon, hydrogen, and nitrogen isotope analysis associated with oxidative transformation of substituted *N*-alkylated aromatic amines. *Environ. Sci. Technol.*, 46:7189–7198, 2012.

[136] S. A. Snyder, P. Westerhoff, Y. Yoon, and D. L. Sedlak. Pharmaceuticals, personal care products, and endocrine disruptors in water: Implications for the water industry. *Environ. Eng. Sci.*, 20:449–469, 2003.

[137] J. E. Sonke. A global model of mass independent mercury stable isotope fractionation. *Geochim. Cosmochim. Acta*, 75:4577–4590, 2011.

[138] S. Spahr, S. Huntscha, J. Bolotin, M. P. Meier, M. Elsner, J. Hollender, and T. B. Hofstetter. Compound-specific isotope analysis of benzotriazole and its derivatives. *Anal. Bioanal. Chem.*, 405:2843–2856, 2013.

[139] S. Spahr, J. Bolotin, J. Schleucher, I. Ehlers, U. Von Gunten, and T. B. Hofstetter. Compound-specific carbon, nitrogen, and hydrogen isotope analysis of *N*-nitrosodimethylamine in aqueous solutions. *Anal. Chem.*, 87:2916–2924, 2015.

[140] D. R. Stapleton, D. Mantzavinos, and M. Papadaki. Photolytic (UVC) and photocatalyic (UVC/ TiO_2) decomposition of pyridines. *J. Hazard. Mater.*, 146(3):640–645, 2007.

[141] A. S. Stasinakis, S. Kotsifa, G. Gatidou, and D. Mamais. Diuron biodegradation in activated sludge batch reactors under aerobic and anoxic conditions. *Water Res.*, 43(5):1471–1479, 2009.

[142] U. E. Steiner and T. Ulrich. Magnetic field effects in chemical kinetics and related phenomena. *Chem. Rev.*, 89:51–147, 1989.

[143] N. Stelzer, G. Imfeld, M. Thullner, J. Lehmann, A. Poser, H. Richnow, and I. Nijenhuis. Integrative approach to delineate natural attenuation of

chlorinated benzenes in anoxic aquifers. *Environ. Pollut.*, 157:1800–1806, 2009.

[144] S. Tajima, S. Shiobara, H. Shizuka, and S. Tobita. Excited-state proton-dissociation of N-alkylated anilinium ions in aqueous solution studied by picosecond fluorescence measurements. *Phys. Chem. Chem. Phys.*, 4:3376–3382, 2002.

[145] K. A. Thorn, P. J. Pettigrew, W. S. Goldenberg, and E. J. Weber. Covalent binding of aniline to humic substances. 2.^{15}N NMR studies of nucleophilic addition reactions. *Environ. Sci. Technol.*, 30:2764–2775, 1996.

[146] M. Thullner, F. Centler, H. Richnow, and A. Fischer. Quantification of organic pollutant degradation in contaminated aquifers using compound specific stable isotope analysis - Review of recent developments. *Org. Geochem.*, 42:1440–1460, 2012.

[147] N. B. Tobler, T. B. Hofstetter, and R. P. Schwarzenbach. Carbon and hydrogen isotope fractionation during anaerobic toluene oxidation by *Geobacter metallireducens* with different Fe(III) phases as terminal electron acceptors. *Environ. Sci. Technol.*, 42:7786–7792, 2008.

[148] N. J. Turro and B. Kraeutler. Magnetic-field and magnetic isotope effects in organic photochemical reations - A novel probe of reaction-mechanisms and a method for enrichment of magnetic isotopes. *Acc. Chem. Res.*, 13:369–377, 1980.

[149] N. J. Turro, V. Ramamurthy, and J. C. Scaiano. *Modern Molecular Photochemistry of Organic Molecules*. 1084 pp. University Science Books, 2010.

[150] J. Van der Zee, D. R. Duling, R. P. Mason, and T. E. Eling. The oxidation of N-substituted aromatic amines by horseradish peroxidase. *J. Biol. Chem.*, 264:19828–19836, 1989.

[151] X. Wang, X. Hu, H. Zhang, F. Chang, and Y. Luo. Photolysis kinetics, mechanisms, and pathways of tetrabromobisphenol a in water under simulated solar light irradiation. *Environ. Sci. Technol.*, 49:6683–6690, 2015.

[152] R. D. Wauchope. The pesticide content of surface water draining from agricultural fields - A review. *J. Environ. Qual.*, 7:459–472, 1978.

[153] E. J. Weber and R. L. Adams. Chemical-mediated and sediment-mediated reduction of the azo-dye disperse-blue-79. *Environ. Sci. Technol.*, 29:1163–1170, 1995.

[154] E. J. Weber, D. L. Spidle, and K. A. Thorn. Covalent binding of aniline to humic substances: 1. Kinetic studies. *Environ. Sci. Technol.*, 30:2755–2763, 1996.

[155] J. Wenk and S. Canonica. Phenolic antioxidants inhibit the triplet-induced transformation of anilines and sulfonamide antibiotics in aqueous solution. *Environ. Sci. Technol.*, 46:5455–5462, 2012.

[156] J. Wenk, U. Von Gunten, and S. Canonica. Effect of dissolved organic matter on the transformation of contaminants induced by excited triplet states and the hydroxyl radical. *Environ. Sci. Technol.*, 45:1334–1340, 2011.

[157] J. Wenk, S. N. Eustis, K. McNeill, and S. Canonica. Quenching of excited triplet states by dissolved natural organic matter. *Environ. Sci. Technol.*, 47:12802–12810, 2013.

[158] J. J. Werner, K. McNeill, and W. A. Arnold. Environmental photodegradation of mefenamic acid. *Chemosphere*, 58:1339–1346, 2005.

[159] P. Westerhoff, Y. Yoon, S. Snyder, and E. Wert. Fate of endocrine-disruptor, pharmaceutical, and personal care product chemicals during simulated drinking water treatment processes. *Environ. Sci. Technol.*, 39:6649–6663, 2005.

[160] R. E. Weston. Anomalous or mass-independent isotope effects. *Chem. Rev.*, 99:2115–2136, 1999.

[161] J. G. Wiederhold, C. J. Cramer, K. Daniel, I. Infante, B. Bourdon, and R. Kretzschmar. Equilibrium mercury isotope fractionation between dissolved Hg(II) species and thiol-bound Hg. *Environ. Sci. Technol.*, 44:4191–4197, 2010.

[162] R. S. Wijker, P. Adamczyk, J. Bolotin, P. Paneth, and T. B. Hofstetter. Isotopic analysis of oxidative pollutant degradation pathways exhibiting large H isotope fractionation. *Environ. Sci. Technol.*, 47:13459–13468, 2013.

[163] R. S. Wijker, J. Bolotin, S. F. Nishino, J. C. Spain, and T. B. Hofstetter. Using compound-specific isotope analysis to assess biodegradation of nitroaromatic explosives in the subsurface. *Environ. Sci. Technol.*, 47:6872–6883, 2013.

[164] R. S. Wijker, K. Zohre, J. C. Spain, J. Bolotin, J. Zeyer, and T. B. Hofstetter. Isotope fractionation associated with the biodegradation of 2- and 4-nitrophenols via monooxygenation pathways. *Environ. Sci. Technol.*, 47: 14185–14193, 2013.

[165] F. Wilkinson, W. P. Helman, and A. B. Ross. Quantum yields for the photosensitized formation of the lowest electronically excited singlet state of molecular oxygen in solution. *J. Phys. Chem. Ref. Data*, 22(1):113–262, 1993.

[166] M. Wolfsberg, A. van Hook, P. Paneth, and L. P. N. Rebelo. *Isotope Effects in Chemical, Geological, and Bio Sciences.* 466 pp. Springer, Heidelberg, 2010.

[167] S. Yan and W. Song. Photo-transformation of pharmaceutically active compounds in the aqueous environment: A review. *Environ. Sci.: Processes Impacts*, 16:697–720, 2014.

[168] Y. Zakon, L. Halicz, and F. Gelman. Bromine and carbon isotope effects during photolysis of brominated phenols. *Environ. Sci. Technol.*, 47:14147–14153, 2013.

[169] T. Zeng and W. A. Arnold. Pesticide photolysis in prairie potholes: Probing photosensitized processes. *Environ. Sci. Technol.*, 47(13):6735–6745, 2013.

[170] L. Zwank, M. Berg, M. Elsner, T. C. Schmidt, R. P. Schwarzenbach, and S. B. Haderlein. New evaluation scheme for two-dimensional isotope analysis to decipher biodegradation processes: Application to groundwater contamination by MTBE. *Environ. Sci. Technol.*, 39(4):1018–1029, 2005.

[171] L. Zwank, M. Elsner, A. Aeberhard, R. P. Schwarzenbach, and S. B. Haderlein. Carbon isotope fractionation in the reductive dehalogenation of carbon tetrachloride at iron (hydr)oxide and iron sulfide minerals. *Environ. Sci. Technol.*, 39:5634–5641, 2005.